AD NUMBER

ADB015191

LIMITATION CHANGES

TO:

Approved for public release; distribution is unlimited.

FROM:

Distribution authorized to U.S. Gov't. agencies only; Test and Evaluation; JUN 1976. Other requests shall be referred to Air Force Armament Laboratory, Attn: DLJF, Eglin AFB, FL 32542.

AUTHORITY

AFATL ltr, 4 Aug 1977

AFATL-TR-76-61

DESIGN AND TEST OF PROTOTYPE SAFE SEPARATION SENSORS (SSS) AND AN INSTRUMENT CONTROL PACKAGE (ICP)

UNIDYNAMICS/PHOENIX, INC.
POST OFFICE BOX 2990
PHOENIX, ARIZONA 85062

JUNE 1976

FINAL REPORT: APRIL 1974 - MAY 1976

AIR FORCE ARMAMENT LABORATORY
AIR FORCE SYSTEMS COMMAND • UNITED STATES AIR FORCE
EGLIN AIR FORCE BASE, FLORIDA

UNCLASSIFIED
SECURITY CLASSIFICATION OF THIS PAGE *(When Data Entered)*

REPORT DOCUMENTATION PAGE

READ INSTRUCTIONS BEFORE COMPLETING FORM

1. REPORT NUMBER: AFATL-TR-76-61
2. GOVT ACCESSION NO.:
3. RECIPIENT'S CATALOG NUMBER: rept.

4. TITLE *(and Subtitle)*: DESIGN AND TEST OF PROTOTYPE SAFE SEPARATION SENSORS (SSS) AND AN INSTRUMENT CONTROL PACKAGE (ICP).

5. TYPE OF REPORT & PERIOD COVERED: Final Apr 1974 through May 1976

6. PERFORMING ORG. REPORT NUMBER: DTR-59

7. AUTHOR(s): Arthur W. Mittendorf

8. CONTRACT OR GRANT NUMBER(s): F08635-74-C-0121 need

9. PERFORMING ORGANIZATION NAME AND ADDRESS:
Unidynamics/Phoenix, Inc.
P. O. Box 2990
Phoenix, Arizona 85062

10. PROGRAM ELEMENT, PROJECT, TASK AREA & WORK UNIT NUMBERS: 25080615 62602F

11. CONTROLLING OFFICE NAME AND ADDRESS:
Air Force Armament Laboratory
Armament Development & Test Center
Eglin Air Force Base, Florida 32542

12. REPORT DATE: June 1976

13. NUMBER OF PAGES: 148

14. MONITORING AGENCY NAME & ADDRESS *(if different from Controlling Office)*: 148p.

15. SECURITY CLASS. *(of this report)*: UNCLASSIFIED

15a. DECLASSIFICATION/DOWNGRADING SCHEDULE

16. DISTRIBUTION STATEMENT *(of this Report)*

Distribution limited to U. S. Government agencies only; this report documents test and evaluation; distribution limitation applied June 1976. Other requests for this document must be referred to the Air Force Armament Laboratory (DLJF), Eglin Air Force Base, Florida 32542.

17. DISTRIBUTION STATEMENT *(of the abstract entered in Block 20, if different from Report)*

18. SUPPLEMENTARY NOTES

Available in DDC

19. KEY WORDS *(Continue on reverse side if necessary and identify by block number)*

Safe Separation Sensors (SSS)
Arming Distances
Conventional Warhead Missiles
Instrument Control Package (ICP)

20. ABSTRACT *(Continue on reverse side if necessary and identify by block number)*

Under Air Force sponsorship Unidynamics conducted a research and development program to demonstrate the ability of a Safe Separation Sensor (SSS) to accurately determine arming distances for conventional warhead missile (S&A). The basic sensing concept was that used in the Air Force SRAM Missile. This device detects single axis acceleration and performs a double integration to provide arming distance information. During this program, the

CONT next p.

DD FORM 1 JAN 73 1473 EDITION OF 1 NOV 65 IS OBSOLETE

UNCLASSIFIED
SECURITY CLASSIFICATION OF THIS PAGE *(When Data Entered)*

* was conducted

356 310

20. device was successfully miniaturized and its g detection range was extended to demonstrate compatibility with conventional munition requirements. Arming range accuracies achieved represent a significant improvement over techniques now used in S&A systems. Prototype SSS's and an Instrument Control Package (ICP) were furnished for sponsor evaluation.

PREFACE

This report documents work performed during the period from April 1974 through May 1976 by Unidynamics/Phoenix, Inc., Post Office Box 2990, Phoenix, Arizona 85062, under contract F08635-74-C-0121 with the Air Force Armament Laboratory, Armament Development and Test Center, Eglin Air Force Base, Florida 32542. Captain J. Williams and later Mr. Firman D. King (DLJF) managed the program for the Armament Laboratory. Program manager and principal investigator for the contractor was Mr. Arthur W. Mittendorf.

This technical report has been reviewed and is approved for publication.

FOR THE COMMANDER

William F. Brockman

WILLIAM F. BROCKMAN, Colonel, USAF
Chief, Munitions Division

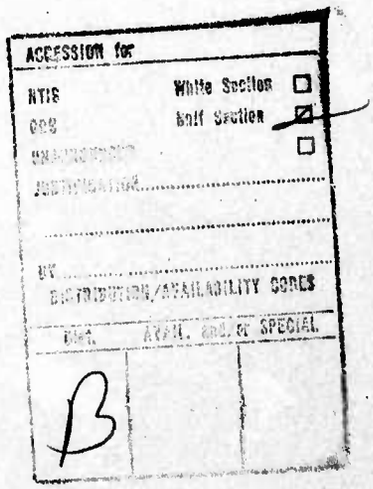

(The reverse of this page is blank)

TABLE OF CONTENTS

TABLE OF CONTENTS (Concluded)

LIST OF FIGURES

LIST OF FIGURES (Concluded)

LIST OF TABLES

(The reverse of this page is blank)

SECTION I

INTRODUCTION

Under Air Force Armament Laboratory sponsorship (Contract No. F08635-74-C-0121) Unidynamics/Phoenix, Inc. conducted a research and development program to demonstrate the feasibility of a Safe Separation Sensor (SSS) to accurately determine arming distances for conventional warhead missile safety and arming (S&A) devices. The basic sensing concept employed here is the approach used in the Air Force SRAM Missile Safe-Arm-Fuze, which was previously developed and manufactured by Unidynamics.

The SRAM device, known as an FES or Flight Environment Sensor, detects single axis acceleration and performs a double integration to provide distance measurement. The FES is designed to integrate acceleration up to 6g with a distance accuracy of approximately 2 percent.

Present conventional S&A's employ acceleration driven mechanical designs to provide pseudo-integrations or timing functions. Their purpose is to arm the S&A on the basis of distance or time. An example of a widely used mechanism consists of an escapement driven by a g weight which responds to missile acceleration. This device yields distance information on the basis of the square root of the applied acceleration; therefore, the arming range is a pseudo value rather than actual range. Assuming this range information to be acceptable for certain missile launch parameters, accuracy is still a significant problem. For example, the performance of the g weight and the escapement gears is modified by varying levels of friction characteristics of the design. This friction can be minimized at increased cost; however, environmental forces introduced by conditions such as missile maneuvering increase the friction and destroy accuracy. Additionally, the typical escapement mechanism cannot respond to zero or negative g acceleration. Because of these problems, arming distances can vary on the order of ± 30 percent. This variation is unacceptable in missile applications where the desired minimum engagement range approaches the minimum allowable launch range for safe separation from the aircraft at impact.

While the existing SRAM FES offers far greater accuracy, its operational specification, size and cost are not compatible with conventional missile S&A applications. The basic objective of the SSS program then has been to utilize the FES technology

in the development of an SSS having extended performance capabilities (-5g to +50g), to simplify the design, and to reduce its size and cost. Accomplishment of these objectives indicates the feasibility of subsequent adaptation of the SSS to conventional S&A's.

To establish the feasibility, a two-part program was conducted. The first part consisted of the design, fabrication, testing and delivery of one breadboard prototype SSS and an Instrument Control Package (ICP). The ICP serves as a testing vehicle which provides power to the SSS and monitors/measures its performance. The second part of the program consisted of fabrication, testing and delivery of five preliminary prototype SSS's, then a motor evaluation followed by the design, fabrication, testing and delivery of five final prototype SSS's. The five preliminary prototype units, built to demonstrate reproducibility, were of the same basic design as the breadboard model of Part 1. Final prototype design was based on the results of the motor evaluation which was conducted to determine if improvements could be made in the design approach used in the previous models.

The chief program goal of demonstrating feasibility of the SSS to provide arming distance information with far greater accuracy than conventional fuzes now being used was adequately demonstrated during this program. During centrifuge testing, the breadboard and preliminary prototypes were tested to 27g and produced an accuracy of ±3 percent. Each of these systems was packaged in a cylindrical container 2.59 inches in diameter by 2.62 inches high, thereby illustrating that the system can readily be placed in the space required by and configuration of existing fuzes. Peak power consumption for the first two prototypes was approximately 100 watts and for the final prototype 25 watts. Electrical requirements are thus compatible with typical weapon systems now in use.

The final prototype was designed to integrate accelerations within the range of ±50g and was intended to represent a significant improvement over the breadboard and preliminary prototype designs. This portion of the effort was partially successful in that the g detection range was nearly doubled in the positive direction, and negative g detection was increased from -5g to -50g. In addition, the final prototype will detect either positive or negative g at the start of a problem, while the first two prototypes must see a positive acceleration before a negative acceleration can be processed. Performance data on the final prototype indicates that very high accuracies (less than 1 percent error) can be achieved; however, an unsolved temperature drift problem hampered the investigations, and full capability was not demonstrated.

Additional details are provided in subsequent sections. General organization of this report is designed to first offer an understanding of the basic SSS concept, including functional and general theoretical design details. This is followed by a description of breadboard and preliminary prototype construction details and operation and test discussions. The same type of information is then presented for the final prototype. Concluding sections of the report include a general failure mode and effects analysis and physical and operational details concerning the ICP.

SECTION II

SYSTEM OPERATIONAL CONCEPT

This section outlines the SSS baseline functional concept and reviews areas of design tradeoff. More precise details of the various functional elements are presented in subsequent sections. As illustrated by the front and side views provided in Figure 1, the SSS consists basically of a DC motor whose principal parts, the stator and rotor, are both free to move. The rotor is supported relative to the stator by the usual means (bearings) to permit rotor displacement when electrical power is applied to the motor. The stator is suspended relative to a mechanical frame (representative of the missile structure) by means of a second set of bearings. These two sets of bearings provide the two-degrees-of-freedom such that application of electrical power will result in equal but opposite motor torques being applied to the rotor and stator. Therefore, with no further design constraints, the rotor and stator will accelerate in opposite directions consistent with their respective moments of inertia.

To sense missile acceleration, an unbalanced mass is placed on the stator (Figure 1). If the system is subjected to missile acceleration in the direction shown, a torque, T_a, will be developed on the stator. This torque will produce counterclockwise motion of the unbalanced mass, hereafter called the null or null mass. When the null crosses the transition line, a sensor (which will be explained later) directs electrical power to the motor such that a motor torque, T_m, is applied to the stator/null assembly in a counterclockwise direction as shown in Figure 1. At the same time, T_m is also applied to the rotor but in the opposite direction. The system is designed such that motor torque, T_m, is always greater than the maximum null acceleration torque, T_a. Therefore, the motor torque stops the null in the on quadrant and accelerates it clockwise toward the off quadrant. When the null arrives at the transition line, the sensor removes electrical power from the motor, thus reducing T_m to zero. Due to its inertia, the null continues into the off quadrant but is eventually stopped by T_a and accelerated back toward the on quadrant. The process is then repeated continuously, and the null/stator motion is oscillatory.

Net null displacement is zero; therefore, the average motor torque is equal to the acceleration torque, and the null can be considered in equilibrium over an extended period.

Or:

$$T_m = T_a \qquad (1)$$

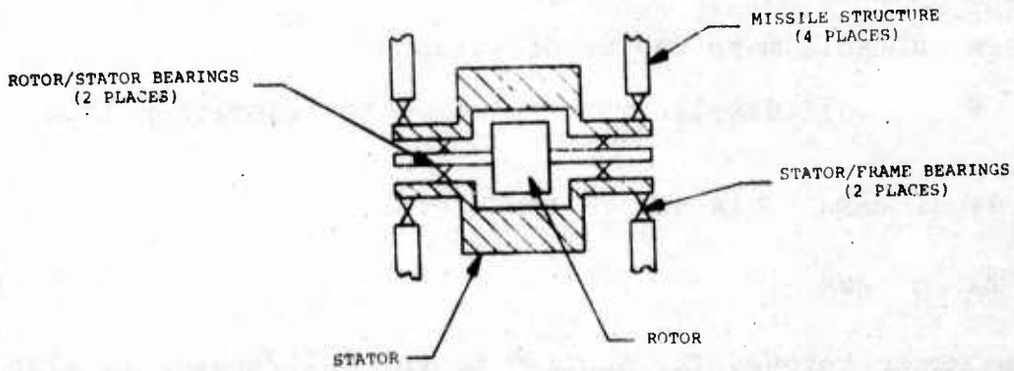

SIDE VIEW

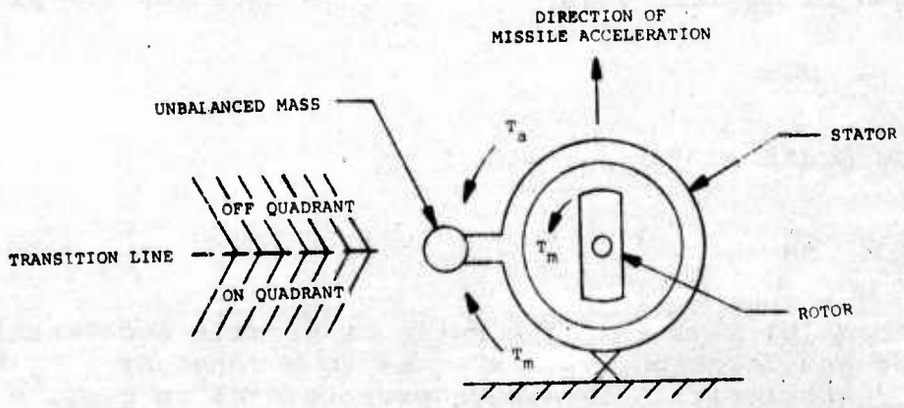

FRONT VIEW

Figure 1. Functional Concept

The acceleration torque, T_a, is equal to:

$$T_a = MaR \cos \theta \tag{2}$$

Where:

M = null mass

a = missile acceleration

R = null mass radius of action

θ = null displacement relative to transition line

In the usual case, θ is small; therefore:

$$T_a = MaR \tag{3}$$

The same motor torque, T_m, applied to the null/stator is also applied to the rotor; therefore:

$$T_m = J_R \alpha_R \tag{4}$$

Where:

J_R = rotor moment of inertia

α_R = rotor angular acceleration

Substitution of Equations (3) and (4) into Equation (1) yields:

$$J_R \alpha_R = MaR \tag{5}$$

Rearranging Equation (5):

$$\frac{a}{\alpha_R} = \frac{J_R}{MR} \tag{6}$$

Equation (6) says that the ratio of missile acceleration, a, to rotor acceleration, α_R, is equal to a constant, J_R/MR. Thus, rotor acceleration is always proportional to missile acceleration because J_R, M and R are unchanging physical parameters. Similarly, the rotor angular velocity and displacement are the analogs of missile velocity and displacement, respectively. The term J_R/MR is referred to as the K factor, or:

$$a = K\alpha_R \tag{7}$$

Taking the integral of Equation (7) yields:

$$v = K\omega_R \tag{8}$$

Where:

v = missile velocity

ω_R = rotor angular velocity

Taking the integral of Equation (8) yields:

$$X = K\theta \tag{9}$$

Where:

X = missile displacement

θ = rotor angular displacement

The K factor has units of feet/radian, and it is clear that the parameters J_R, M or R may be adjusted to provide the desired a/α_R or X/θ ratio. For example, K can be set such that one rotor revolution (2π radians) is equal to 1 foot; therefore, missile range can be determined by counting the rotor revolutions. When the accumulated count is equal to the desired range, the appropriate arming commands are given.

Range can be accumulated in a variety of ways. In the SRAM FES, a set of brushes installed between the rotor and stator provides three electrical output pulses per rotor revolution. By means of slip rings, these pulses are routed to a stepping motor which in turn rotates a gear train a fixed number of degrees per pulse. This gear train then actuates a series of switches, each located at an angular position representative of a specific missile distance displaced.

A second technique is to electronically accumulate the range by counting the rotor revolutions. This is the technique used in the present program.

Null sensing can also be accomplished in a variety of ways. Figure 2 illustrates the approach used in the SRAM FES. The arrangement shown is attached to and part of the null assembly and therefore oscillates with it. Operation is as follows: A plus voltage is applied to the conductor via a slip ring. When the null mass is above the transition line

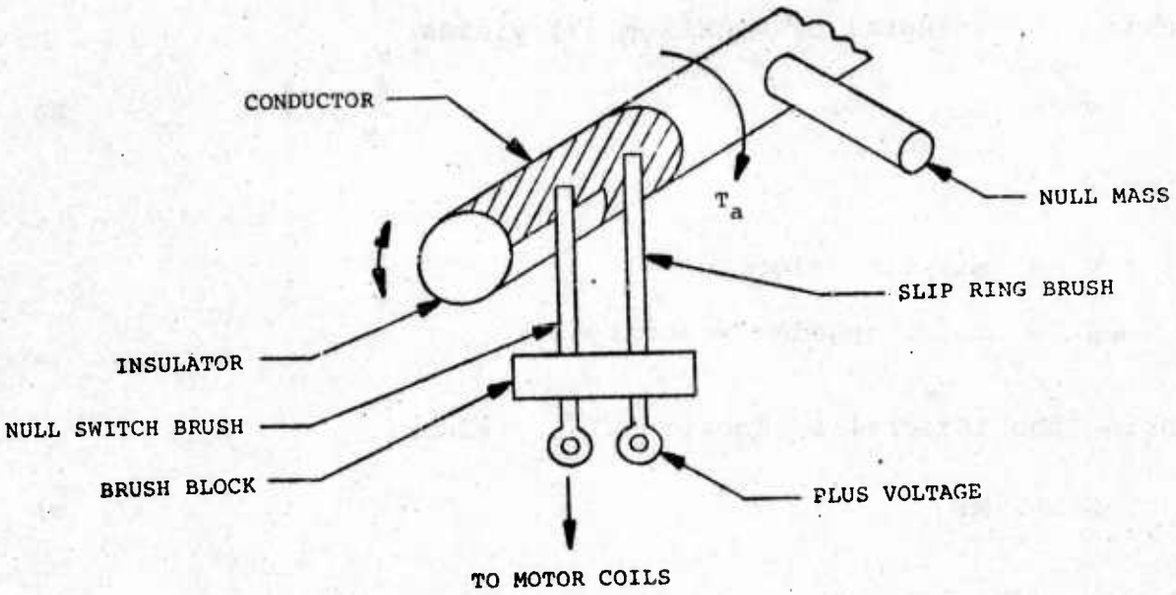

Figure 2. Bang-Bang Null Sensor

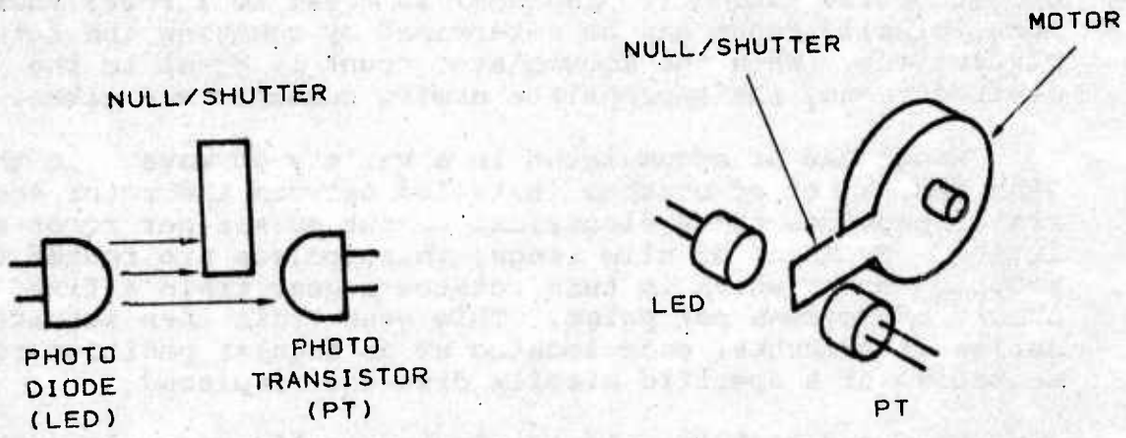

Figure 3. Photo Null Sensor

shown in Figure 1, the null switch brush is in contact with the insulator, and power is removed from the motor. When the null is in the on quadrant or rotated clockwise beyond the transition line, the null brush is in contact with the conductor, and power is supplied to the motor. Because the brushes are mounted relative to the missile structure, the approach introduces friction into the null assembly to influence null motion and affect accuracy. To eliminate this friction, a second approach can be used.

Figure 3 illustrates a null sensing technique which does not introduce friction into the system. It consists of a photo diode and a photo transistor mounted in opposition such that light emitted by the photo diode is received by the photo transistor unless interrupted by the null mass, which serves as a shutter. The photo transistor is wired into a motor control circuit such that when light is cut off by the null, the motor is on; otherwise, it is off. To improve system accuracy, this approach was used in all SSS designs described herein. It also provides the option of using a tracking null approach where $T_a = T_m$ at all times. With the brush design, only the bang-bang or oscillating null approach can be used. Though the photo approach is used in all designs of this program, the oscillating mode was used in the breadboard and preliminary prototype systems, and the tracking mode was used in the final prototype. The rationale for this will be explained in detail in later sections of this report.

To provide further information and define terms which will be used throughout the report, a more detailed description of the oscillating null is presented. Figure 4 shows a plot of null displacement as a function of time.

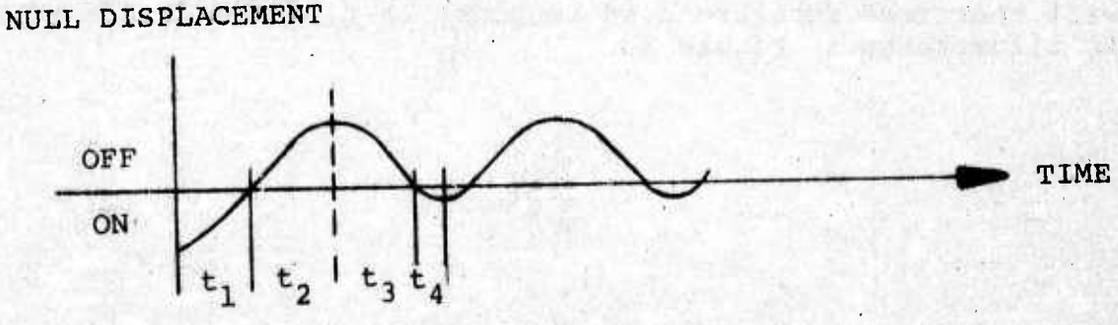

Figure 4 - Null Displacement Versus Time

One null cycle is defined as the sum of the times t_1 through t_4. The duty cycle is defined as the on-time ($t_1 + t_4$) divided by the full-cycle time ($t_1 + t_2 + t_3 + t_4$). During each on-time interval, full motor torque, T_m, is applied; therefore, the average motor torque applied for a given time is equal to T_m times the duty cycle, D. Because the average motor torque is equal to the acceleration torque, T_a, the following equation results:

$$T_a = T_m D \tag{10}$$

The torque, T_m, which a motor can provide is a fixed value; therefore, the duty cycle will vary with T_a. Stated differently for a large missile acceleration, T_a will be large and will result in a larger duty cycle. This means that in response to larger missile acceleration, the average motor on-time increases, thus producing a greater rotor angular acceleration. The maximum rate of acceleration occurs when the duty cycle is 100 percent.

Because the null is oscillating, the rotor motion will also be oscillatory. For example, when the null is on, the rotor will accelerate in response to the applied T_m. However, when the null is off, the rotor will decelerate in response to internal motor friction between the stator and rotor. If the rotor and stator are fully coupled, that is, the friction seen by the rotor is also seen by the stator in the opposite direction, then the net effect of such friction will automatically be compensated and no error will result. To explain this feature, internal drag or frictional torques tend to slow the rotor. This frictional torque, T_B, is in opposition to the motor torque, T_m. The same is true for the stator assembly; therefore, T_B is in the same direction as T_a with respect to null operation. Positive T_a causes a particular duty cycle, as previously explained, and T_B has the same effect. Stated differently, the presence of T_B results in a greater duty cycle and thus a larger average applied motor torque. The increase in average motor torque is equal to T_B, and the rotor will therefore accelerate in response to T_a. The effect of T_B is illustrated in Figure 5.

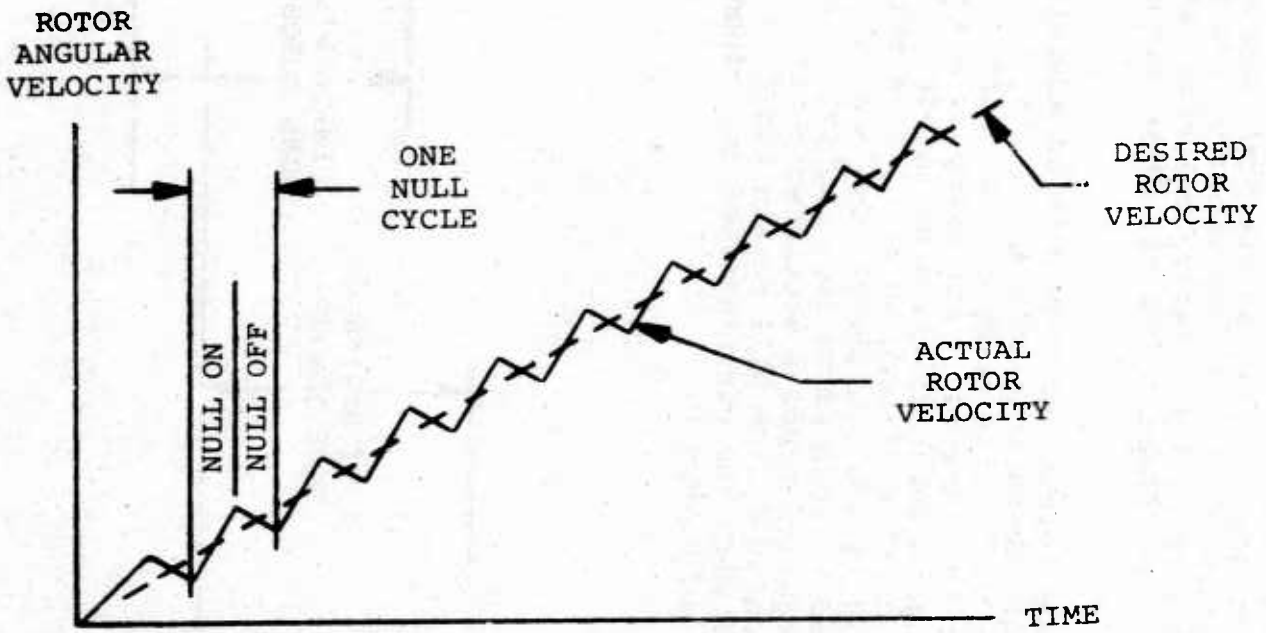

Figure 5 - Motor Velocity Versus Time

Figure 5 plots rotor angular velocity versus time for a system under the influence of a constant missile acceleration. As shown, the velocity oscillates about the desired curve, but the average increase is equal to the desired rate. The deceleration portions are due to the internal friction, T_B.

In addition to Coulomb friction torque, T_B, which is due to the internal bearings and brushes, an air drag component also exists. This drag is of the viscous variety, and the resulting torque is related to the relative velocity between the rotor and stator. The effect of the air drag torque is the same as T_B.

Coulomb and viscous torques provide both an advantage and a disadvantage. Without these loss torques, a single power supply polarity system would only respond to a maximum positive T_a or positive missile acceleration. For example, assume a system could be designed without friction to integrate an acceleration range or profile of zero to 30g. If a frictional torque equivalent to 5g is now introduced, the peak acceleration which can be integrated is reduced to 25g. However, the system can now integrate a negative missile acceleration of -5g. Therefore, this particular system will retain the full integration range of 30g, but with the curve shifted in response to loss torques as shown in Figure 6.

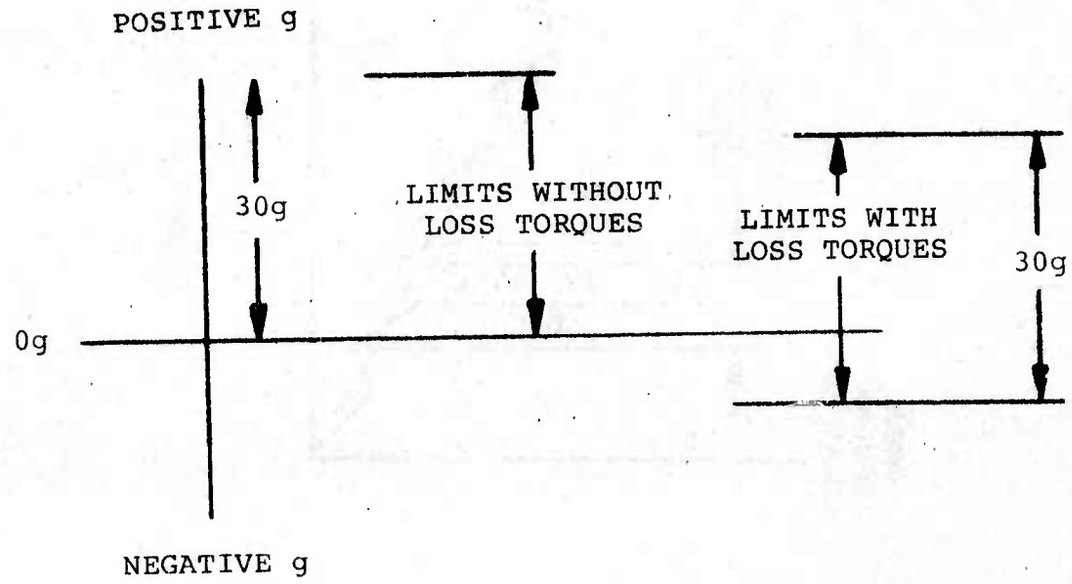

Figure 6 - SSS g Limits

The system described in Figure 6 uses a single polarity electrical source, and motor torque, T_m, is applied in one direction only. If the electrical circuit is designed such that motor current is reversed rather than set to zero when the null is in the position defined previously as the off quadrant, then the system can integrate equal magnitudes of positive and negative acceleration from a standing start. If positive g is applied first followed by negative g, a larger negative g can be sensed than positive due to the internal loss torques which will always exist to some extent. The reverse situation, application of negative then positive acceleration, is also true provided the rotor velocity is never reversed from the initial direction.

Two of the SSS designs which were investigated during this effort feature a motor commutation design accomplished by means of light in a manner similar to the photo diode/transistor pair used for the null. This approach eliminates brushes and reduces the internal Coulomb frictional torque, T_B. In the same models, stator and rotor surfaces are smooth and uninterrupted. This reduces viscous torques thereby increasing the peak positive acceleration which can be detected. The final prototype SSS motor commutation was accomplished by brushes, and coil windings were exposed, resulting in viscous drag. The details of these designs are expanded in subsequent sections.

Design limitations of the system are primarily due to a Coulomb frictional torque between the stator/null and missile structure. In the conventional approach, this friction is due to the bearings, motor access power brushes and the null switch. Stated simply, such frictional torque, T_c, must be less than the minimum T_a, and T_m must be greater than the maximum T_a plus T_B and the peak viscous torque. Therefore, the motor torque which must be developed is determined by the maximum expected T_c. Without T_c, there is no limit on the range of g which can be detected except within the constraints of system dynamic balance. For example, T_a can be set as small as desired if there are no other unbalanced stator conditions, i.e., the stator is dynamically balanced. For a given motor, reducing the lg T_a increases the g range which can be sensed.

The first two SSS models were mounted to the structure via ball bearings, and null sensing was accomplished by photo means. Motor electrical access was provided by small wires connected directly from the motor to the control circuit. The null frictional content was therefore due primarily to the bearings. The final prototype was mounted to the structure

via torsional springs, thereby eliminating all T_c frictional content. Electrical access was provided through the springs, and null photo sensing was used in this model to secure the zero T_c feature. With no T_c, a very small, low-power motor can be used to sense in excess of 50g, both positive and negative; however, introduction of the springs produced other problems. Further details are provided on all designs in subsequent sections.

SECTION III

ANALYSIS OF PROGRAM REQUIREMENTS - PART I

The first portion of this program consisted of design, fabrication and testing of a breadboard prototype of the SSS. To test and demonstrate the device, it was necessary to design and construct an Instrument Control Package (ICP). The SSS and ICP were to be compatible to the extent that various arming ranges could be selected and the run time to the selected ranges measured. The ICP also provided the necessary power for SSS operation. The breadboard SSS configuration was to be a right circular cylinder 2.655 inches in diameter and 2.2 inches in length. Specified accuracy goal was $\pm$0.5 percent at a range of 1300 feet, and the device was to be capable of integrating an acceleration profile of -5g to +50g. A launch lock solenoid was to be incorporated for uncaging the SSS motor. Testing was to consist of unspecified levels of temperature (high and low) and vibration.

At the start of the program, Unidynamics' design experience in this area was limited to the SRAM FES DT&E program. This device integrated acceleration profiles of up to 6g and provided an arming range in excess of 13,000 feet. The package size was about three times that specified for the breadboard prototype. This much smaller size coupled with the significantly larger acceleration profiles provided the primary design challenge.

The breadboard and preliminary prototype SSS's delivered to the sponsor were 2.59 inches in diameter by 2.620 inches high, or about 0.4 inch larger than the specified height. This was necessary to accommodate the electronic circuits. These prototypes were tested to 27g, which is less than the goal of 50g; however, the device will accelerate at the 50g rate for a limited period. System accuracy achieved was about 3 percent, less than the goal of 0.5 percent.

SECTION IV

BASIC THEORETICAL ANALYSIS AND DESIGN GUIDELINES

In the paragraphs that follow, two theoretical analyses are presented. The first analysis is the design procedure used to establish or select motor and other parameters required by a basic set of relationships which can be used to evaluate system performance and to determine parameter interdependence. Because there are numerous techniques which may be used to implement the basic concept, it is not practical to provide a comprehensive set of relationships for all of them. Those provided below are characteristic of most systems which may be considered, including the breadboard and preliminary prototypes investigated in this program. Detailed relationships governing the final prototype are provided in a subsequent section dealing with that design.

Design Procedure. The DC motor is the heart of any SSS design, and the capability of an SSS to meet specified performance requirements is dependent on its operational parameters. With one exception all other parameters which characterize the system are considered peripheral and are controlled by implementation techniques (count accumulation, control electronics, envelope, etc.). The peripheral parameter which must be considered in the design procedure is T_c, the frictional torque between the null assembly and missile structure. Considering accuracy and motor operational parameters, it is the most important parameter in a bang-bang design. Selection or determination of the magnitude of T_c is the first step in the design procedure because all other motor parameters are based on this value.

To provide the necessary null performance, the torque, T_a, on the unbalanced mass due to missile acceleration must always be greater than T_c. Otherwise the null can stick in the off quadrant and integration will cease. To provide a margin of safety and to ensure accuracy, T_a should be at least three times T_c. Because T_a and T_c are variables due to loading effects, their magnitudes are selected on the basis of a 1g load condition. Preliminary design procedure has been established by assuming both T_c and T_a will vary as a function of the acceleration profile. That is, the ratio of T_a to T_c will be essentially constant, and the 1g condition can be used for convenience. In the SRAM FES, it was found that an appropriate maximum value for T_c at 1g was 0.008 ounce-inch. The minimum value of T_a at 1g is

set at three times T_c, or 0.024 ounce-inch. At 50g, T_a will be (50) (0.024) = 1.2 ounce-inches.

Internal motor loss torques appear at the null in the same direction as T_a, or in opposition to the motor torque. Coulomb frictional torque caused by the motor bearings will be approximately the same value as the null bearings and will vary with loading as previously explained for T_c. If brushes are used for commutation, the resulting friction is dependent on side-loading or maneuvering acceleration only, since these brushes can be oriented as desired. Because photo commutation is used in the breadboard and preliminary prototypes, only the bearing friction is applicable to the Coulomb component. At 1g then, T_B will be about 0.008 ounce-inch, or at 50g, 0.4 ounce-inch.

An additional loss parameter which must be considered is windage or viscous torque. This loss torque is equal to the product of an air drag coefficient (A) and the motor angular velocity ($\dot{\theta}$). This coefficient was found to be approximately 0.0008 ounce-inch/radian/second in the SRAM FES. However, the motor design used here features smoother internal surfaces and a coefficient of 0.0004 ounce-inch/radian/second was assumed for design purposes. To determine the motor torque necessary to offset the effects of air drag, the motor velocity must be known. This velocity is the analog of missile velocity; therefore, all missile acceleration profiles must be evaluated to determine the worst case g-time product.

In this instance, the sponsor stated that an acceleration level of 25g for a period of 0.4 second followed by a negative g is representative of a typical worst case condition. For this profile, the worst case missile velocity will occur at the 0.4 second point, since the motor torque demand is the greatest at that time. In other profiles, further accumulation of velocity is acceptable if such an increase is due to a lower acceleration. The objective here is to ensure that sufficient motor torque is available to overcome loss torque and still provide the acceleration torque being demanded. Because the viscous loss torque is velocity dependent, correct integration can continue and additional velocity can be accumulated if less torque is needed for acceleration. In the 0.4 second, 25g profile, the maximum missile velocity is calculated to be 322 feet/second. To increase the sensing capability of the device to integrate 50g for 0.4 second, the motor peak velocity can be maintained by doubling the rotor moment of inertia.

At 322 feet/second, the motor velocity will be 161 revolutions/second if a K factor of 2 feet/revolution is selected. This angular velocity is 1011.59 radians/second, or 9660 RPM. The value for air drag torque is then $A\dot{\theta}$, or

(0.0004) (1011.59) = 0.4 ounce-inch. For the 50g then, the total motor torque required to secure null action is summarized below:

T_a @ 50g:	(0.024) (50)	= 1.2
T_c @ 50g:	(0.008) (50)	= 0.4
T_B @ 50g:	(0.008) (50)	= 0.4
$A\dot{\theta}$ @ 1011 rads/sec:	(0.0004) (1011)	= 0.4
TOTAL		2.4 ounce-inches

By way of comparison, at 25g the total is 1.4 ounce-inches. It should be noted that the motor must be capable of delivering these levels of torque for the duration of the applied g.

To summarize this portion of the analysis, the reader is reminded of the effect of T_C, the null frictional content. If there is no T_C, any T_a may be selected and any motor can provide the correct integration properties. That is, the g profile which can be detected is limited only by the ability of the rotor to accelerate under the applicable loading conditions primarily due to T_B, the internal motor friction. The remaining motor parameters can now be investigated. Shown below are simplified relationships for the typical DC motor:

$$V = IR + K_B\dot{\theta} \tag{11}$$

$$T_m = K_T I \tag{12}$$

$$K_B = K_T/141.6 \tag{13}$$

Where:

V = available source voltage

I = motor current

R = motor resistance

K_B = motor back emf constant

$\dot{\theta}$ = motor velocity

T_m = motor torque

K_T = motor torque sensitivity constant

Examination of Equation (11) shows that the motor current will decrease (at constant applied voltage) as motor velocity increases. Therefore, the available motor torque also decreases. To ensure sufficient motor torque to accomplish integration, the value for K_T must be carefully selected. For example, if a large K_T is selected, then as seen in Equation (13), the back emf constant is also large and the motor current will drop off quickly with an increase in velocity. Required torque sensitivity can be determined by substituting Equations (12) and (13) into Equation (11) as follows:

$$\dot{\theta} K_T^2 - 141.6\ V K_T + 141.6\ T_m R = 0 \qquad (14)$$

There are two unknowns in this relationship, motor torque sensitivity (K_T) and motor resistance (R). These two parameters are related, and both are related to motor size. For example, K_T is equal to NAB where:

N = number of armature turns

A = pole face area

B = magnet field density

And, the resistance is related to N and A. Both N and A are related to motor size. For a given motor size, the space allotment for windings is fixed. If the number of windings is increased to increase K_T, the wire size will be reduced and the resistance will increase accordingly. From another viewpoint, power can be minimized by maximizing resistance. Maximum resistance is determined by use of the quadratic equation for determination of roots. At 25g, which requires a torque of 1.4 ounce-inches, and with an applied voltage of 28 VDC, Equation (14) becomes:

$$1011\ K_T^2 - 3965\ K_T + 198\ R = 0 \qquad (15)$$

Using the quadratic equation for determination of roots yields:

$$K_T = \frac{3965 \pm [3965^2 - (4)\ (1011)\ (198)\ R]^{1/2}}{(2)\ (1011)} \qquad (16)$$

Then to determine the maximum value of R, the radical term is set to zero, or:

$$R = 3965^2 / [(4)\ (1011)\ (198)] = 19.63 \text{ ohms} \qquad (17)$$

For 50g:

$$R = 3965^2/[(4)\ (1011)\ (340)] = 11.43 \text{ ohms} \qquad (18)$$

In both instances, K_T is equal to:

$$K_T = 3965/(2)\ (1011) = 1.96 \text{ ounce-inches/ampere} \qquad (19)$$

Here it is shown that for minimum power the motor size will increase with an increase in g level. This is because the same number of turns gives the same K_T; however, to obtain the lower resistance for the higher g level case, larger wire is needed and more space is necessary. This additional space increases the size of the motor. It can also be seen from the analysis that the maximum velocity affects both power consumption and the selection of K_T. If the rotor moment of inertia is doubled, the velocity will be halved and K_T can be doubled. The current will also be halved, and at a given applied voltage the power too is halved. It is interesting to note that power consumption can be reduced by increasing the size of the motor in an attempt to increase K_T (thus reducing current necessary to produce the required T_m) and reduce the resistance. This can be more clearly seen if Equation (14) is solved for its roots as follows:

$$K_T = \frac{3965 \pm [3965^2 - (4)\ (1011)\ T_m\ R]^{1/2}}{2(1011)} \qquad (20)$$

Here for a given T_m and a reduced R, a larger K_T is permitted. The applicable radical sign is always positive. This is because the IR voltage drop is reduced and the voltage gained permits a larger back emf at the applicable velocity without affecting the needed torque. With the higher K_T, the current needed drops, and thus the power consumed is reduced.

In this design, the space limitations require the use of a small motor. Thus, a two-winding motor was selected with each winding having a resistance of 8 ohms and a K_T of 1 ounce-inch/ampere. Total resistance is then 4 ohms, and total K_T is 1.414 ounce-inches/ampere. With this motor and a 22-volt source, the total torque available is 4.2 ounce-inches at a velocity of 1011 radians/second. Only 2.4 ounce-inches were required; therefore, the current needed was 2.4/1.414 = 1.7 amperes and the power consumption is 37.3 watts. For a 25g case, the torque required is 1.4 ounce-inches and the necessary current is then about 1 ampere. Power consumption is 22 watts.

Exclusive of commutation, the motor size is 1 inch in diameter by 0.35 inch thick.

To reduce the torque requirements of the breadboard and preliminary prototype design, it was necessary to reduce the loss torques. This was accomplished by use of the photo null detector to reduce T_C and photo commutation to reduce T_B. The effects of windage A were reduced by using a cylindrical shaped rotating magnet and a molded armature, thus providing smooth internal surfaces. In the final prototype design, torsional springs were used to mount the null, thus eliminating T_C and permitting the use of a small T_a at lg. Further details on the final prototype are provided in a subsequent section.

Equations of Motion. The equations that follow are the more comprehensive relationships which govern system performance. There are two moving assemblies, the null/stator and the rotor. Figure 7 depicts the system and the free body diagrams of the two moving assemblies.

The summation of torques for both diagrams provide the equations of motion as follows:

Stator/Null:

$$T_m - T_a - T_B - A\dot{\theta} + J_N\ddot{\theta}_N \pm T_C = 0 \qquad (21)$$

Rotor:

$$- T_m + A\dot{\theta} + T_B + J_R\ddot{\theta}_R = 0 \qquad (22)$$

Where:

T_m = motor torque

T_a = acceleration torque

T_B = internal motor Coulomb friction torque

A = windage coefficient of friction

$\dot{\theta}$ = $\dot{\theta}_R - \dot{\theta}_N$

$\dot{\theta}_N$ = null velocity

$\dot{\theta}_R$ = rotor velocity

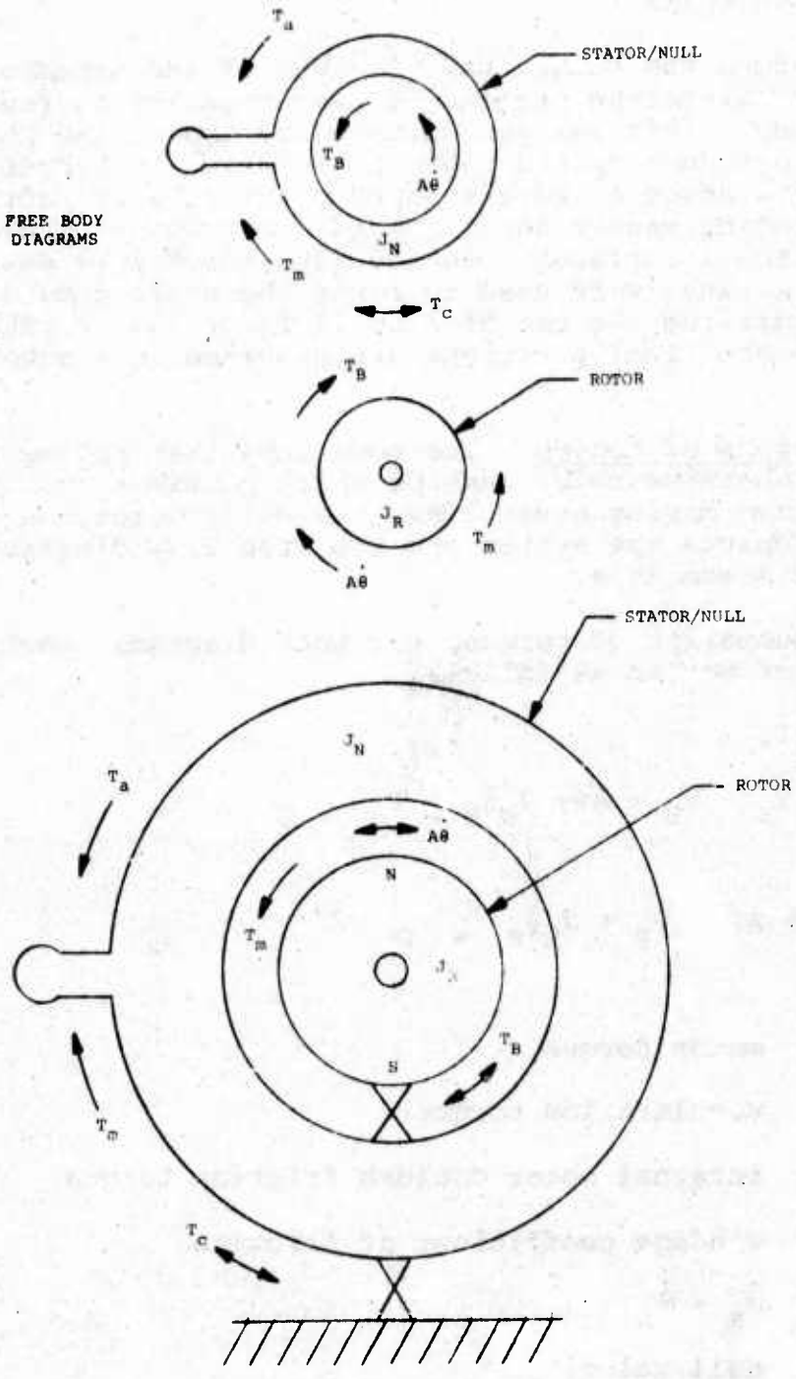

Figure 7. Motion Diagrams

$\ddot{\theta}_N$ = null acceleration

$\ddot{\theta}_R$ = rotor acceleration

T_c = null Coulomb friction torque

The term T_c is dependent on the null velocity because of the oscillating motion; therefore, Equation (21) is modified as follows:

$$T_m - T_a - T_B - A\dot{\theta} + J_N\ddot{\theta}_N + T_c|\dot{\theta}_N|/\dot{\theta}_N = 0 \quad (23)$$

To find T_m, it is necessary to use the motor equations. These are developed as follows.

There are two windings in the motor wound in quadrature (offset 90 degrees). Winding number one will deliver a torque as follows:

$$T_{m1} = K_{T1}I_1 \cos\theta \quad (24)$$

Winding two torque is given by:

$$T_{m2} = K_{T1}I_2 \sin\theta \quad (25)$$

Where:

$$\theta = \theta_R - \theta_N$$

The total torque, T_m, is then:

$$T_m = T_{m1} + T_{m2} = K_{T1}I_1|\cos\theta| + K_{T1}I_2|\sin\theta| \quad (26)$$

The currents I_1 and I_2 are found as follows:

$$V = I_1R_1 + K_{B1}\dot{\theta}|\cos\theta| + L_1\dot{I}_1 \quad (27)$$

$$V = I_2R_2 + K_{B2}\dot{\theta}|\sin\theta| + L_2\dot{I}_2 \quad (28)$$

Absolute values are the result of commutation, and L is the inductance of each winding. Because the windings are identical, R, L, K_T and K_B are the same value for each of the relationships. It should be noted that simulation of this

system on a computer requires that the commutation effects be included. For example, the current direction in each winding is reversed each 180 degrees of relative rotor/stator motion. Figure 8 illustrates the commutation procedure.

This concludes the analysis of the breadboard and preliminary prototype design approaches. The next section includes a description of these systems. Subsequent sections present the final prototype details.

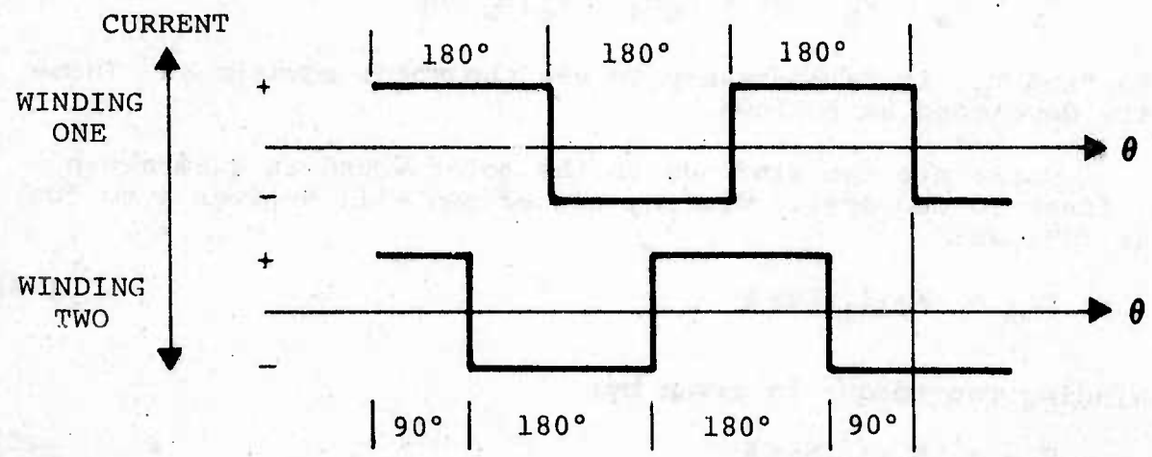

Figure 8. Commutation Procedure

SECTION V

BREADBOARD PROTOTYPE DESIGNS

The basic SSS concept was presented in a previous section of this report. This section shows how the concept was implemented for construction of the breadboard and preliminary prototype designs. The presentation is structured as an assembly process, thereby revealing each design feature and functional detail. As the design unfolds, the motivation for the selection of a particular configuration will be explained. Evolutionary changes which were made during the investigation process are also discussed.

Motor Selection. As indicated in the theoretical analysis section, motor size is dependent on a number of factors. The space envelope limitation coupled with the g detection range and loss torques dictate motor selection. At the start of the program, the general magnitude of loss torques was not known. To ensure the availability of sufficient motor torque to provide a broad g range capability, a motor configuration was selected which permitted optimization of the loss torques. The standard torquer motors have this property in that rotor magnets may be made cylindrical and stators may be molded to provide smooth surfaces, thereby reducing air drag. In addition, this type motor uses an Alnico V magnet, which has a very large B field or flux density. The flux density which can be achieved across the air gap between the rotor and stator relates to the motor torque which can be developed.

Despite the above advantages, torquer motors are limited displacement devices which are not commutated and have only one winding. A one winding motor can be commutated to achieve the normal motor RPM characteristics, but in various starting positions (rotor relative to stator) the motor may not run when power is applied. If it does run, it may run in either direction. Thus it is necessary to have at least two windings. On this basis, Aeroflex Inc., a torquer motor manufacturer, was asked to modify an existing motor to include two coils wound in quadrature. Unidynamics then chose to commutate the motor by photo means, thereby eliminating brush friction to increase the g range capability. With the motor designed in this way, the Coulomb friction (between stator and rotor) was limited to that in the motor ball bearings, and the air drag was minimized.

The next task involved selection of a commutation technique. The most obvious approach, which was attempted,

involved use of a disk attached to the rotor. This disk contained cutouts which shuttered two sets of photo diode/photo transistor pairs at the appropriate angular displacement. The system was constructed and bench tested but did not integrate correctly. This technique also exhibited an unacceptable increase in air drag. The metal cutout disk was then replaced with a transparent plastic disk painted to shutter the light. This significantly reduced drag and improved the integration results slightly. It was discovered that the integration problem was due to insufficient air drag coupling between the rotor and stator. Attempts to accomplish full coupling with this design configuration failed, and other techniques were investigated. The approach finally selected is discussed in the following paragraph.

Figure 9 shows a sketch of the motor rotor. The rotor is a cylindrical Alnico V permanent magnet 0.614 inch in diameter by 0.240 inch thick. The 0.125 inch diameter shaft is installed through the magnet axis as shown, and the end of the rotor shaft is machined in the shape of a wedge. This wedge serves as a shutter between two photo diode/photo transistor pairs to perform motor commutation. Figure 10 shows how commutation is accomplished.

As the rotor and wedge rotate, as shown by the arrow, each photo transistor receives light from its opposing photo diode (LED) during 180 degrees of rotation. During the remaining 180 degrees, the wedge shutters the light. Because the photo pairs are mounted 90 degrees apart, the resulting signals are also offset by 90 degrees. Figure 11 is a plot of each photo transistor output voltage as a function of angular displacement.

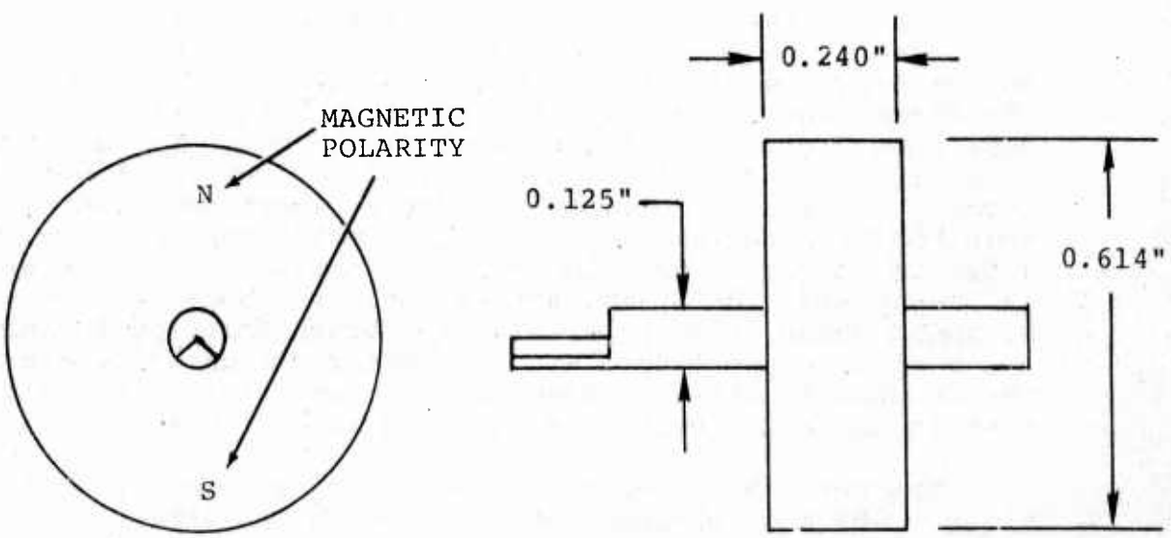

Figure 9. Motor Rotor (Alnico V Magnet)

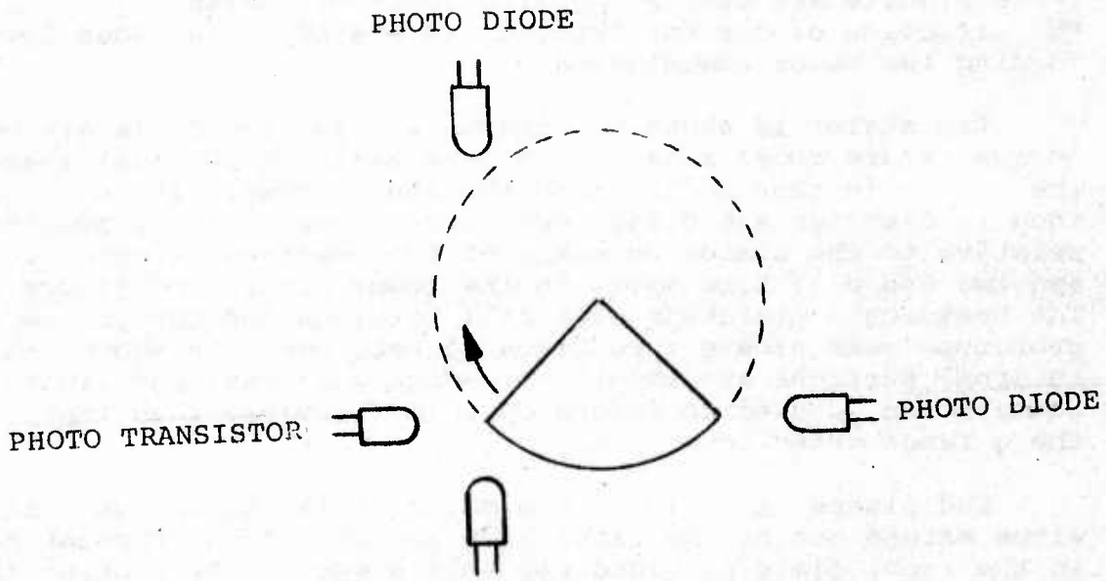

Figure 10. Commutation Shutter

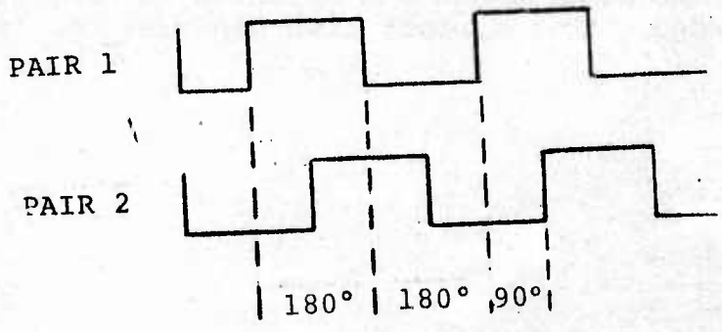

Figure 11. Commutation Signals

These signals are used along with a circuit network to control the direction of current through two stator coils, thus performing the motor commutation.

The stator is shown in Figure 12. Its two coils are wound in quadrature about a laminated core having a toroidal shape. The stator is then molded into the shape shown. It is 0.960 inch in diameter and 0.350 inch thick. The rotor is mounted relative to the stator by means of two bearings. a motor collar and two end plates as shown in the lower portion of Figure 12. The breadboard prototype uses ball bearings and the preliminary prototype uses sleeve type Oilon 80 bearings. As shown, all internal surfaces are smooth to reduce air drag, and light commutation is used to reduce Coulomb friction, thus improving the g range detection.

End plates are held to the motor collar by screws. Stator wires extend out of the right side and are routed through holes in the right plate provided for this purpose. By routing the wires in this manner, they are placed near the centerline of the assembly and can be hard-wired to the commutation drive circuit without introducing drag, except to the extent of a negligible torsional spring effect.

The motor subassembly just described is installed into a motor mount as shown in Figure 13. As shown, the motor is supported relative to the mount by means of two ball bearings to provide the second degree of freedom. Shims are placed between the motor and bearings at each side to provide thrust support. For additional frame support, a heat sink is bolted to the mount in the position shown. This part is used to mount the commutation transistors and provide a path for heat flow.

The commutation wedge extends out the left side. A photo diode/photo transistor support is shown in Figure 14.a. It is mounted to the motor mount and oriented to correctly function with the wedge. This support also captures the left null bearing.

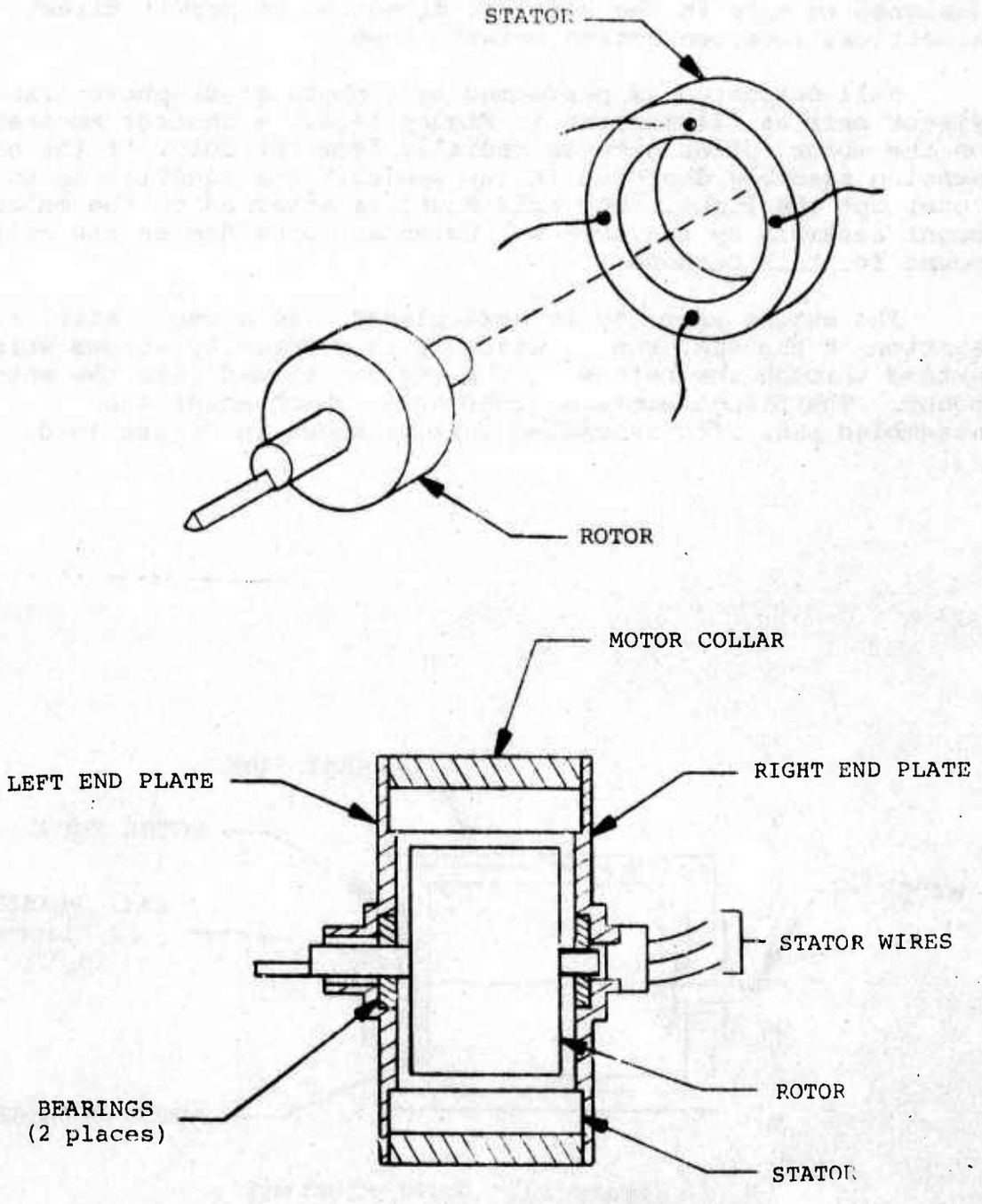

Figure 12. Rotor/Stator Design

Three printed circuit boards are used in the design. These boards are mounted to the heat sink plate by means of bolts and spacers as shown in Figure 14.b. Also shown is a cover. This part is mounted in the same manner as the PC boards but also supports the electrical connector. Connector leads extend through to the next board and are soldered. The boards are designed to mate in the vertical direction to permit direct electrical interconnection between them.

Null detection is performed by a photo diode/photo transistor pair as illustrated in Figure 14.c. A shutter mounted on the motor collar extends radially from the motor to the null sensing assembly depicted in the sketch. Its function is to interrupt the light. The null mount is attached to the motor mount assembly by two screws. Holes are provided in the null mount for this purpose.

The entire assembly is next placed into a can. After insertion in the can, the subassembly is secured by screws which extend through the bottom of the can and thread into the motor mount. The flange contains four holes which mount the assembled SSS. The assembled unit is shown in Figure 14.d.

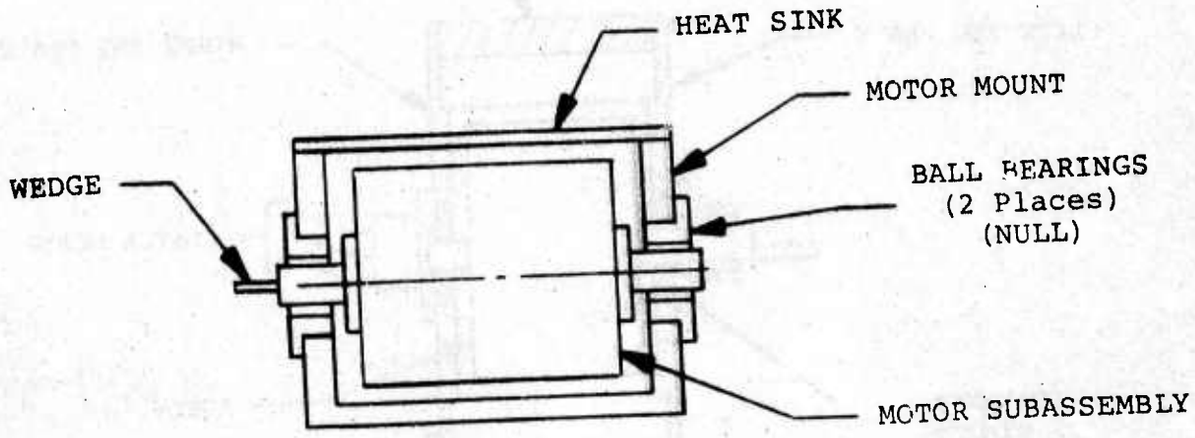

Figure 13. Motor Mounting

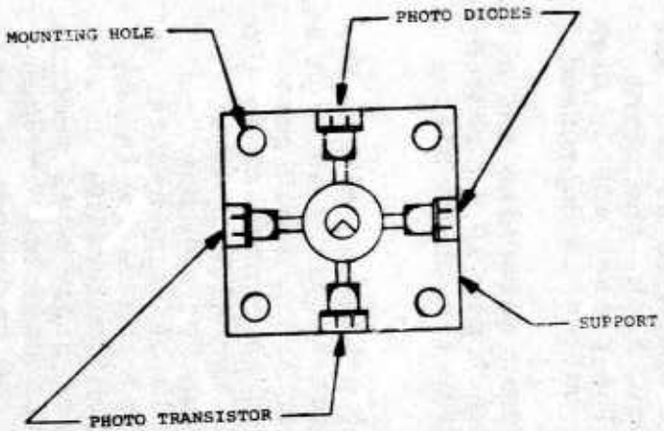

a. *Commutator Mounting*

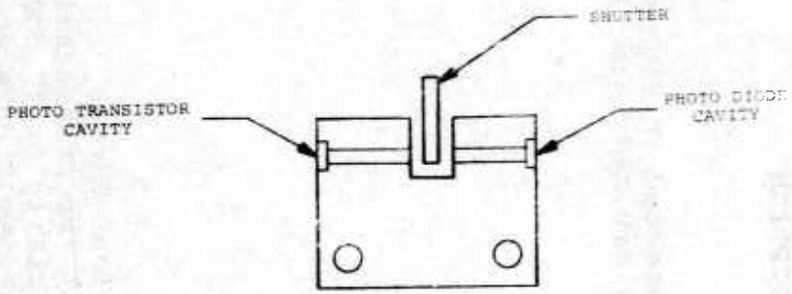

c. *Null Shutter*

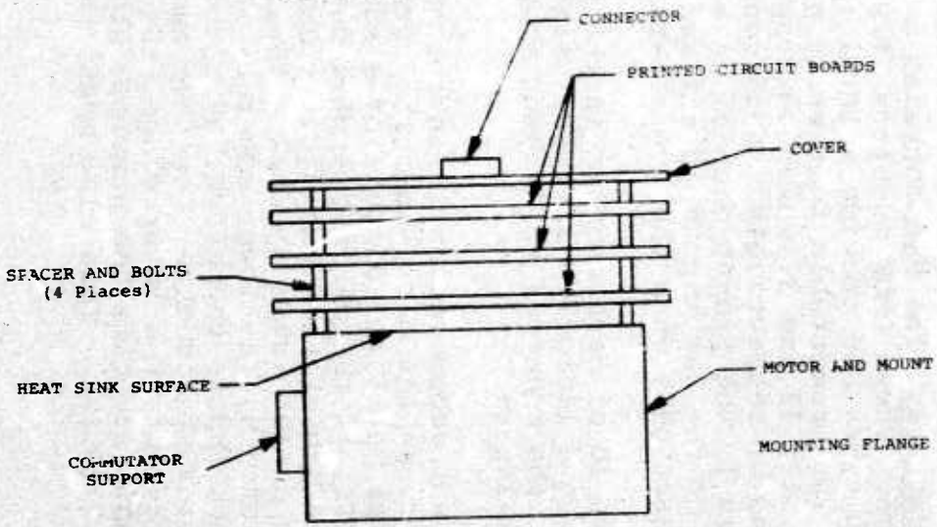

b. *SSS and Electronic Layout*

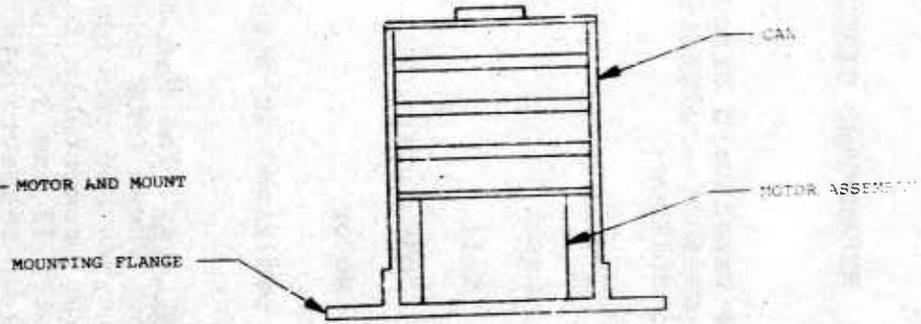

d. *Container*

Figure 14. Breadboard Prototype Physical Layout

SECTION VI

BREADBOARD CIRCUIT FUNCTIONAL DESCRIPTION

The breadboard circuit schematic is presented in Figure 15. For purposes of explanation, this circuit is divided into five parts as follows:

- Counters
- Clock
- Null
- Commutation
- Motor

Each is explained in detail below.

Counters. The SSS contains a total of four decade counters. These CMOS counters (P/N CD4029AE) are presettable up/down types and provide a total range capability of 10,000 feet. The presettable feature is provided by jam inputs at pins 4, 12, 13 and 3, which correspond to the logic numbers 1, 2, 4 and 8, respectively. Each counter operates as follows: When pin 1, the preset enable, is a logic high, the count placed on the jam inputs is entered. The preset enable high is present only when the ICP set-reset button is depressed.

Pin 10 of each counter is the up/down selection and counts down when a logic low is used. Since each pin 10 is routed to ground, the counters will count down from the count placed on the jam inputs.

Count accumulation is inhibited by a high on pin 5, referred to as the carry-in. The carry-out at pin 7 is high at all times until all outputs of a counter are a logic zero. Therefore, if the carry-out of a counter is connected to the carry-in pin of the next digit counter, the higher digit counter cannot advance until a total count of ten has been accumulated by the lower counter. Pin 15 of each counter is the clock input; therefore, by connecting the carry-in and clock pins of a counter together and then connecting them to the carry-out of a lower stage, the upper digit will receive one count each time the previous stage counter has accumulated 10 counts. This also means that the carry-out of the

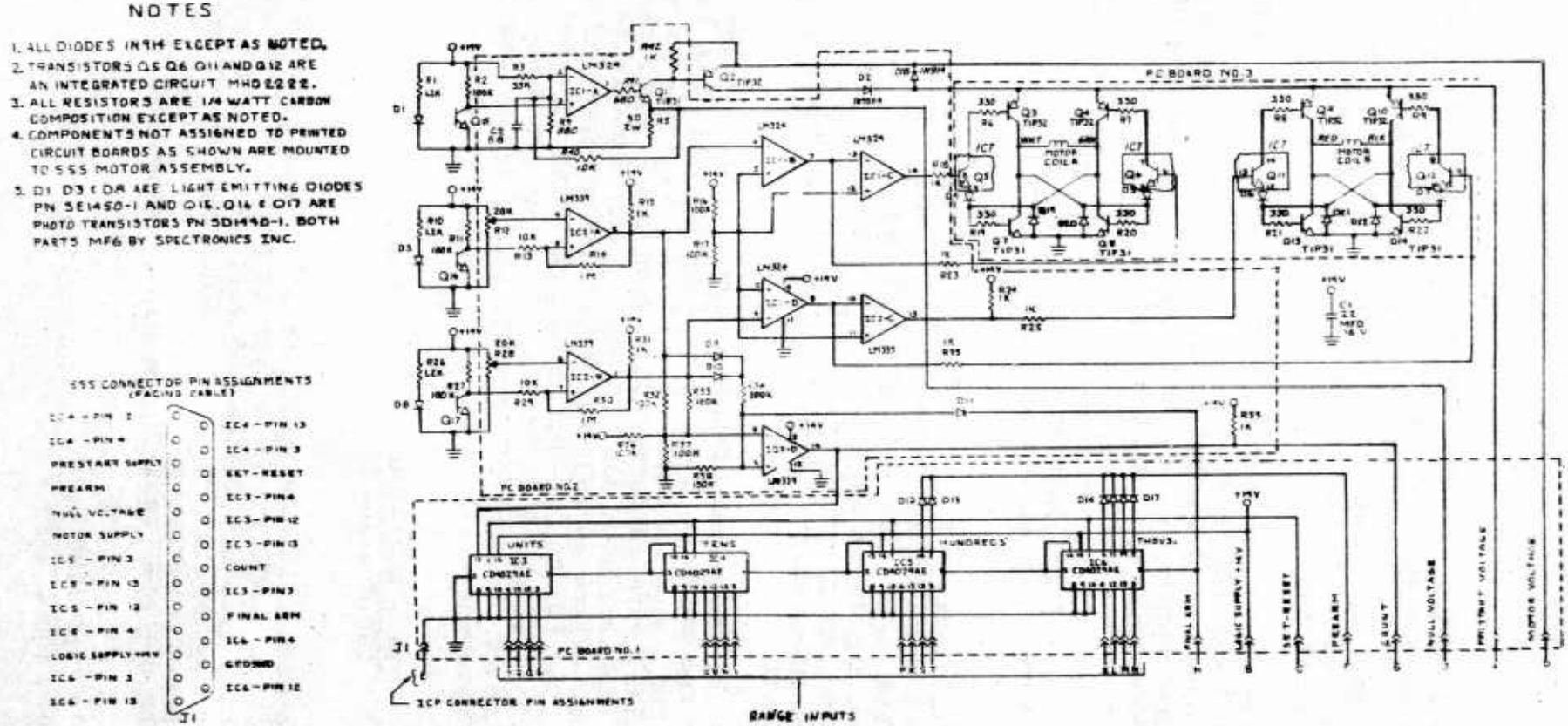

Figure 15. Breadboard Prototype Safe Separatioon Sensor Schematic

last counter in a string will be high at all times until all previous stages have 0 at their outputs. Then when pin 7 of IC6 becomes low, the counters have accumulated the total range placed on the jam inputs at the start of a run. On this basis, only 1 pin is needed to decode the point where the correct range is reached.

To determine the prearm point, which is set at 400 feet from the end of final arm, 6 diodes, D12 through D17, are used. These diodes are connected to the 1, 2, 4, and 8 output pins of the last counter IC6 and the 4 and 8 pins of the previous counter IC5. When any of these outputs is at a logic one, the signal at connector pin F will be a logic one. For pin F to be a logic zero, all diode-connected outputs must be low. This occurs 400 feet from final arm. The only function this performs is to turn on an indicator light on the ICP control panel.

Clock. The clock is formulated by IC2-D which is 1/4 of an LM339, a quad comparator. This circuit functions as an exclusive OR gate to provide a K factor of two counts per revolution. The two inputs to this circuit are commutation outputs derived from pin 1 of IC2-B and pin 2 of IC2-A. These two signals and the IC2-D circuit are shown in Figure 16 to aid in the explanation.

To follow the operation of this circuit, start at the point shown by the arrow on the signal diagram. At this time, pin 1 is high and pin 2 is low. With pin 2 low, resistor R32 is now in parallel with resistor R36. With pin 1 high, resistor R33 is in parallel with R36. Since a logic high is 14 volts, there now exists an equivalent circuit at pin 8 of a voltage divider of two 50,000-ohm resistors being supplied by 14 volts. Therefore, pin 8 is at 7 volts. The pin 9 voltage results from the pin 1 input of 14 volts which is divided by R34 and R38 to provide:

$$V_{\text{Pin 9}} = \frac{(14 - 0.7)\ 150\ \text{K}}{150\ \text{K} + 100\ \text{K}} = 8\ \text{volts} \qquad (29)$$

Since pin 9 is at 8 volts and pin 8 is at 7 volts, pin 14 will be high. The next condition is a high at both pin 1 and pin 2. The pin 9 voltage will not change and will remain at 8 volts. At pin 8 there now exists a voltage divider equivalent circuit of three 100,000-ohm resistors in parallel, or 33,000 ohms in series with 100,000 ohms (R37). The pin 8 voltage will then be:

$$V_{\text{Pin 8}} = \frac{14\ (100\ \text{K})}{100\ \text{K} + 33\ \text{K}} = 10.5\ \text{volts} \qquad (30)$$

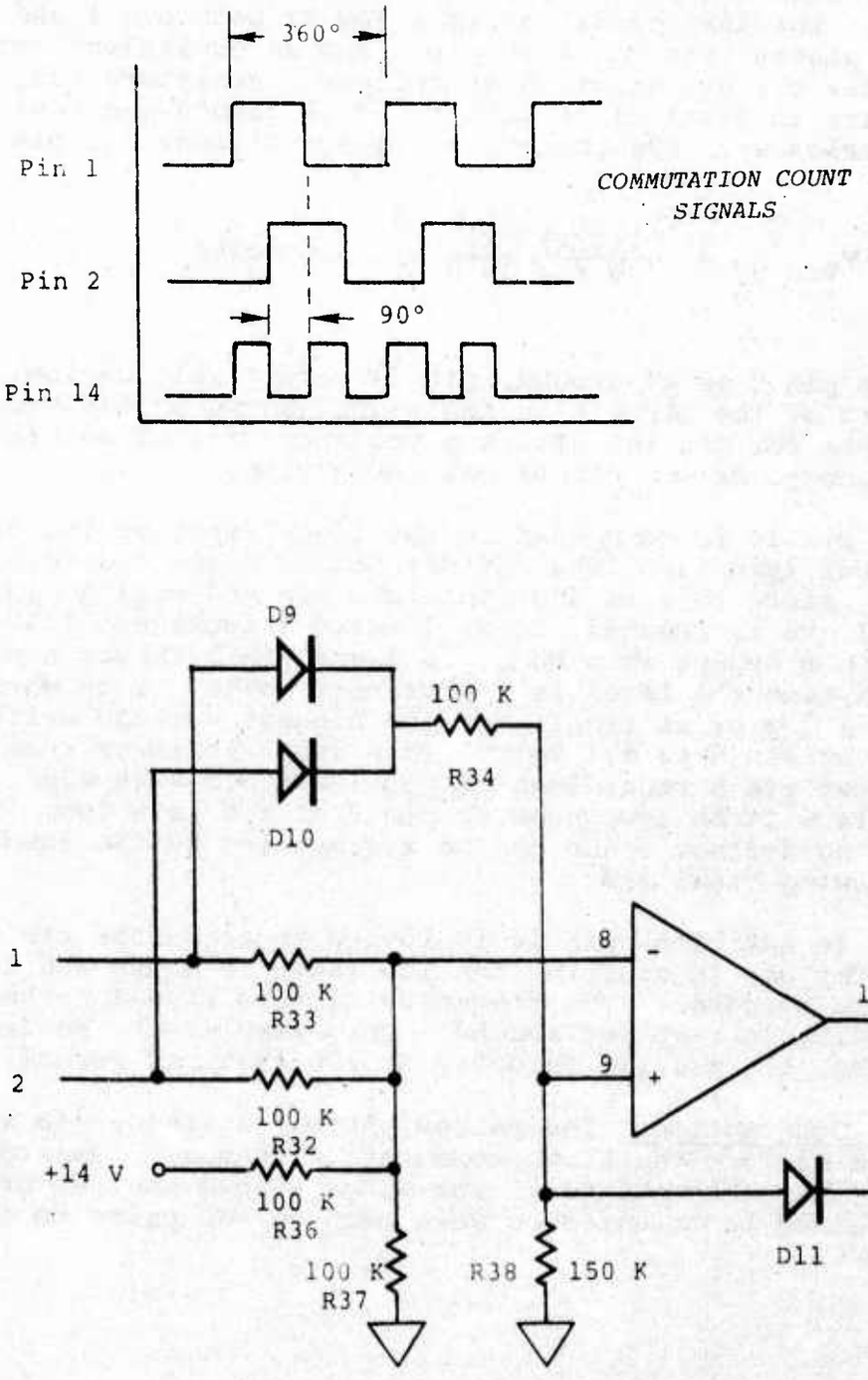

Figure 16. Clock Functions

The pin 8 voltage is now higher than the pin 9 voltage and the pin 14 output will be low. The next condition is a low at pin 1 and a high at pin 2. This is the same condition as for pin 1 high and pin 2 low; therefore, the pin 14 output will be high. The last condition is a low at both pin 1 and pin 2. This places zero volts at pin 9 and an equivalent voltage divider circuit at pin 8 as follows. Resistors R33, R32 and R37 are in parallel to ground. This 33,000-ohm resistance is in series with R36 to form a voltage divider for pin 8 of:

$$V_{\text{Pin 8}} = \frac{(14)(33\ \text{K})}{100\ \text{K} + 33\ \text{K}} = 3.5 \text{ volts} \qquad (31)$$

Since pin 9 is at ground, pin 14 output will be low. The net result of the circuit is the signal shown on the Figure 16 diagram for pin 14. It is a sequence wave of double the motor frequency, or two counts per revolution.

Pin 14 is connected to the clock input of the first counter (pin 15). The divider D11 is connected to pin 7 of IC6. Since this is the final arm pin and will go low when final arm is reached, it will force a permanent 0.7-volt level at pin 9 except when both pin 1 and pin 2 inputs are low, at which time the level is low or zero volts. Then when pin 7 of IC6 is low or at final arm, the highest voltage which can be seen at pin 9 is 0.7 volt. This level is lower than will be seen at pin 8 regardless of pin 1 and pin 2 levels. Therefore, pin 14 will be low whenever pin 7 of IC6 is a low. This means that no further count can be accumulated by the range counters following final arm.

In addition, pin 14 is routed to connector pin G of the ICP for use in clocking the ICP range counters and for monitoring purposes. The frequency of this signal is the missile velocity in feet per second. For example, if the frequency is 200 Hz, the missile velocity is 200 feet per second.

Commutation. The paired photo transistor Q16 and photo diode D3 form the first commutation channel. Pair Q17 and D8 form the other channel. The wedge shaped shutter previously explained is oriented between each of the pairs to form the

basic commutation signals. Since the first pair is oriented 90 degrees from the second pair, the relative signals will be 90 degrees apart. Whenever a pair is shuttered or the light is cut off, the photo transistor collectors will be high. Uninterrupted light will result in a low at the collectors. Therefore, by alternately interrupting and opening the light path between the photo diode and photo transistor, the continuous signals seen at the collectors will be as shown in Figure 17:

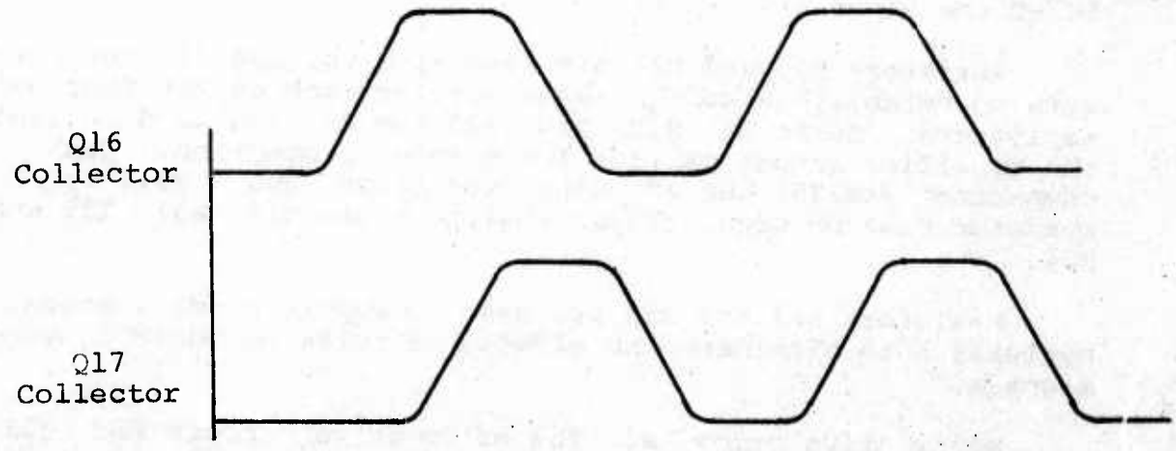

Figure 17. Photo Commutator Signals

These signals are fed to the positive inputs of comparators IC2-A and IC2-B, which are used to square up the commutation signals. The trigger points are adjustable by means of variable resistors R12 and R28, which serve as adjustable voltage dividers. It is necessary to formulate a square wave

for use as the commutation signal for most efficient motor performance. That is, the direction of current through a motor coil should exist for 180 degrees of rotation and then reverse for the next 180 degrees. The variable resistors R12 and R28 are used for this purpose, to set the square wave duty cycle at 50 percent or 180 degrees for each condition.

In addition to supplying the count signal, the commutation waveforms are fed to IC1-B and IC1-D, which serve as buffer amplifiers. The output of IC1-B is fed through R23 to the base of Q6 and to the inverting input of IC1-C. The net result of this connection is that when Q6 is on, its counterpart Q5 is off. Similarly, with Q6 off, Q5 will be on. As will be explained later, this procedure sets the current through coil A in one direction for 180 degrees and then in the other direction for the next 180 degrees. The same procedure is used for the other coil, with IC1-D driving one side (Q12) and IC2-C the other side (Q11).

Resistors R16 and R17 are used as a voltage divider network to establish a common reference for each of the four buffer amplifiers. Resistors R18, R23, R25 and R35 are used to limit the amplifier output current for burnout protection. Each comparator (LM339) has an output collector, and a pull-up resistor must be used. These resistors are R15, R31, R39 and R24.

Resistors R14 and R30 are used to supply a small amount of hysteresis to eliminate the effects of noise on their input signals.

Motor Drive Circuits. The motor drive circuit for coil A consists of transistors Q3, Q4, Q5, Q6, Q7, Q8 and associated resistors. As stated earlier, when Q5 is on, Q6 is off. With Q5 on, base current flows in Q3, turning it on. The collector of Q3 is fed to the base of Q8 via R20 to turn it on. Current can now flow through coil A from the collector of Q3 through the coil and then to ground through the collector of Q8. The current is reversed by shutting off Q5 and turning on Q6. With Q6 on, base current flows in Q4, turning it on. Its collector turns on Q7 via R19, and a current path now exists for the coil from the collector of Q4 through the coil to the collector of Q7 and then to ground.

Diodes D4 and D5 protect Q5 and Q6 from excessive reverse biasing. Resistors R6 and R7 set the base current levels for Q3 and Q4.

Coil B is operated in the same way as coil A except the phase is offset by 90 degrees. Diodes D19 through D22 are used to reduce the effects of back emf on ground. The coil back emf is sometimes negative, which can result in ground noise, but this noise is held to a one-diode drop by the means shown.

Null Circuits. The null circuits consist of photo diode D1, photo transistor Q15, operational amplifier IC1-A, transistors Q1 and Q2, and related circuitry. The collector of the photo transistor is connected to the positive input of IC1-A, and the shutter operates to shut off greater amounts of light with increased g's. Therefore, the input to IC1-A increases with an increase in g level. The resulting output of IC1-A at pin 1 is an increasing voltage with increased g. Pin 1 output drives Q1, which in turn supplies base current for Q2. Transistor Q1 serves as a voltage controlled current sink, since the emitter is fed back to the negative input of the amplifier. Therefore, the total gain of IC1 and Q1 is approximately one.

Since it is not possible to bring the Q15 collector to ground when it is completely turned on, some offset is necessary for the amplifier negative input. This is accomplished by R3 and R4. In other words, when the null shutter is open or the null mass is high, all power should be shut off to the motor. Without the offset connection, some power would always be supplied regardless of null position. Because it is necessary to use the offset connection, diode D18 is also required since the 50-ohm resistor would swamp out the offset voltage in the feedback loop.

Capacitor C2 is the key to accomplishing the tracking null design since without this capacitor the null would oscillate. It will also oscillate if the gain is increased by placing resistance in series with D18. The capacitor serves as a unidirectional null mass velocity control. For example, suppose the system is in equilibrium, or tracking. Then the voltage at pin 2 will be only a few microvolts less than the voltage at pin 3. For purposes of this program, the positive input voltage and the feedback or negative input voltage to the operational amplifier are equal. Therefore, capacitor C2 is charged to the null or input voltage. This capacitor can charge very rapidly from the emitter of Q1 through diode D18, but can discharge slowly through R4. On this basis, suppose the null suddenly has too much motor torque being applied and the shutter starts up. The result of this action is a reduction in voltage at pin 3, the positive input. Since the capacitor cannot discharge as fast as the charge at pin 3, the negative input voltage will be larger than the positive input. Therefore, the amplifier output at pin 1 will go to ground, shutting off Q1 and Q2. This means that the null does

not have to travel very far to remove sufficient motor current to correct for a need of torque reduction. The reverse is also true. For a demand for greater torque, a slight increase in Q15 collector voltage will result in an increase in the Q1 current; however, this voltage is fed back immediately to charge C2. The net effect of the circuitry is a quick responding null voltage with a slight change in null position. Transistor Q1 controls the Q2 base current which in turn controls the current to the motor.

Diode D2 is used to keep the prestart voltage off the Q2 collector. The prestart voltage, which is applied to the motor bus via connector pin A, is used to establish an initial motor RPM for testing purposes. The RPM is adjusted by varying the prestart voltage at the ICP. Normal motor voltage is applied at pin D, which is connected to the Q2 emitter. Capacitor C1 filters the logic supply, +14 volts. When the motor coils are switched, large inductive spikes are created. To control this the filter capacitor is used.

SECTION VII

INITIAL BREADBOARD PROTOTYPE TESTING

The breadboard prototype unit was subjected to centrifuge testing and to environmental testing consisting of exposure to high and low temperature plus sine and random vibration. Both evaluations are described below.

Centrifuge Tests. The centrifuge tests were conducted first and were witnessed by the sponsor. During the setup procedure for these tests, an attempt was made to set the Instrument Control Package (ICP) outside the centrifuge and route signals through the centrifuge slip rings. To collect operational data (null and RPM information), a visicorder was used. The remaining range and time information were recorded on the ICP.

Two problem areas were found to exist. First, the cabling distance between the SSS and ICP was too great, resulting in distortion of signal information that prevented reliable ICP processing. Second, sufficient drive power was not available from the ICP to drive the visicorder directly. To solve these problems, the ICP was mounted inside the centrifuge as close to the axis of rotation as possible, and signals used for driving the visicorder were amplified by external electronics. The ICP was modified to accept a remote control box to accomplish the functions of starting, stopping, and resetting. A TV camera was mounted in front of the ICP to monitor the range and time data.

The SSS was mounted at a distance of 32 inches from the centrifuge axis of rotation. Because there is some difficulty in setting and maintaining the exact centrifuge RPM, the actual RPM was recorded immediately prior to the run, and the actual g-level imposed on the SSS was calculated with the following relationship:

$$a = R\omega^2 \tag{32}$$

Where:

a = acceleration

R = radius

ω = angular velocity

Appropriate substitution of units and rearranging yields:

$$g = 9.0818 \times 10^{-4} (Z)^2 \quad (33)$$

or:

$$Z = 33.1829\ g^{1/2} \quad (34)$$

Where:

Z = centrifuge angular velocity in revolutions per minute.

Runs were made at 6, 11 and 17g levels and the data collected is presented in Tables 1 through 3 which are set up as follows:

- Column 1 - The run number.
- Column 2 - The centrifuge RPM and g level using the relationship above.
- Column 3 - The final arm distance set on the ICP.
- Column 4 - The recorded run time to the distance selected.
- Column 5 - The calculated rate of acceleration based on the selected run distance and recorded time.
- Column 6 - The actual distance, calculated from the g-level and run time.
- Column 7 - The percentage distance error.

Two sources of error exist in the measurement apparatus of the system: (1) the centrifuge will vary during a run by an estimated 0.2 percent, and (2) the counting mechanism is accurate to within ± 1 count or ± 1 foot. At 6g (400-foot run distance) these factors amount to a total error of 0.45 percent. (The error due to 1 foot in 400 is 0.25 percent.) At 11g (run distance of 140 feet) the error is 0.71 percent plus the centrifuge error of 0.2 percent or a total possible error of 0.91 percent in range. At 17g (run distance of 100 feet) the total error is 1.2 percent.

TABLE 1. RUN SERIES NO. 1 - 6g

Run	RPM/g	Distance (feet)	Time (sec)	Acceleration (g)	Actual Distance	Percent Error
1	81.13/5.977	400	2.048	5.923	403.6	0.9
2	81.11/5.975	400	2.047	5.929	403.1	0.8
3	81.07/5.969	400	2.017	6.107	391.0	2.25
4	81.11/5.975	400	2.036	5.993	398.8	0.31
5	81.08/5.970	400	2.055	5.883	405.9	1.48
6	81.13/5.977	400	2.043	5.952	401.6	0.40
7	81.10/5.973	400	2.042	5.958	401.0	0.25
8	81.10/5.973	400	2.031	6.023	396.7	0.83
9	81.22/5.991	300	1.739	6.162	291.7	2.77
10	81.13/5.977	300	1.760	6.015	298.1	0.64
11	81.12/5.976	300	1.777	5.901	303.8	1.27

TABLE 2. RUN SERIES NO. 2 - 11g

Run	RPM/g	Distance (feet)	Time (sec)	Acceleration (g)	Actual Distance	Percent Error
12	109.84/10.957	140	0.897	10.807	141.9	1.35
13.a	109.84/10.957	140	0.881	11.203	136.9	2.21
13.b	109.84/10.957	140	0.883	11.153	137.5	1.78
13.c	109.84/10.957	140	0.880	11.229	136.6	2.43
13.d	109.84/10.957	140	0.882	11.178	137.2	2.00
13.e	109.84/10.957	140	0.881	11.203	136.9	2.21
13.f	109.84/10.957	140	0.880	11.229	136.6	2.43
13.g	109.84/10.957	140	0.883	11.153	137.5	1.78
13.h	109.84/10.957	140	0.881	11.203	136.9	2.21
13.i	109.84/10.957	140	0.884	11.127	137.9	1.50
13.j	109.84/10.957	140	0.881	11.203	136.9	2.21
14	109.83/10.958	108	0.781	10.998	107.6	0.39
15	109.89/10.967	149	0.928	10.746	152.1	2.05
16	109.87/10.963	150	0.934	10.680	154.0	2.67

TABLE 3. RUN SERIES NO. 3 - 17g

Run	RPM/g	Distance (feet)	Time (sec)	Acceleration (g)	Actual Distance	Percent Error
17	136.79/16.993	97	0.601	16.680	98.8	1.86
18	136.80/16.996	100	0.602	17.139	99.2	0.80

In the 6g series. the worst range error was 2.77 percent, and the bulk of the runs were within 1 percent. The 11g runs, however, presented a different picture. In runs 13.a. through 13.j., no effort was made to adjust the null caging mechanism to the correct starting position. Consequently, the null struck the PC boards several times at the beginning of each of these runs. Whenever the system is not caged correctly, the null mass may be down, which opens the shutter to permit excessive motor torque at the start. This accelerates the null upward to a large displacement. Since the PC boards are mounted very close to the sides of the system, such deflections will result in the null impacts.

When the null strikes the PC board, it bounces back with sufficient speed again to proceed deep into the open shutter condition, resulting in another instance of excessive acceleration. This process is repeated several times until correct stability is established. The net result is that the system runs too fast and provides a short run time.

The puzzling factor for runs 13.a. through j. is the consistent performance. Since the number of impacts was not the same for each run, it is expected that the times would have been different from run to run. However, as the data show, the maximum deviation was 4 milliseconds. Despite the impacts, the maximum error was 2.43 percent.

Runs 12, 14, 15 and 16 may be considered as representative of a correctly caged system, and the data provided from these tests is within 2.67 percent.

At 17g only two runs were made, with the worst error being 1.86 percent. The problem here was that the caging mechanism would not maintain cage under the high levels of acceleration. To correct this problem, it was necessary to mount the caging mechanism at 90 degrees to the axis of acceleration. This change is reflected in the design tested later.

Environmental Testing. The breadboard SSS was subjected to high temperature (165° F), low temperature (-65° F), sine vibration and random vibration. Results are shown in Tables 4 through 7. As the data show, performance in the high temperature and random vibration series was adequate; however, large errors were seen in low temperature and sine vibration testing.

Low Temperature Tests. Each of these was conducted at 1g. Since the system is self-compensating to a large degree within the motor, the most probable source of error is in null effects. These effects usually are manifested as increased

TABLE 4. HIGH TEMPERATURE TESTS

Run	Distance (feet)	Time (sec)	Acceleration (ft/sec^2)	Actual Range	Percent Error
1	1000	7.839	32.55	989.3	1.07
2	1000	7.918	31.90	1009.4	0.94
3	1300	9.133	31.17	1342.9	3.30
4	1300	8.963	32.36	1293.4	0.51
5	1300	9.017	31.98	1309.0	0.69
6	1300	9.056	31.70	1320.4	1.57
7	1300	8.996	32.13	1302.9	0.22
8	1300	9.102	31.38	1333.8	2.60
9	1300	9.139	31.13	1344.7	3.44
10	1300	9.064	31.65	1322.7	1.75

TABLE 5. LOW TEMPERATURE TESTS

Run	Distance (feet)	Time (sec)	Acceleration (ft/sec^2)	Actual Range	Percent Error
1	1000	8.310	28.96	1111.8	11.18
2	1000	8.072	30.70	1049.0	4.90
3	1300	9.442	29.16	1435.3	10.41
4	1300	9.324	29.91	1399.7	7.67
5	1300	9.177	30.87	1355.9	4.30
6	1300	9.226	30.19	1370.4	5.42
7	1300	9.209	30.66	1365.4	5.03
8	1300	9.416	29.33	1427.4	9.80
9	1300	9.307	30.02	1394.6	7.28
10	1300	9.367	29.63	1412.6	8.66

TABLE 6. SINE VIBRATION

Run	Range (ft)	Frequency (Hz)	Time (sec)	Acceleration (ft/sec^2)	Actual Range (ft)	Percent Error
1	1000	1019	7.821	32.70	984.8	1.52
2	1300	1019	9.323	29.91	1399.4	7.65
3	1300	1251	9.301	30.05	1392.8	7.14
4	1300	1793	9.336	29.83	1403.3	7.95

TABLE 7. RANDOM VIBRATION

Run	Range (ft)	Frequency (Hz)	Time (sec)	Acceleration (ft/sec^2)	Actual Range (ft)	Percent Error
5	1300	3.8 g RMS	9.013	32.01	1307.9	0.61
6	1300	3.8 g RMS	9.042	31.80	1316.3	1.25
7	1300	3.8 g RMS	8.823	33.40	1253.3	3.59
8	1300	3.8 g RMS	8.942	32.52	1287.3	0.98
9	1300	3.8 g RMS	9.058	31.69	1321.0	1.61
10	1300	5.0 g RMS	9.026	31.91	1311.6	0.89
11	1300	5.0 g RMS	8.862	33.11	1264.4	2.74

friction due to interference fit changes or unwanted materials in the bearings. Interference fit changes could occur in the low temperature tests, since the bearings were exposed to the air for long periods during assembly and testing. Accumulation of foreign materials is the result of non-clean procedures. At low temperature the viscosity of these materials will change and thus cause the frictional changes.

In the cold tests, attempts were made to eliminate the effects of moisture by installing the assembly into a plastic bag to allow a continuous flow of dry nitrogen across the SSS. This was done during the 3-hour soaking and during testing. However, it may not have been entirely successful. When there is increased friction in the null, the result is long run times or less acceleration. The preliminary prototype design facilitated bearing cleaning and replacement and thus eliminated the problem.

Vibration Testing. The sine vibration tests were conducted by first running a resonance sweep, then running the SSS at the resonance frequencies. Results are shown in Figure 18. It should be noted that the test frequency was slightly different than the sweep resonance. Since it was found during the runs that the resonance points changed slightly, the peak point was set and the system run. It is believed that such resonances are set by the bearings.

Random vibration results were within the normal limits of error for the device. It was therefore concluded that random effects were minimal.

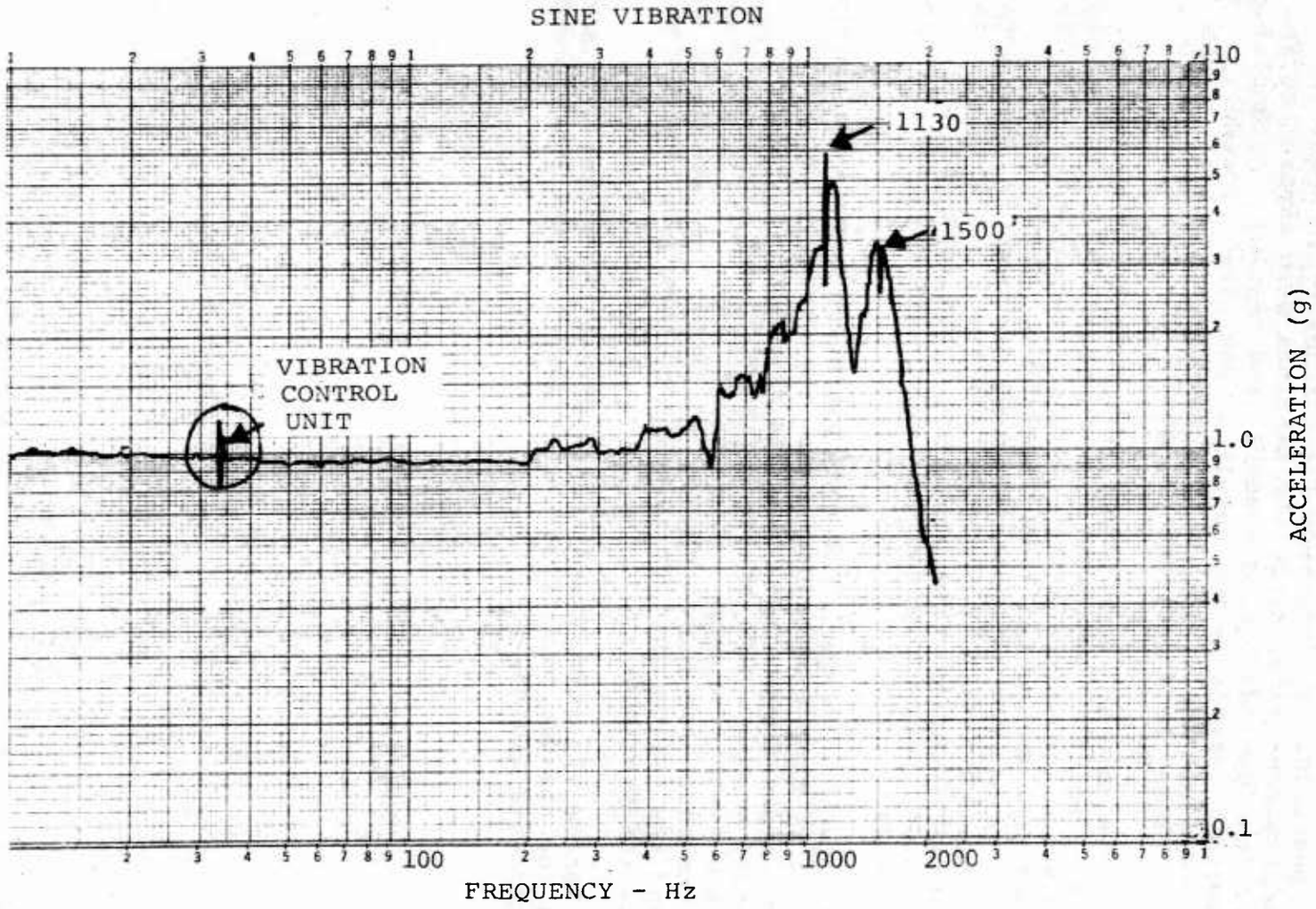

Figure 18. Vibration Test Raw Data (Search)

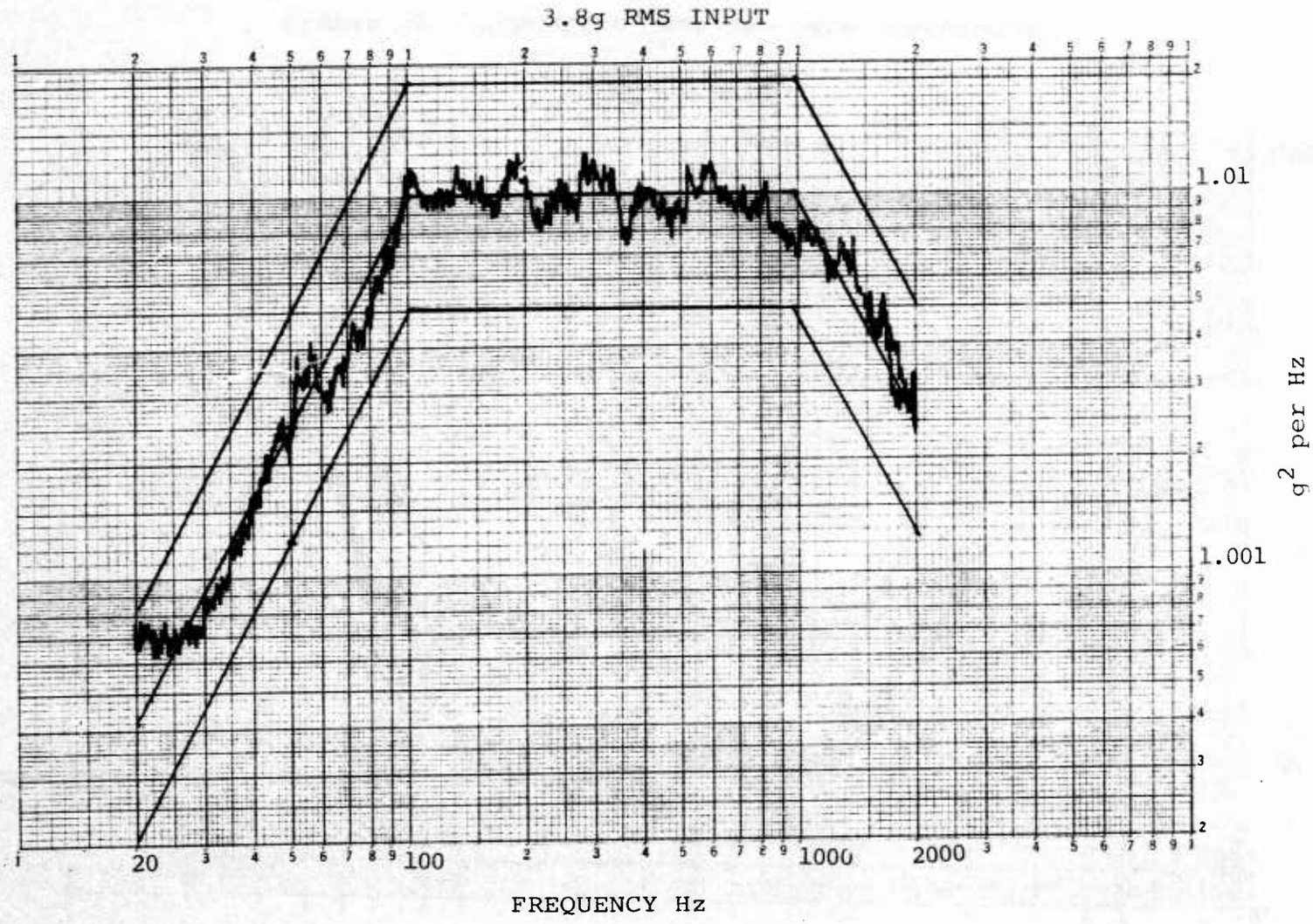

Figure 18. Vibration Test Raw Data (Continued)

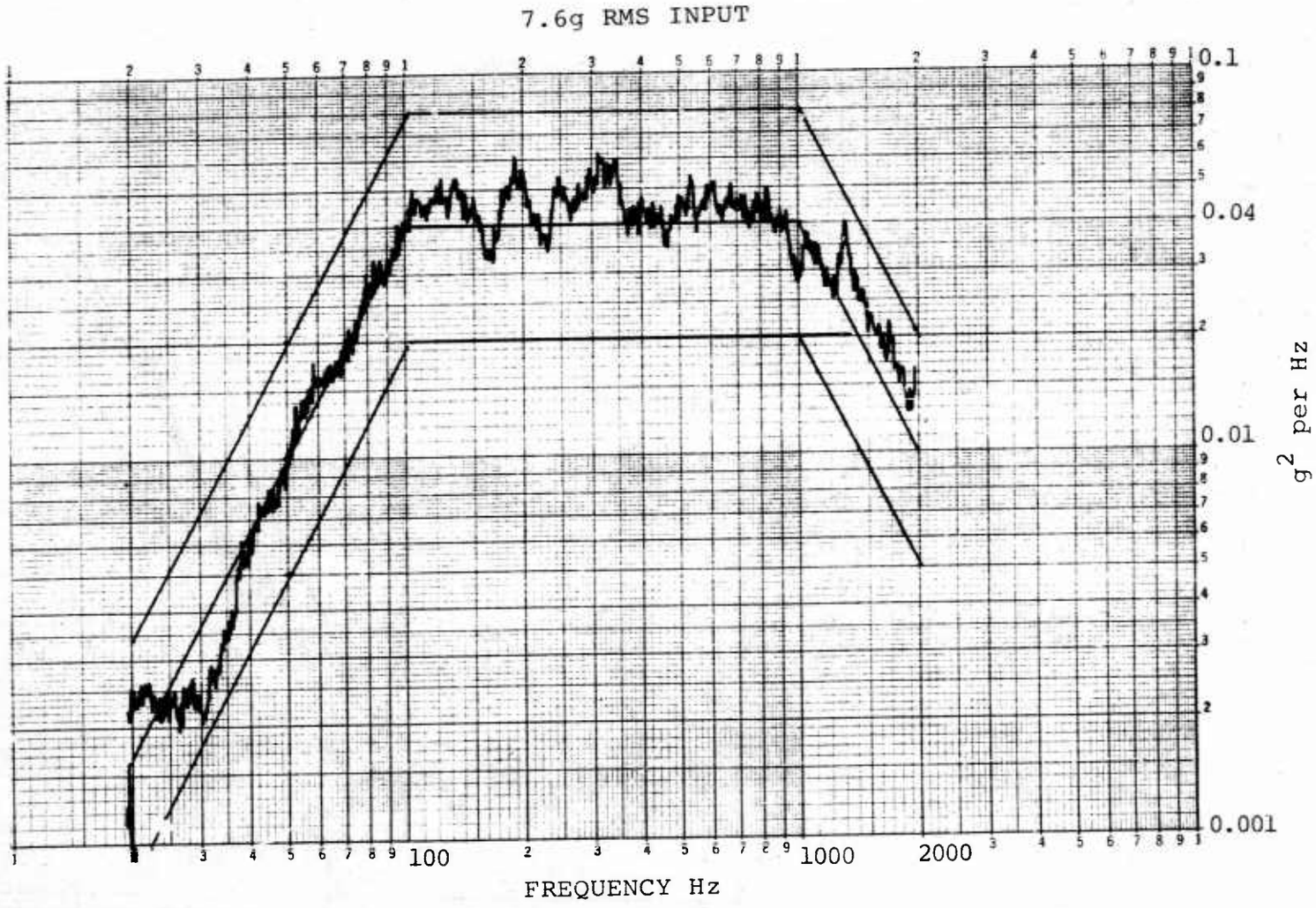

Figure 18. Vibration Test Raw Data (Concluded)

SECTION VIII

FINAL BREADBOARD PROTOTYPE TESTING

This section discusses centrifuge tests conducted on the breadboard prototype delivered to Eglin. Numerous runs were made at each of 6, 11, 17 and 27g levels. The data along with an error analysis is provided below.

The first series of 20 runs were accomplished with the centrifuge set at 6g. No effort was made to calibrate the SSS beyond that accomplished at one g; therefore, the calibration will be in error with the null mass slightly on the heavy side. For the 6g runs, the count error amounts to about 3 milliseconds in run-out time and therefore is not considered in the percent error calculations. As shown in Table 8, the error range is -2.54 to +2.54 percent. The error was calculated on the basis of a median g of 6.11.

For the 11g runs, the median selected was 11.397g, and the error range was -15.81 to +2.18 percent. It should be noted that at the end of the positive g testing for all levels, attempts to run the device at zero or negative g failed because of difficulty in setting the initial run velocity. The SSS was then run at one g. It was found that the internal motor bearings were sticking and/or freezing up periodically, particularly as the system became heated. These bearings were dry, i.e., no lubrication was used.

It is interesting to note from Table 9 that if the four runs noted with an asterisk are eliminated and the one count error corrected, the calculated range occurs in 15 of the 19 runs considered and the error range (based on $\pm$68 feet) is 2.94 percent or considered on a median basis $\pm$1.47 percent. Since 68 feet is the bulk range, sticking bearings can account for the 66 and 67 foot runs of which there are four.

For 17g a similar occurrence is seen. Three of the four runs noted with an asterisk are at low range, again indicating sticking bearings. The 117-foot run (No. 9) is not understood. The range of error here is -10.24 percent to 2.38 percent. Again eliminating the four runs noted with an asterisk and correcting for one count measurement error, the error range is 2.88 percent based on 104 feet. If a median is used, $\pm$1.44 is seen. Thirteen of the 21 runs provided a range of 104 feet.

TABLE 8. SUMMARY OF 6g (6.11g) RUNS

Run	Range (feet)	Time (seconds)	g	Percent Error
1	1300	3.682	5.956	2.54
2	1300	3.651	6.058	0.87
3	1300	3.636	6.107	0.07
4	1300	3.614	6.182	1.15
5	1300	3.629	6.131	0.33
6	1300	3.654	6.048	1.03
7	1300	3.648	6.067	0.72
8	1300	3.620	6.162	0.83
9	1300	3.643	6.084	0.44
10	1300	3.651	6.058	0.87
11	1300	3.644	6.081	0.49
12	1300	3.611	6.192	1.31
13	1300	3.596	6.244	2.13
14	1300	3.589	6.269	2.52
15	1300	3.620	6.162	0.83
16	1300	3.622	6.155	0.71
17	1300	3.611	6.192	1.31
18	1300	3.591	6.262	2.41
19	1300	3.588	6.270	2.54
20	1300	3.612	6.189	1.26

TABLE 9. SUMMARY OF 11g (11.397g) RUNS

Run	Range (feet)	Time (seconds)	g	Percent Error	Calculated Range	Percent Error
1	66	0.602	11.312	-0.77	67	1.47
2	68		11.654	+2.18	68	0.00
3	68		11.654	+2.18	68	0.00
4	65		11.140	-2.28	66	2.94
5	68		11.654	+2.18	68	0.00
6	68		11.654	+2.18	68	0.00
7	67		11.483	+0.72	68	0.00
8	68		11.654	+2.18	68	0.00
9	65		11.140	-2.28	66	2.94
10	67		11.483	+0.72	68	0.00
11	57*		9.769	-14.31		
12	68		11.654	+2.18	68	0.00
13	68		11.654	+2.18	68	0.00
14	65		11.140	-2.28	66	2.94
15	67		11.483	+0.72	68	0.00
16	68		11.654	+2.18	68	0.00
17	67		11.483	+0.72	68	0.00
18	67		11.483	+0.72	68	0.00
19	59*		10.111	-11.31		
20	56*		9.598	-15.81		
21	68		11.483	+0.72	68	0.00
22	68		11.483	+0.72	68	0.00
23	56*	0.602	9.598	-15.81		

*Erroneous data, see discussion.

At 27g, the results are consistent with previous data. This time the correct range is 71 feet, and the corrected calculation provides an error of 4.23 percent or ±2.17 percent if a median is used. In this instance, 15 of the 21 runs considered resulted in 71 feet. It is interesting to note that heating played a large role in the results. The runs were all made in rapid succession to reduce the effects of centrifuge RPM drift. Therefore, the SSS became more heated with each run. Between g levels, cooling occurred and the effects can be seen. For the 11, 17 and 27g runs (Tables 10 and 11) erratic data began to appear at run 11, run 9 and run 12, respectively. With sticking bearings, it is possible to record both fast and slow runs. For example, if the bearing sticks to the extent where the null must drop to a point of very high torque before breaking loose, then the rotor does break loose and a sudden drop in friction occurs. The null will then accelerate rapidly and strike the PC board mounts above the motor. It has been found that fast runs occur when the null impacts a stop in its off cycle. The reverse is true for the lower stop.

If the friction level is excessive but not sufficient to cause null impact with the upper or lower stops, the run-out range will be small for a fixed time run. The data show that most of the poor runs fit into the short range category. It should be indicated that this device, when first assembled, was running at one g to 1000 feet within ±20 milliseconds, or better than 0.5 percent. Several hundred runs were made on the device at one g before making the centrifuge tests. Since the bearings were dry and brass shims were used, it is likely that the bearings were contaminated. Following the centrifuge tests and before shipping the device to Eglin, these bearings were changed and lubricated devices were used, again with brass shims. Microscopic examination of the removed bearings confirmed the contamination and scouring of races. Aside from normal value, this data is also important from the standpoint of determining performance effects when malfunctioning bearings are used.

Analysis of the data also indicates that the starting position of the null probably played an important role in corrected performance. The caging mechanism is now mounted 90 degrees to the detection axis; therefore, the acceleration level does not affect the solenoid directly. However, with a torque on the null mass, the solenoid plunger is forced inward against its spring. Because there is friction within the solenoid, the starting null point will vary from run to run. Since consistency is the prime consideration, the null starting point is important. In a tracking or oscillating null system, the null should be started against the lower stop or at the 0g point. In subsequent testing, the null will be started at a

TABLE 10. SUMMARY OF 17g (17.685g) RUNS

Run	Range (feet)	Time (seconds)	g	Percent Error	Calculated Range	Percent Error
1	104	0.6	17.943	1.44	104	0.00
2	99*		17.080	3.41		
3	104		17.943	1.44	104	0.00
4	101		17.426	1.46	102	1.92
5	105		18.116	2.38	105	0.95
6	104		17.943	1.44	104	0.00
7	104		17.943	1.44	104	0.00
8	104		17.943	1.44	104	0.00
9	117*		20.186	12.39		
10	104		17.943	1.44	104	0.00
11	100		17.253	2.43	101	2.88
12	104		17.598	0.49	103	0.96
13	102		17.598	0.49	103	0.96
14	103		17.771	0.48	102	1.92
15	104		17.943	1.44	103	0.96
16	92*		15.873	10.24		
17	104		17.943	1.44	104	0.00
18	103		17.771	0.48	103	0.96
19	104		17.943	1.44	104	0.00
20	104		17.943	1.44	104	0.00
21	103		17.771	0.48	104	0.00
22	103		17.771	0.48	104	0.00
23	98*		16.908	4.39		
24	103		17.771	0.48	104	0.00
25	103	0.6	17.771	0.48	104	0.00

*Erroneous data, see discussion.

TABLE 11. SUMMARY OF 27g (26.980g) RUNS

Run	Range (feet)	Time (seconds)	g	Percent Error	Calculated Range	Percent Error
1	70	0.4	27.174	0.71	71	0.00
2	71		27.562	2.11	71	0.00
3	71		27.562	2.11	71	0.00
4	70		27.174	0.71	71	0.00
5	71		27.562	2.11	71	0.00
6	69		26.786	0.72	70	1.41
7	71		27.124	2.11	71	0.00
8	68		26.398	2.15	69	2.82
9	71		27.562	2.11	71	0.00
10	70		27.174	0.71	71	0.00
11	69		26.786	0.72	70	1.41
12	81*		31.444	14.20		
13	66*		25.621	5.04		
14	71		27.562	2.11	71	0.00
15	70		27.174	0.71	71	0.00
16	70		27.174	0.71	71	0.00
17	67		26.009	3.50	68	4.23
18	71		27.562	2.11	71	0.00
19	70		27.174	0.71	71	0.00
20	70		27.174	0.71	71	0.00
21	69		26.786	0.72	70	1.41
22	70		27.174	2.11	71	0.00
23	68	0.4	26.398	2.15	69	2.82

*Identified null impact with printed circuit board. Erroneous data, see discussion.

given position to determine the effects of starting variation. Improvements in null tracking will permit starting to be accomplished at the lower stop without excessive upper excursions. If correct damping is used, the null should travel to the tracking position quickly without excessive overshooting.

SECTION IX

ANALYSIS OF PROGRAM REQUIREMENTS - PART II

The second portion of this program involved fabrication and testing of a preliminary prototype and design, fabrication and testing of a final prototype. Five of the preliminary prototype designs were to be constructed, and one was to be temperature, vibration and centrifuge tested. This design is the same as the breadboard prototype described in the previous sections of this report.

Before designing the final prototype, a motor evaluation was conducted to ascertain if improvements in performance and cost could be made. Following this evaluation, five final prototypes were to be constructed with one unit subjected to temperature, vibration and centrifuge testing. After the above activities, each of the five preliminary prototypes and five final prototypes were to be calibrated and shipped to the sponsor. A failure mode and effects analysis was also conducted and is provided in Section XV.

SECTION X

MOTOR EVALUATION

Before formulating a design for the final prototype SSS, a motor evaluation was conducted. The purpose of this effort was to determine if significant improvements in the performance and cost of the SSS could be achieved, and results of the evaluation were to be used in the final prototype design. This section includes a discussion of the motor study and a presentation of the final prototype design approach.

During the breadboard and preliminary prototype design efforts, two parameters were found which contribute to range error. These were frictional torque, T_c, between the null and mechanical ground and the null oscillation effect on rotor performance. Although these are sources of error, the amount of range variation is dependent on the value of other parameters. For example, in an oscillating null system or bang-bang system, a null duty cycle of about 35 percent will exhibit little range error due to T_c. In addition, the null oscillation effect on rotor performance can be minimized by adjusting other parameters such as null assembly moment of inertia to increase null frequency or decrease amplitude. The oscillation effect is also negligible for applications where the run time to range is large compared with the number of null cycles which occur during the period.

Of the two error sources, frictional torque is the most significant. As was shown in Section IV of this report, T_c not only contributes to system error but influences the entire design in terms of SSS size and power consumption. For a system requiring the detection of a large g range, the value of T_c becomes even more critical. If this parameter could be eliminated or reduced to zero, any DC motor could be used to detect almost any level of acceleration and produce very accurate results. Without T_c, the principle limitation would be the size of the null mass relative to the level of dynamic balance which could be achieved in the null assembly. On this basis then, if a technique could be found to eliminate T_c, motor evaluation would be reduced to a selection based primarily on small size and low power consumption. In general, there is a motor cost relationship to size in that larger motors cost more than smaller sizes. Small motors also offer packaging advantages and low power consumption consistent with the needs of typical weapons systems.

The technique developed for mounting the motor relative to the mechanical structure in a way which eliminated T_c consisted of a torsional spring approach. This concept amounts to removal of the null bearings, which are replaced by the springs. A schematic of the procedure is shown in Figure 19.

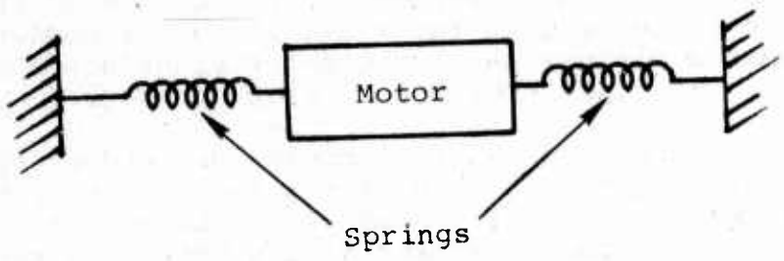

Figure 19. Mounting Procedure

With this design, it was theorized that spring effect could be minimized by configuring the system to control null displacement to within a very limited range. It is clear that an ordinary spring cannot be used to support the system, since only angular motion can be permitted. To prevent side or vertical motion, the spring must be configured to provide the necessary support.

A torsional spring design which can provide the necessary features is illustrated in Figure 20.

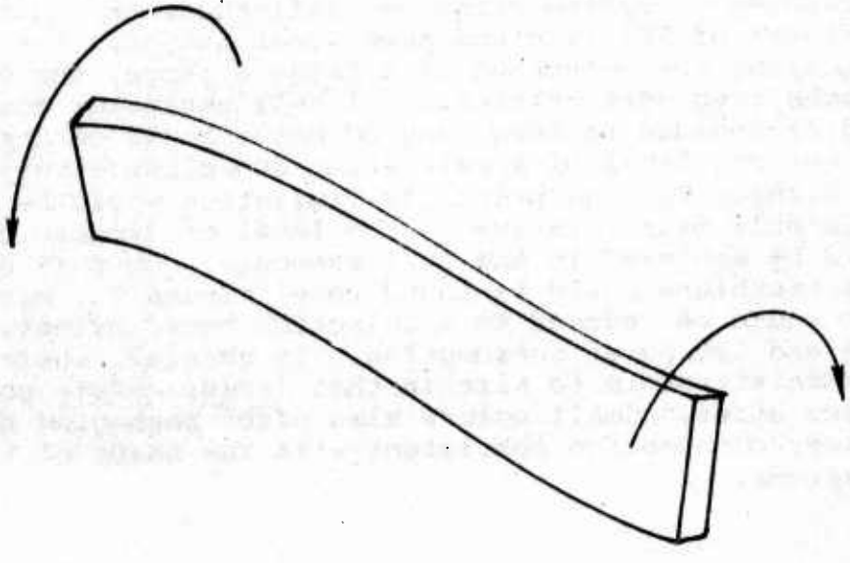

Figure 20. Torsional Spring

Here a small slab shaped piece of metal is used with a torque couple applied. This shape permits the torsional displacement and provides vertical support. Another such slab placed 90 degrees to the one shown will provide the necessary support in all directions. Such a spring is an available shelf item manufactured by Bendix. The exact configuration is shown in Figure 21.

Components used to provide electrical access to the motor also contribute to T_c. In the typical SSS design, electrical access is accomplished by slip rings and brushes. The torsional spring approach solves this problem, since electrical power can be provided through the springs. Two springs are required, one for each side of the motor. One side provides the positive polarity and the other the negative or ground. These two parameters, electrical access friction and null bearing friction, make up T_c and are eliminated by the spring approach.

In the spring design, it is necessary to limit null deflection to the smallest possible angle. If this can be accomplished, then the null acceleration torque, T_a, will be equal to the motor torque as desired for accuracy. To provide this the null must track or be a stable device with no oscillation. By accomplishing the tracking feature, the second error source, the null oscillation effect, will be eliminated. For these reasons then, the torsional spring design was selected for use in the final prototype SSS.

The next step is motor selection. It is apparent that available spring support is limited and motor weight must therefore be as low as possible. In addition, the rated spring loading is a function of the spring rate. That is, if a small spring rate is desired, the loading in other directions which it can accommodate is also small. Normally, a small rate is desirable from the standpoint of reducing spring effects due to null deflection. It is also necessary to pick a motor whose torque output is large compared with the spring torque at a given deflection. On this basis, the smallest spring available was selected. Its rate was 0.176 ounce-inch/radian. The motor selected was a Micromo Electronics 060 device 0.5 inch in diameter by 0.5 inch long.

Detailed performance data are provided in a subsequent section. It is important to note here that power consumption of this device is less than two watts. As a comparison, the breadboard and preliminary prototype motors consume about 45 watts. In addition to the power advantage, the motor selected has a unique rotor design of low inertia that permits acceleration to 33,000 RPM in about 50 milliseconds. With this capability, more than 100g positive and negative acceleration can be detected.

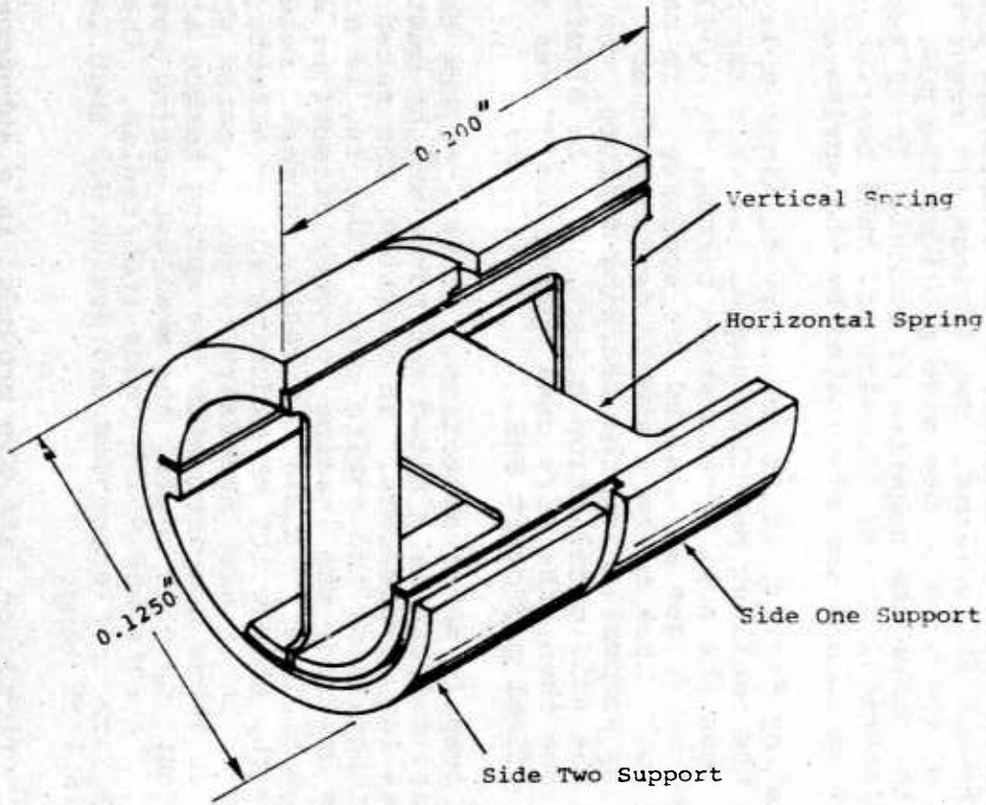

Figure 21. Torsion Spring

On the basis of the promise of greater accuracy, larger g detection range, lower power consumption, reduced cost and a smaller package, this approach was selected for use in the final prototype. It was not within the scope of this program to study every possible DC motor which may be used, and because the spring approach indicated the use of an optimum motor (small size, low power, low cost, etc.), the motor evaluation was reduced to implementation of the design concept.

Before proceeding to the later sections which describe this portion of the effort, it will be useful to provide preliminary information on the implementation procedure. To accomplish the tracking null design, servo mechanism design procedures must be used to establish compensation circuits. These circuits are used to ensure null stability, i.e., the closed loop performance of the system must be stable and have a fast transient response and a high gain to minimize spring deflections. The first step in such a procedure is to derive the open loop equation for each part of the system with no electronic compensation. The various parameters are then measured and substituted into the equations. These relationships are then confirmed by running a frequency response of the open loop system. If the relationships are correct and characterize system performance, then electronic compensation techniques can be formulated. This is the general approach used as detailed in subsequent sections of this report. Before proceeding to a theoretical analysis, further conceptual details are provided.

The basic SSS concept was discussed in Section II. This concept applies to all three designs (breadboard, preliminary, and final prototypes); however, the theoretical analysis is somewhat different for the final prototype. All designs are servo mechanisms, but the breadboard and preliminary prototypes are positional types, because the null responds to applied acceleration on the basis of locations. That is, the application of null torques is always in a direction which tends to restore the null to the transition line. Because springs are used in the final prototype, the system is a torque servo mechanism. Figure 22 shows this feature.

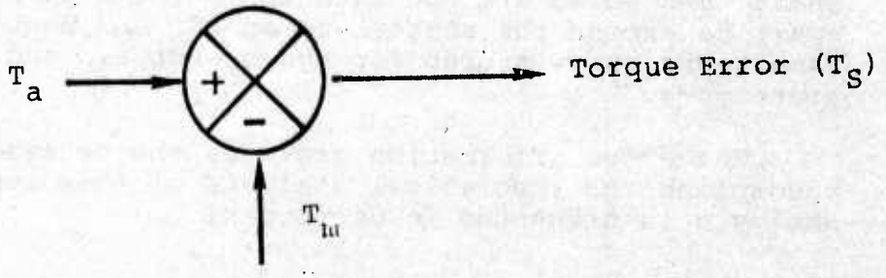

Figure 22. Summing Junction

At the springs, an acceleration torque is applied by the unbalanced mass. This results in spring deflection and torque error, T_s (spring torque). If this deflection is sensed and motor current supplied, then a motor torque, T_m, results as shown. This torque is applied to reduce the torque error to a value where T_m is almost equal to T_a. This is the desired result, since the motor rotor will accelerate under the influence of T_a as explained in Section IV. It is clear then that the system error will be minimized if the spring torque is close to zero. This can be accomplished if the spring deflection error signal is subjected to a very large electronic gain. For reasons which are discussed later, an extremely large gain may not be practical. To improve this situation, a spring having a low spring rate should be used. The smallest torsional spring rate found is provided by a spring (Part No. 5004-800) manufactured by Bendix Fluid Power Division. This spring, having a spring rate of 0.176 ounce-inch per radian, is shown in Figure 21. Here the two orthogonally oriented torsional springs are supported on each end by cylindrical shaped sleeves. Weld joints are used in the construction.

The Micromo Electronics 060 motor and its functional parameters and construction are shown in Figure 23. This motor has a no-load speed of 33,600 RPM at the rated six volts. The ironless rotor construction shown produces a very low moment of inertia; therefore, at the level of torque indicated, the rate of acceleration is very large. Maximum speed is reached in about 50 milliseconds.

Figure 24 shows schematically how the motor and springs are used to mount the system to a structure. Two supports are first installed onto the motor. The first is pressed in place and the second threaded as shown. Springs are then pressed into the supports on their inboard ends and into insulator sleeves at the outboard ends. The sleeves are pressed into the mounting structure for support. They are made of insulating material because they serve as conductors. Each motor terminal is connected to a spring via a wire (not shown).

To determine the range, a shutter is inserted on the rotor shaft, and holes are cut into the motor support 180 degrees apart to expose the shutter to an LED and photo transistor. The same technique was used for the breadboard and preliminary prototypes.

The above information provides the necessary background to accomplish the theoretical analysis of this approach. The analysis is presented in Section XI.

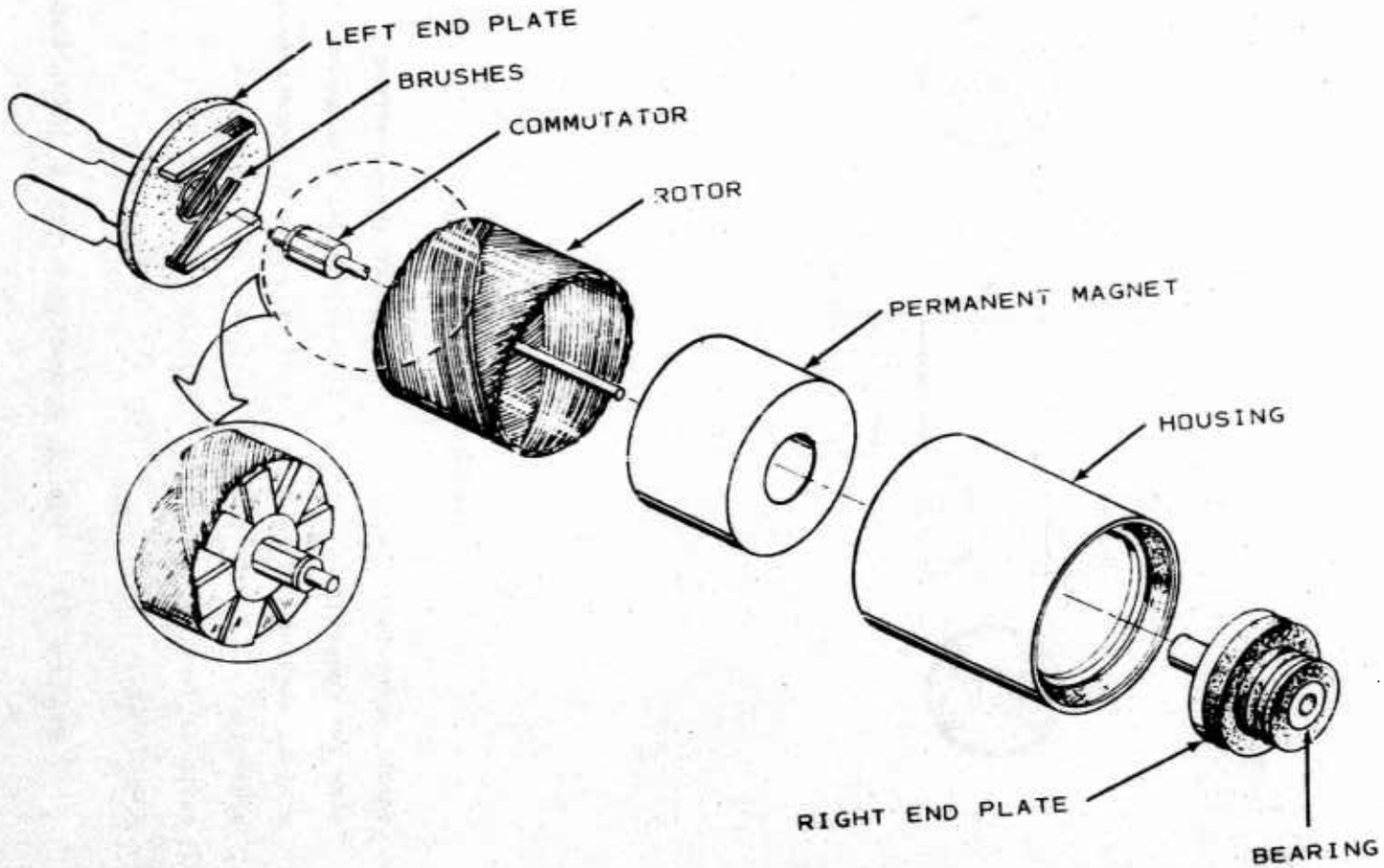

Figure 23. Final Prototype Motor

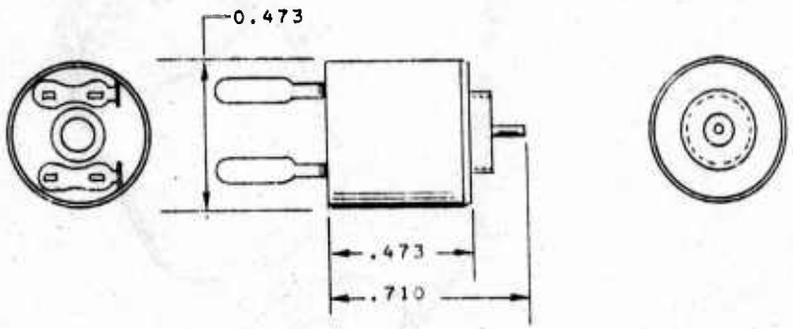

MOTOR PARAMETERS

TORQUE SENSITIVITY, K_T	- 0.229 OUNCE-INCHES/AMPERE
BACK EMF CONSTANT, K_B	- 0.0016 VOLTS/RADIAN/SECOND
VISCOUS DAMPING CONSTANT, A	- 1.05×10^{-6} OUNCE-INCHES/RADIAN/SECOND
RESISTANCE, R	- 19 OHMS
RATED VOLTAGE, V	- 6 VOLTS
INDUCTANCE, L	1×10^{-4} HENRY

Figure 23. Final Prototype Motor (Concluded)

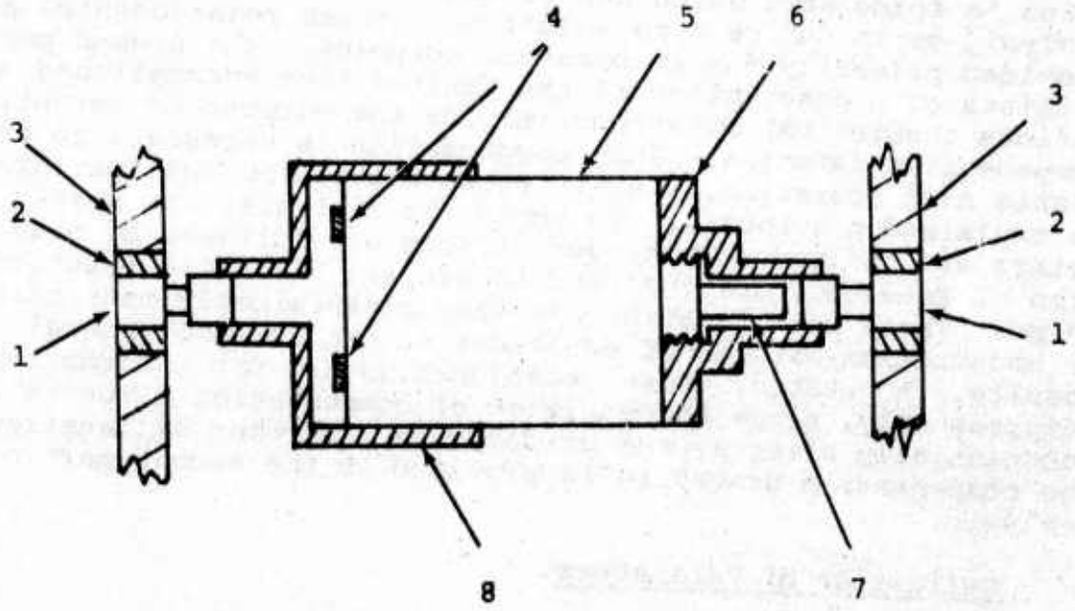

LEGEND

1 - Torsional Spring
2 - Insulator Sleeve
3 - Mounting Structure
4 - Motor Electrical Terminals
5 - Motor
6 - Motor Support - 1
7 - Rotor Shaft
8 - Motor Support - 2

Figure 24. Motor Mounting Schematic

SECTION XI

FINAL PROTOTYPE THEORETICAL ANALYSIS

This section presents a two part theoretical analysis of the final prototype. In the first part a general set of relationships is formulated which can be used to conduct computer analysis or to derive time solutions. These relationships are provided primarily for information purposes. The second part consists of a description of the manipulation accomplished on various theoretical relationships for the purpose of establishing compensation networks. Such compensation is necessary to provide stable null operation, i.e. to produce tracking null performance as explained previously. To begin the analysis, the system parameters are defined. These definitions are followed by presentation of free-body designs used to prepare the basic relationships. These relationships are then algebraically manipulated in conjunction with motor equations to produce the general results. As stated, those relationships are for information purposes only, since the addition of compensation circuits will substantially alter system performance. Further explanation of the compensation procedure is provided in the second part of the analysis.

Definition of Parameters.

K_T = torque constant (ounce-inches/ampere)

K_B = back emf constant (volts/radian/second)

A = viscous friction coefficient (ounce-inch/radian/second)

J_R = rotor moment of inertia (ounce-inch-seconds^2)

J_N = stator moment of inertia (ounce-inch-second^2)

K_S = torsional spring rate (ounce-inch/radian)

R = motor resistance (ohms)

L = motor inductance (henry)

V = motor voltage (volts)

I = motor current (amperes)

θ_R = rotor displacement (radians)

θ_N = null displacement (radians)

T_B = motor Coulomb friction torque (ounce-inches)

T_V = viscous friction torque (ounce-inches)

T_D = motor torque developed (ounce-inches)

T_a = null acceleration torque (ounce-inches)

Tm = net motor torque on rotor (ounce-inches)

Free body diagrams of the null and rotor assemblies are shown in Figure 25. Using these diagrams, the equations of motion are as follows:

rotor:

$$T_D - T_V - T_B - J_R\ddot{\theta}_R = 0 \tag{35}$$

stator/null:

$$T_D - T_a - T_V - T_B + K_S\theta_N + J_N\ddot{\theta}_N = 0 \tag{36}$$

The Tm term is defined above as the net motor torque, or:

$$T_D - T_V - T_B = Tm \tag{37}$$

Substituting Equation (37) into Equation (35) yields:

$$Tm = J_R\ddot{\theta}_R \tag{38}$$

If it can be shown that T_a = Tm, then Equation (38) becomes $T_a = J_R\ddot{\theta}_R$, the desired result. To show this, Equation (37) is first substituted into Equation (36) as follows:

$$T_a - Tm = J_N\ddot{\theta}_N + K_S\theta_N \tag{39}$$

This relationship shows that to provide T_a = Tm, $\ddot{\theta}_N$ and θ_N must be zero. If a tracking/stable null is realized, then $\ddot{\theta}_N$ will equal zero and Equation (39) reduces to:

$$T_a - Tm = K_S\theta_N = T_S \text{ (spring torque)} \tag{40}$$

Equation (40) represents the torque summing junction discussed previously. It can be seen that if T_a = Tm is to be realized, then θ_N must be zero or very small. To develop a sensor signal,

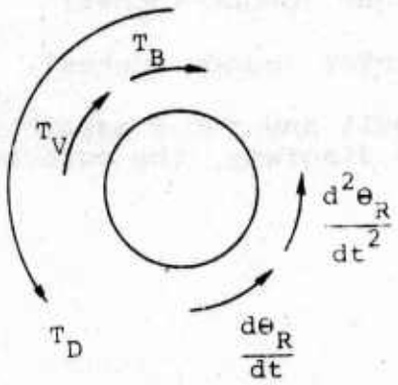

ROTOR ASSEMBLY
FREE-BODY DIAGRAM

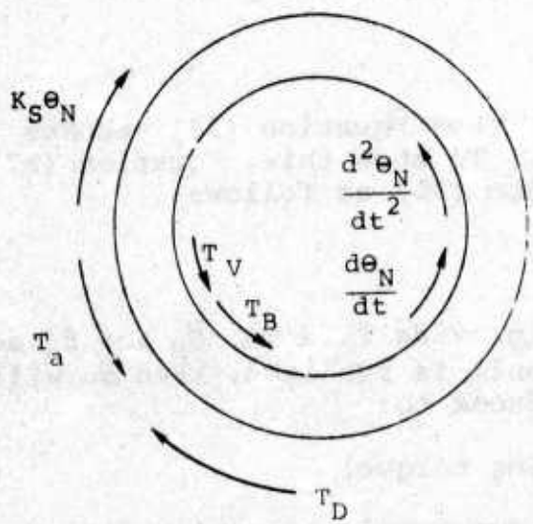

STATOR ASSEMBLY
FREE-BODY DIAGRAM

Figure 25. Final Prototype Free-Body Diagrams

θ_N cannot be zero except when $T_a = 0$; therefore, it is necessary to make θ_N small by using a sensor with very high gain. Then $T_a = Tm$ as desired. It will be shown later that for all values of T_a, $Tm = B\ T_a$, where B is a constant almost equal to one.

To complete the analysis, further definition of T_D and T_V is necessary. The torque, T_V, is due to the internal motor windage and is therefore related to rotor and null motion as follows:

$$T_V = A\ (\dot{\theta}_R - \dot{\theta}_N) \tag{41}$$

The developed motor torque, T_D is related to K_T and I as follows:

$$T_D = K_T I \tag{42}$$

The motor relationship is:

$$V = IR + K_B\ (\dot{\theta}_R - \dot{\theta}_N) + L\dot{I} \tag{43}$$

Taking the LaPlace of Equations(42) and (43) then solving Equation (43) for I and substituting into Equation (42) yields T_D as follows:

$$T_D = K_T \frac{V - K_B\ (\theta_R S - \theta_N S)}{R + SL} \tag{44}$$

Taking the LaPlace Equation of (35), (36) and (41) and substituting T_V of Equation (41) and T_D of Equation (44) into Equations (35) and (36) provides the final result:

$$K_T \frac{V - K_B\ (\theta_R S - \theta_N S)}{R + SL} - A\ (\theta_R S - \theta_N S) - T_B - J_R S^2 \theta_R = 0 \tag{45}$$

$$K_T \frac{V - K_B\ (\theta_R S - \theta_N S)}{R + SL} - T_L - A\ (\theta_R S - \theta_N S) - T_B \tag{46}$$

$$+ K_S \theta_N + J_N S^2 \theta_N = 0$$

These are the relationships which define the system if compensation is not used. The task now is to establish the necessary compensation. This comprises part two of the analysis.

Before beginning part two, it is necessary to establish the ground rules. First, the basic relationships must be linearized because linear compensation will be used. Therefore, T_B, the internal motor frictional torque, will not be considered at this time. In addition, T_a is set equal to zero in Equation (39) because the compensation will apply for all values of T_a including the zero g case. Next, motor inductance may be eliminated from the analysis because it was found during investigations to create a corner well below zero db. Each of these conditions simplify the analysis and provide the desired result. On this basis then, four equations are written as follows:

First from Equation (38):

$$T_M = J_R S^2 \theta_R \tag{47}$$

Next from Equation (39):

$$-T_M = J_N S^2 \theta_N + K_S \theta_N \tag{48}$$

T_M is found to be the difference between the motor torque developed, T_D, and the loss torques T_V and T_B. Since T_B was set to zero:

$$T_M = \overbrace{K_T I}^{T_D} - \overbrace{(AS\theta_R - AS\theta_N)}^{T_V} \tag{49}$$

Finally from Equation (43) with L = 0:

$$V = IR + K_B S\theta_R - K_B S\theta_N \tag{50}$$

Equations (47) through (50) can now be manipulated to isolate the various parts of the system in terms of transfer functions. The problem now is to develop a technique which can be used to isolate the various transfer functions. Examination of the physical system as explained in a previous section shows that the summing junction of Figure 26 applies:

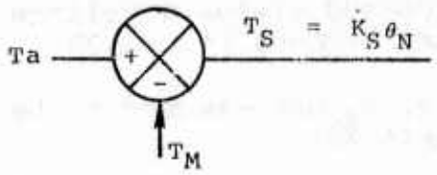

Figure 26. Summing Junction

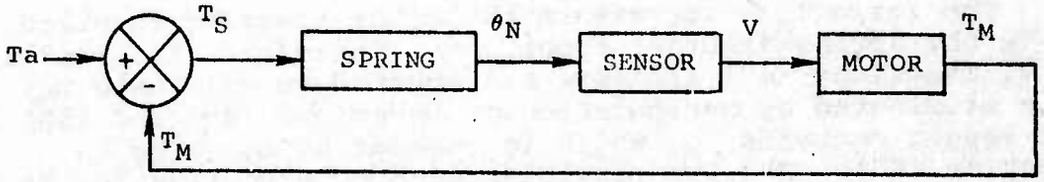

Figure 27. Basic Functional Diagram

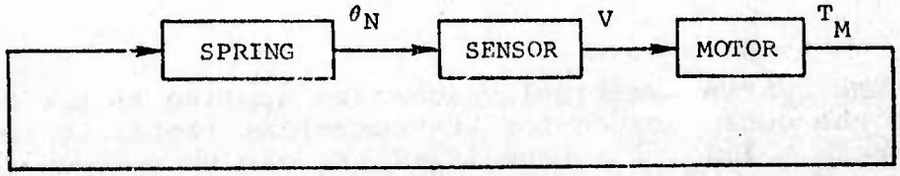

Figure 28. Basic Diagram With Ta = 0

The term T_S is the spring torque related as shown. This condition is detected by the null sensor which measures θ_N, applies amplification and yields a voltage, V, proportional to θN. The diagram then becomes Figure 27.

In the analysis, T_a was assumed to be zero, and the block diagram becomes Figure 28.

If the loop is opened at the sensor and the transfer function θ_N/V is determined, then a relationship made up of spring and motor parameters exists.

If the transfer function θ_N/TM is found next, it can be applied to θ_N/V to find T_M/V as follows:

$$\frac{T_M}{\theta_N} \quad \frac{\theta_N}{V} = \frac{T_M}{V} \tag{51}$$

The ratio T_M/V represents the motor transfer function and θ_N/T_M the spring transfer functions. Therefore, to first find θ_N/V, Equations (47) and (48) are equated to eliminate T_M. Next, I is eliminated by manipulation of Equations (49) and (50) and the result contains T_M, which is removed by equating to Equation (47). The two resulting equations contain θ_N, θ_R and V, which are then manipulated to eliminate θ_R. The result is as follows:

$$\frac{\theta_N}{V} = \frac{-\dfrac{J_R K_T S}{K_S(AR + K_T K_B)}}{\dfrac{J_R J_N R}{K_S(AR + K_T K_B)} S^3 + \dfrac{(J_R + J_N)}{K_S} S^2 + \dfrac{J_R R}{AR + K_T K_B} S + 1} \tag{52}$$

If the system numerical values are applied to the denominator and the cubic solved for its numerical roots, it is found that for $J_N > 10J_R$, the term $(J_R+J_N)K_S$ can be reduced to J_N/K_S without appreciably affecting the results. After making the substitution J_N/K_S for $(J_R+J_N)/K_S$ and factoring, θ_N/V becomes:

$$\frac{\theta_N}{V} = \frac{-KS}{\left(\dfrac{1}{\omega_N^2} S^2 + 1\right)\left(\dfrac{1}{\omega_1} S + 1\right)} \tag{53}$$

Where:

$$\omega_N = \left(\frac{K_S}{J_N}\right)^{1/2} \tag{54}$$

$$\omega_1 = \frac{A}{J_R} + \frac{K_T K_B}{J_R R} \tag{55}$$

$$K = \frac{J_R K_T}{K_S (AR + K_T K_B)} \tag{56}$$

Next, the transfer function θ_N/T_M is found by manipulating Equation (48) as follows:

$$\frac{\theta_N}{T_M} = - \frac{\frac{1}{K_S}}{\frac{J_N}{K_S} s^2 + 1} \tag{57}$$

Or from Equation (54):

$$\frac{\theta_N}{T_M} = - \frac{\frac{1}{K_S}}{\frac{1}{\omega_N^2} s^2 + 1} \tag{58}$$

The motor transfer function, T_M/V, can now be found as previously explained. The result is:

$$\frac{T_M}{V} = \frac{K_M s}{\frac{1}{\omega_1} s + 1} \tag{59}$$

Where:

$$K_M = \frac{J_R K_T}{AR + K_T K_B} \tag{60}$$

The block diagram of the system can now include the transfer functions as shown by Figure 29.

Now in Figure 29, the ω_N term represents the undamped natural frequency of the spring, and the T_M/V term represents motor performance. Each of the applicable parameters were measured, and the results are tabulated below:

K_T = 0.229 ounce-inch/ampere

K_B = 1.618×10^{-3} volts/radian/second

A = 1.05×10^{-6} ounce-inches/radian/second

J_R = 1.389×10^{-5} ounce-inches-second^2

J_N = 1.16×10^{-4} ounce-inches-second^2

K_S = 0.352 ounce-inches/radian (2 springs)

R = 19 ohms

ω_1 = 1.48 radian/second

ω_N = 54.93 radian/second

Substituting the above values into Equation (52) leads to the following Bode plot shown by Figure 30.

As illustrated by Figure 30, applying gain to the system without providing compensation will result in instability. With sufficient gain the plot will cross zero db rolling off at -40 db/decade, and the phase shift will be at least 180 degrees. Such a gain is necessary to reduce spring effects, and compensation is necessary to achieve null stability. Before presenting the compensation technique, sensor information is provided. As indicated by the block diagram of Figure 31, the null sensor is placed between the spring and the compensation circuits. The sensor will then produce an output voltage, V, in response to a null displacement, θ_N. This voltage is acted on by the compensation to produce a motor voltage which results in a motor torque fed back to the torque summing function. The difference between T_a and T_M acts through the spring to produce θ_N. The sensor consists of a pair of photo diodes and a pair of LED's. Further sensor information is provided in the next section; however, it is emphasized here that for stability to be maintained once compensation is applied, the sensor gain must be linear. This is because the sensor contributes to the total system gain which in turn affects stability.

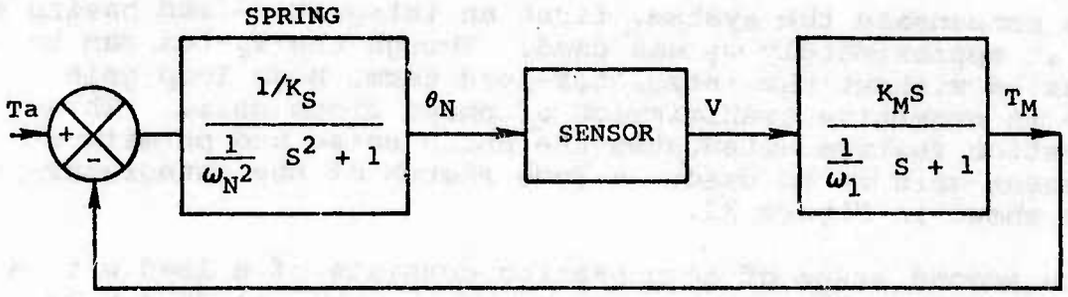

Figure 29. Uncompensated Block Diagram

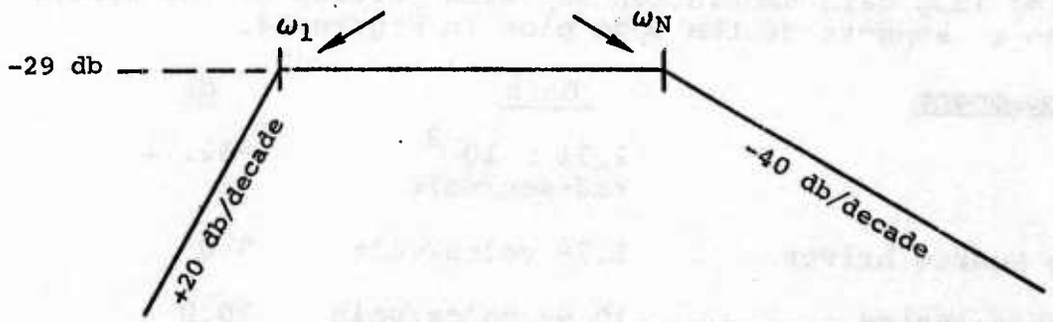

Figure 30. Bode Plot

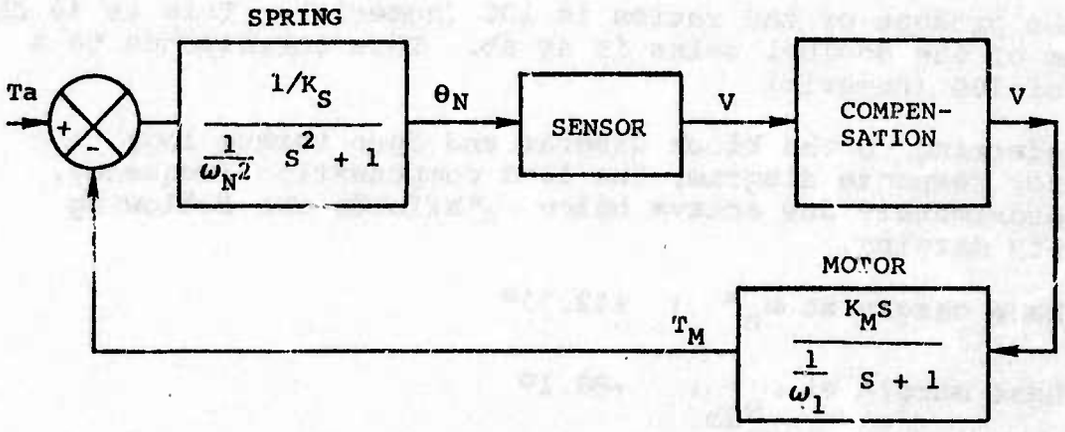

Figure 31. Compensated Block Diagram

To compensate the system, first an integrator-lead having a corner at approximately ω_1 was used. Though the system can be compensated without the integrator-lead term, high loop gain results in excessive transmission of photo diode noise. This compensation feature attenuates the photo noise and permits a high sensor gain to be used. A Bode sketch of the integrator-lead is shown in Figure 32.

The second stage of compensation consists of a lead with a corner ω_2 placed prior to ω_N. This reduces the -40 db/decade slope to -20db/decade, and the phase shift cannot exceed 90 degrees. The lead sketch is shown in Figure 33.

Figure 34 shows a total open loop plot of the sensor, hardware, compensation and the motor driven circuit. The following loop gain tabulation for each portion of the system is given in support of the Bode plot in Figure 34.

Component	Gain	db
K_m/K_S	2.31×10^{-2} rad-sec/volt	-32.71
Voltage Source Driver	1.78 volts/volt	5.0
Lead Compensation	10.97 volts/volt	20.8
Integrator-Lead Compensation	1.11 sec^{-1}	0.94
Torsion Angle Sensor	200 volts/rad	46.02

The product of the ratios is 100 (numeric). This is 40 db. The sum of the decibel gains is 40 db. This corresponds to a ratio of 100 (numeric).

Referring to the block diagram and open torque loop frequency response diagram, the lead compensation frequency, ω_2, approximately one octave below ω_n" affords the following stability margins:

Phase margin at ω_n" : $+42.73^o$

Phase margin at $\omega_{o_{db}}$: $+86.1^o$

The slope of -20db/decade in the region of the 0db frequency implies a phase margin at unity gain that approaches +90 degrees.

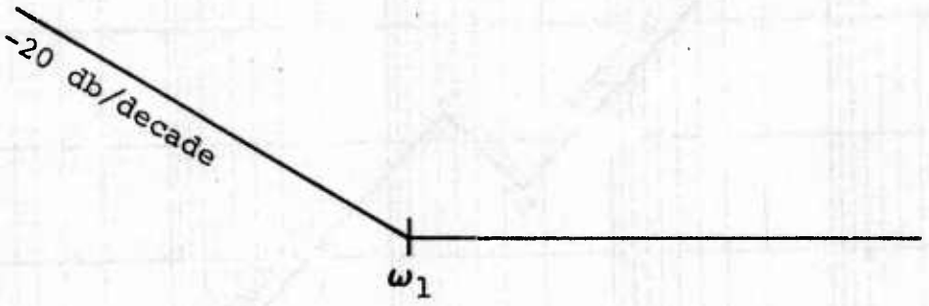

Figure 32 - Integrator-Lead Plot

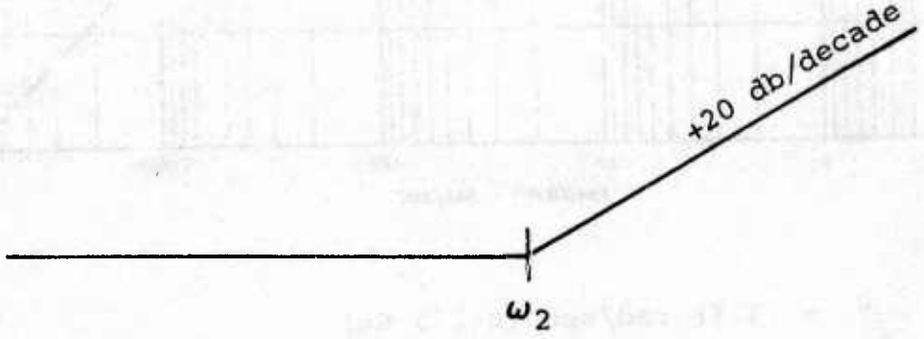

Figure 33 - Lead Plot

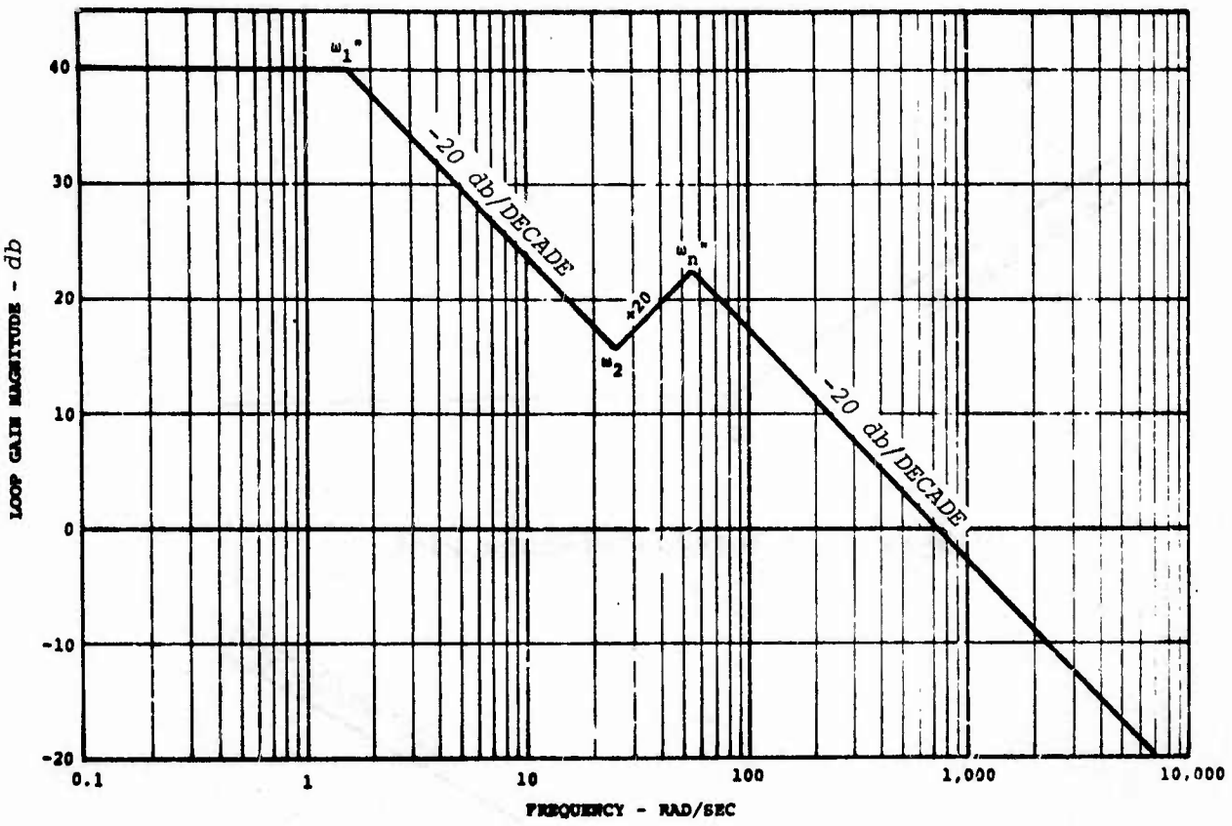

$\omega_1"$ = 1.48 rad/sec (0.235 Hz)

ω_2 = 24.9 rad/sec (3.96 Hz)

$\omega_n"$ = 54.9 rad/sec (8.74 Hz)

$\omega_{o_{db}}$ = 720 rad/sec (114.59 Hz)

Figure 34. Open Torque Loop Frequency Response

The 720 radians/second (114.59 Hz) 0db frequency given by the open torque loop frequency response diagram implies a closed loop bandwidth (3db down frequency) of 114.59 Hz for the closed torque loop transfer function, T_M/T_a. This corresponds to a 10 to 90 percent T_M torque rise time of 3.052 milliseconds for T_a step inputs. This is equivalent to a time constant of 1000/720 = 1.389 milliseconds for T_a step inputs. The closed loop relationship is as follows:

$$\frac{T_M}{T_a} = \frac{0.99 \left(\frac{1}{24.9} S + 1\right)^2}{\left(\frac{1}{16.6} S + 1\right)\left(\frac{1}{41} S + 1\right)\left(\frac{1}{663} S + 1\right)} \qquad (61)$$

Because the product of the first two terms in the denominator of Equation (61) is nearly equal to the squared term in the numerator, they can be cancelled to simplify the relationship for examination. Equation (61) then reduces to:

$$\frac{T_M}{T_a} \approx \frac{0.99}{\frac{1}{663} S + 1} \qquad (62)$$

Treating T_a as a step function, the time relationship is:

$$\frac{T_M}{T_a} = 0.99 \left(1 - e^{-633t}\right) \qquad (63)$$

This relationship shows that in response to T_a the system will reach 95 percent of its tracking condition in about 4.7 milliseconds. When the system is in the tracking mode, the motor torque is equal to 0.99 T_a, or a one percent error exists because the desired result is $T_M = T_a$. This error can be calibrated by increasing the null mass by one percent, or:

$$T_M = 1.01\, T_a\, (0.99) = T_a \qquad (64)$$

Earlier in this section it was stated that for all values of T_a, $T_M = BT_a$ and in this instance B = 0.99, or near unity.

Based on the above information calculations indicate the dynamic range of the system to be ±50g. As an example, the following calculated parameters for 50g applied are presented:

T_a = 0.123 ounce-inches

T_M = 0.122 ounce-inches

θ_N = 3.47×10^{-3} radians

To make the analysis more complete, the assumptions made earlier are treated. First, to simplify the analysis, the motor inductance was not considered. In the block diagrams it was shown that a voltage, V, input to the motor will result in a torque, T_M, output. This transfer function was determined to be:

$$\frac{T_M}{V} = \frac{K_M S}{\omega_1 S + 1} \tag{65}$$

where:

$$K_M = \frac{J_R K_T}{AR + K_T K_B} \tag{66}$$

$$\omega_1 = \frac{A}{J_R} + \frac{K_T K_B}{J_R R} \tag{67}$$

If the resistance term, R, is replaced by the total motor impedance term, R + SL, the inductance effect can be examined. Following substitution, the result is:

$$\frac{T_M}{V} = \frac{(K_T/L)\ S}{S^2 + \left(\frac{R}{L} + \frac{A}{J_R}\right) S + \frac{1}{LJ_R}\ (RA + K_T K_B)} \tag{68}$$

Equation (68) shows that two roots exist in the denominator rather than one as seen in Equation (65). To find these roots, the numerical values given previously and 1×10^{-4} henry for the inductance are used. The roots are:

$$\omega_1 = 1.473 \text{ radians/second} \tag{69}$$

$$\omega_L = 1.9 \times 10^5 \text{ radians/second} \tag{70}$$

The corner at ω_1 is the same as before. The additional corner due to the inductance is more than 2 decades above the zero db crossing as seen in Figure 34. Therefore, this corner is not significant with regard to stability.

To examine the assumption that $T_a = 0$, Equation (39) is rewritten below:

$$T_a - T_M = J_N\ddot{\theta}_N + K_S\theta_N \tag{71}$$

Using LaPlace, Equation (71) becomes:

$$T_a - T_M = (J_N S^2 + K_S)\ \theta_N \tag{72}$$

or:

$$\frac{\theta_N}{T_a - T_M} = \frac{\frac{1}{K_S}}{\frac{1}{\omega_N{}^2} S^2 + 1} \tag{73}$$

This relationship results in the summing junction illustrated by Figure 35.

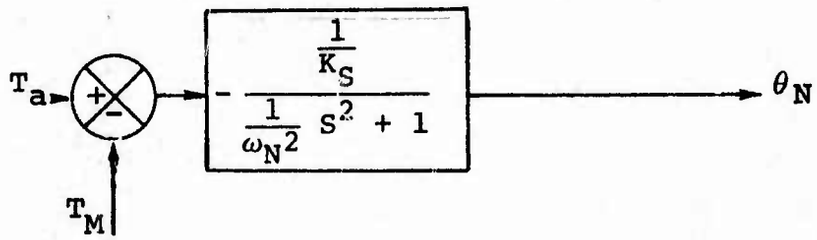

Figure 35. Summing Junction - General Case

This is the condition used in the previously presented block diagrams. It represents the general case. Use of the general case equation ($T_a = 0$) would have complicated the compensation procedure considerably.

The remaining assumption was that the internal motor Coulomb functional torque, T_B, equals zero. It is clear that $T_B \neq 0$; however, T_B is nonlinear and therefore not easily treated by linear compensation techniques. T_B is applied to the rotor in a direction which tends to cause deceleration. T_B is also applied to the null/stator but in the direction which results in greater motor torque, thus offsetting the deceleration effect. Transient effects due to changing T_B are probably similar to changing T_a, but this was not confirmed.

To summarize this section, it is necessary to indicate that the compensation presented was the final compensation design approach. Several other techniques were attempted by altering the location of corners and gain. This was accomplished by altering both electrical and mechanical parameters. These investigations were conducted to eliminate electrical noise and stray corners which caused system oscillations. It should be emphasized that the analysis indicates the system has the capability of responding to large and small levels of acceleration at high accuracy. The difficulties encountered stemmed primarily from hardware implementation. This is discussed in greater detail in the next section.

SECTION XII

FINAL PROTOTYPE DESIGN

The final prototype design can best be understood by describing the various problems which were encountered during the program. These problems led to the final design configuration and therefore provide a more comprehensive picture of the system. The reader is reminded of the basic objectives which were defined in the motor evaluation section of this report. These objectives included the formulation of an SSS design having large g sensing capability at high accuracy, low cost, low power consumption and minimum envelope. As will be shown, the final prototype will sense a large g range and the power consumption is considerably less than the breadboard and preliminary prototypes, but it did not meet the original expectations. The space consumed is the same as the first two prototypes, and high accuracy is indicated from testing but was not substantiated. In addition, the cost of this system as it evolved will be larger than the other systems. However, additional work which is explained later should improve this situation. The system description presented below will provide the rationale for the above statements. The principle source of the design problems was the sensor which is discussed first.

As stated earlier, system stability can be achieved only if sensor gain is linear in the normal region of null operation. A single photo diode and LED pair as used in the first two prototypes does not produce the desired response due to the variations in LED light intensity in the cross section. In other words, the light cut off by the shutter will not be linear with null displacement. It was found that linearity can be achieved over the desired range of θ_N by employing two pairs of LED's and photo diodes if a common mode rejection technique is used. That is, a photo diode is connected to each input (inverting and non-interting) of an operational amplifier. Meanwhile, the shutter is designed to expose one diode while the other is being shuttered. A curve of the result is shown in Figure 36.

It was found that any unbalance in the rotor or the application of external vibration causes an unwanted displacement of the motor relative to the springs. This displacement is detected by the sensor and is mistaken for T_a. To solve this problem, one photo diode/LED pair is mounted on each side of the motor as shown in Figure 37.

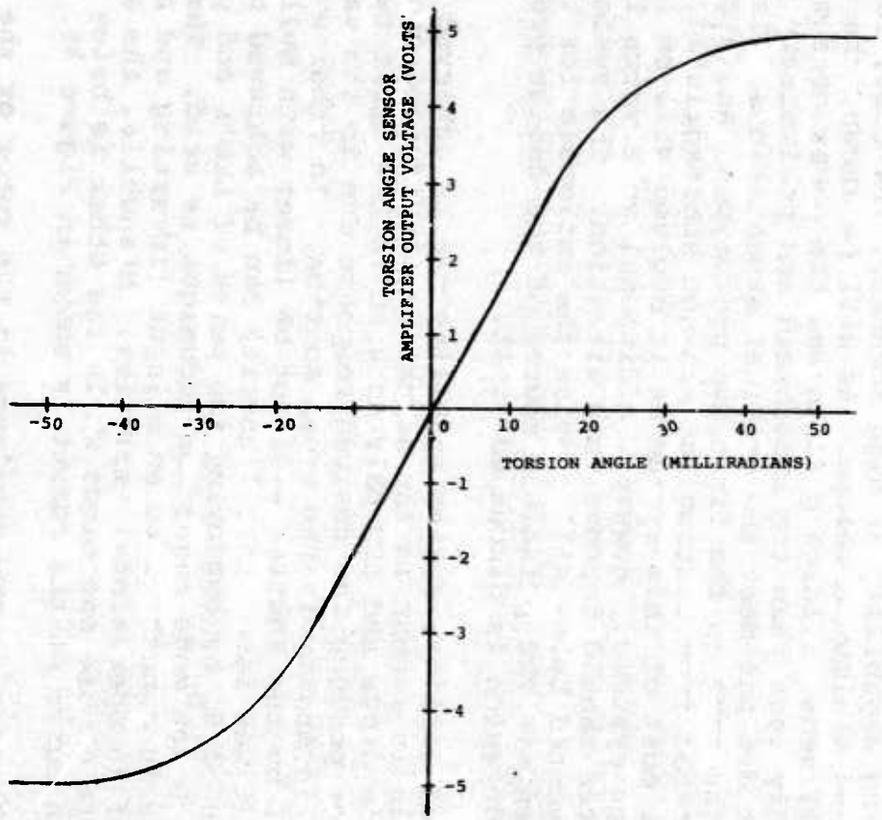

Figure 36. Torsion Angle Sensor/Amplifier Transfer Characteristic Curve

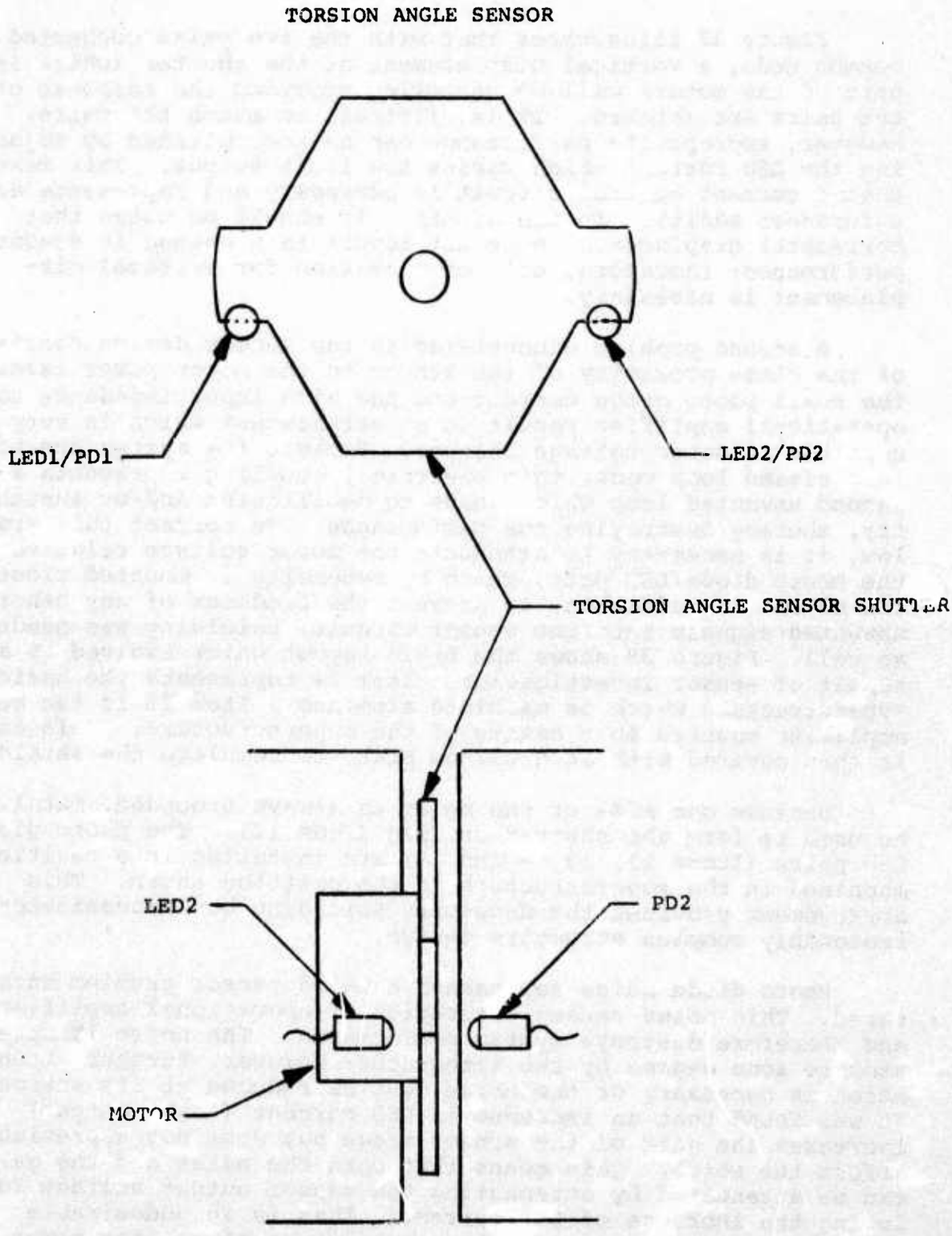

Figure 37. Final Prototype Shutter Arrangement

Figure 37 illustrates that with the two pairs connected in common mode, a vertical displacement of the shutter (which is part of the motor) will be cancelled provided the response of the pairs are matched. It is difficult to match the pairs; however, appropriate performance can be accomplished by adjusting the LED current which varies the light output. This means that a current control circuit is necessary and represents an unforeseen addition to the system. It should be noted that horizontal displacement does not result in a change in sensor performance; therefore, only compensation for vertical displacement is necessary.

A second problem encountered in the sensor design consists of the close proximity of the sensor to the motor power terminals. The small photo diode current and the high input impedance to the operational amplifier result in an arrangement which is very susceptible to motor voltage changes. Because the system operates in a closed loop mode, this electrical coupling represents a second unwanted loop which leads to oscillation and/or instability, thereby destroying the performance. To correct this problem, it is necessary to attenuate the motor voltage relative to the photo diode/LED pair, which by necessity is mounted close to the motor. In addition, to prevent the feedback of any other unwanted signals into the sensor circuit, shielding was needed as well. Figure 38 shows the basic layout which evolved as a result of sensor investigation. Item 24 represents the basic superstructure which is machined aluminum. Item 25 is the sensor amplifier mounted in a cavity of the superstructure. This cavity is then covered with an aluminum plate to complete the shielding.

Because one side of the motor is always grounded, metal can be used to form the shutter or flag (Item 12). The photo diode/LED pairs (Items 11, 13, 9 and 19) are installed into cavities machined in the superstructure in the position shown. This arrangement provides the necessary shielding but necessitates a reasonably complex structure design.

Photo diode noise represents a third sensor problem encountered. This noise causes saturation of operational amplifiers and therefore destroys system performance. The noise is attenuated to some degree by the integrator; however, further attenuation is necessary or the noise must be reduced at its source. It was found that an increase in LED current (light output) increases the gain of the sensor stage but does not appreciably affect the noise. This means that both the noise and the gain can be attenuated by attenuating the sensor output voltage following the increase of LED current. This is an undesirable feature because it requires the consumption of greater power.

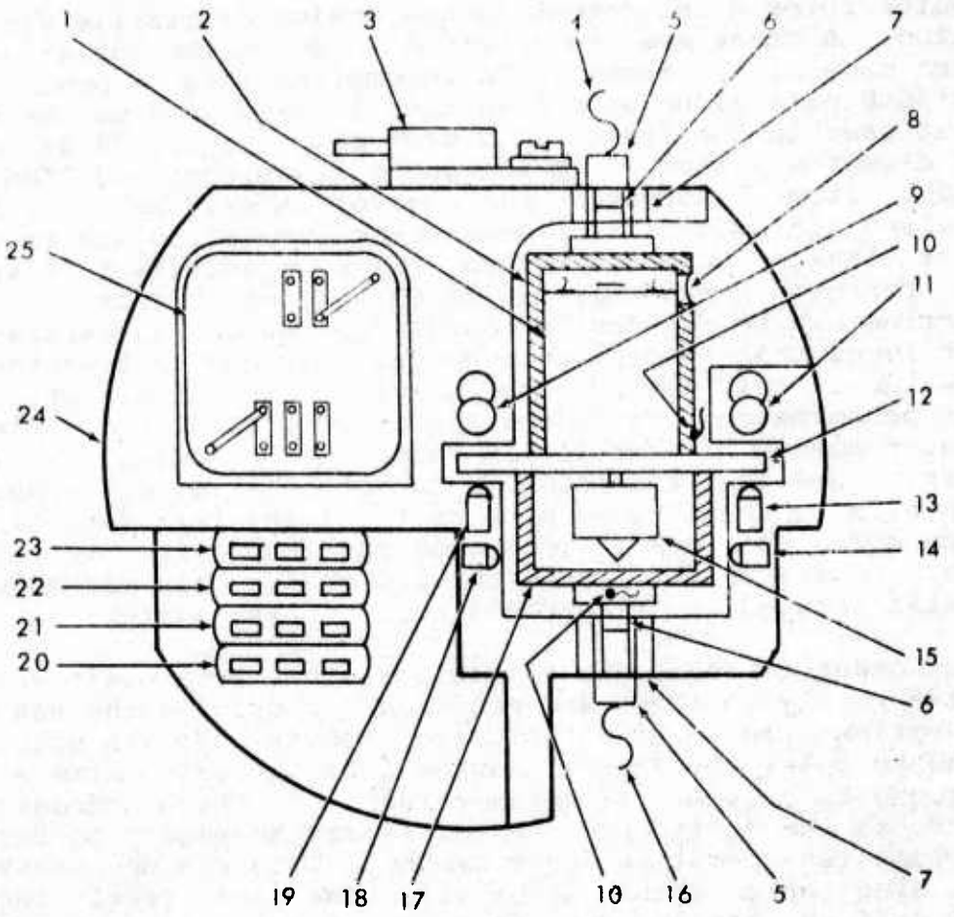

LEGEND

1 - MOTOR
2 - MOTOR HOUSING (BRASS)
3 - Q6, Q7
4 - CIRCUIT GROUND
5 - SLEEVE
6 - TORSION SPRING
7 - INSULATING BUSHING
8 - STATOR MASS VOID
9 - PD2
10 - MOTOR LEAD TERMINATIONS
11 - PD1
12 - TORSION ANGLE SENSOR FLAG (BRASS)
13 - LED 1
14 - LED 3
15 - FLYWHEEL
16 - SERVO AMPLIFIER OUTPUT
17 - FLYWHEEL ENCLOSURE (INSULATING MATERIAL)
18 - PT1
19 - LED 2
20 - MC7818 VOLTAGE REGULATOR
21 - MC7918 VOLTAGE REGULATOR
22 - MC7812 VOLTAGE REGULATOR
23 - MC7912 VOLTAGE REGULATOR
24 - SUPERSTRUCTURE
25 - TORSION ANGLE SENSOR AMPLIFIER

Figure 38. Top View of Final Prototype Superstructure Assembly

Motor rotor displacement is the analog of missile distance traveled. A means must be provided to count the number of revolutions made by the member. To accomplish this, a photo transistor/LED pair along with a shutter is used in a manner similar to that used in the first two prototypes. Figure 39 depicts these elements. Item 6 is the photo transistor and Item 2 is the LED. Item 7 serves as the shutter as well as a flywheel. Two pulses are provided for each rotor revolution due to the shutter blanking twice each turn. Close examination of the equations presented previously indicates that the effect of spring deflection can be reduced for large J_R. During investigations, it was found that temperature changes resulted in unwanted spring deflections. This destroys calibration and causes a drift in system performance. To reduce the effects of spring deflection, the rotor moment of inertia was increased by adding the flywheel shutter. Note that the rotor moment of inertia, J_R, appears as a gain term in the forward path of the loop; therefore, increasing the moment of inertia increased the loop gain. To restore the gain to its former level, the integrator gain was adjusted. This also reduced the electronic noise in the system.

In order to formulate a stable system, both positive and negative supply voltages are required for driving the sensor, compensation stages and motor drive circuit. It was originally planned to split the 28-volt source into two parts with a floating ground to provide ±14 volts relative to the electronics; however, as the design progressed, it was necessary to form separate supplies operating about ground. This was necessary to ensure electronic circuit stability. The final result included use of voltage regulators to produce ±18 volts and ±12 volts. These are mounted on the side of the structure as shown in Figure 38, Items 20 through 23. In addition, two motor drive transistors are mounted on the structure, Item 3, for heat sinking purposes. Although considerable difficulty was experienced in the heat effects on the springs, there was no other area where these transistors could be sinked within the assembly.

With regard to heat effects on the springs, this is an unsolved problem. Although emphasis was placed on the spring mounting procedure, the calibration is affected by temperature changes. To ensure structure spring hole cavity alignment, drilling was accomplished with one drill pass. It is clear, however, that the procedure for mounting the springs onto the motor could be improved.

The remaining system circuits are contained on three printed circuit boards mounted atop the structure in a manner similar to that used in the first two prototypes. The assembly is then placed into the same size and configuration can as used in the

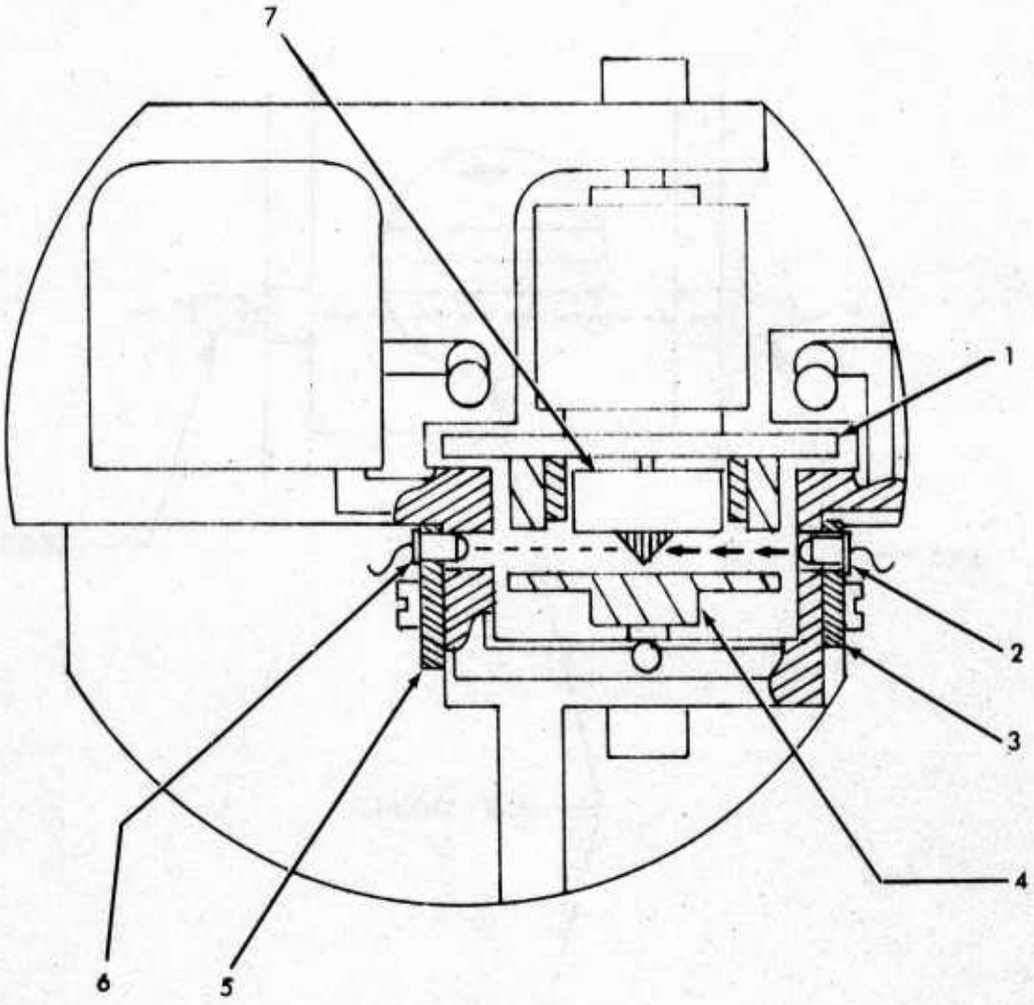

LEGEND

1 - TORSION ANGLE SENSOR FLAG
2 - LED-3
3 - LED-3 HOLDER
4 - FLYWHEEL ENCLOSURE
5 - PT-1 HOLDER
6 - PT-1
7 - FLYWHEEL/SHUTTER

Figure 39. Rotor Revolution Sensing Detail

ROTOR REVOLUTION SENSOR

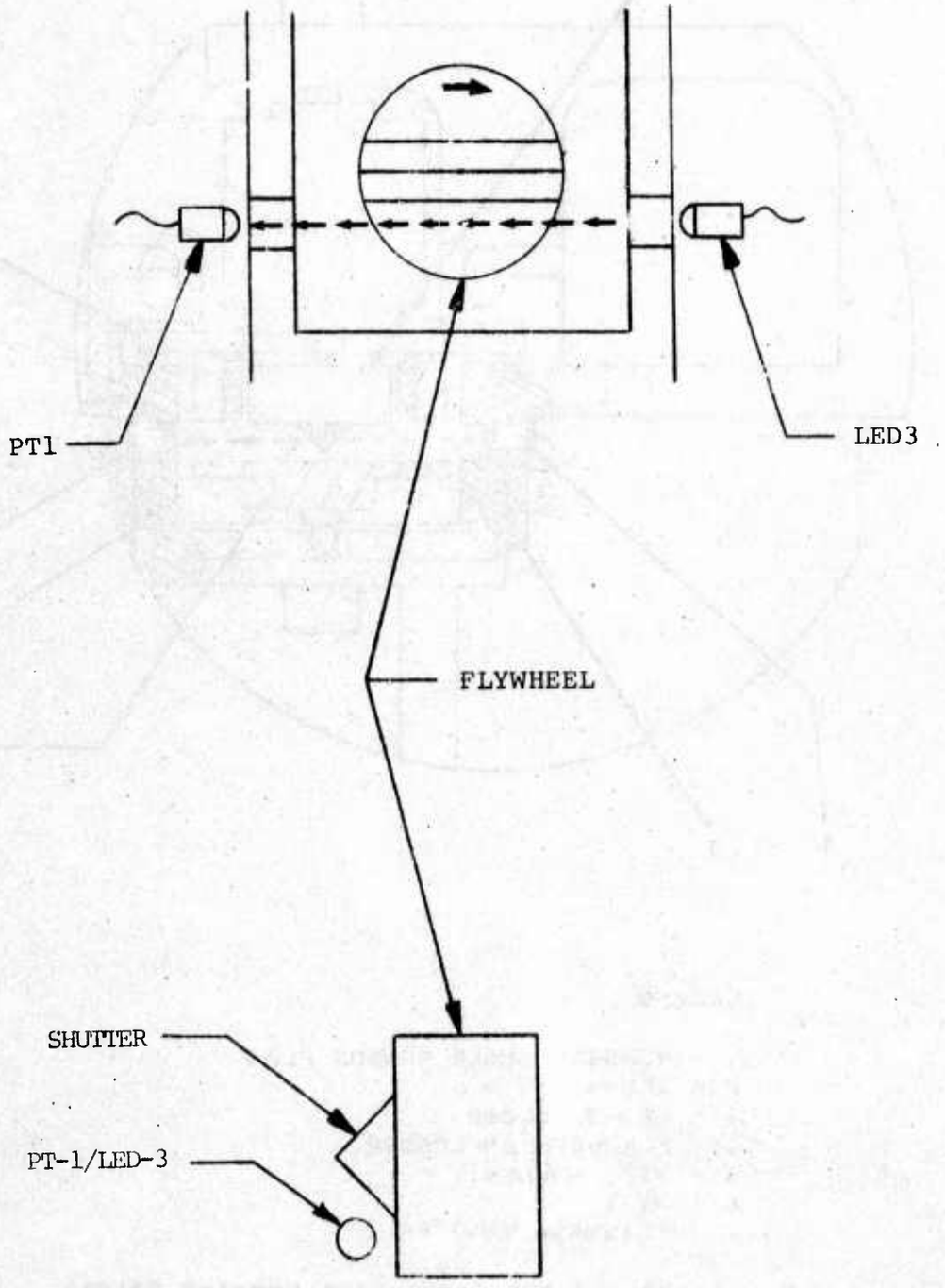

Figure 39. Rotor Revolution Sensing Detail (Concluded)

first two prototypes. Figure 40 depicts the general layout of the system. This concludes the description of the basic assembly. Operation of the system is presented in greater detail in Section XIII.

QTY REQD	SYM	CAGE IDENT	PART OR IDENTIFYING NO	DRAWING OR SPECIFICATION NO	NOMENCLATURE OR DESCRIPTION	ITEM NO
						36
4					SCR, PAN HD	35
2					SCR, FLAT HD	34
						33
						32
2					PIVOT	31
1				1/4 INCH	GROMMET	30
					MOTOR	29
3					L.E.D	28
1			50-749-2		PHOTO TRANSISTOR	27
2			50-751-22		PHOTO DIODE	26
1			MMB 102-2551	25 PIN PT	CONNECTOR	25
						24
1					CKT BD, LOGIC	23
1					CKT BD, CURRANT SW	22
1					CKT BD, SERVO AMP	21
1					CKT BD, SENSOR	20
1			50-7594-1		CASE ASSY	9
2			50-7590-1		HOLDER, PHOTO DIODE	8
2			50-7592-1		BUSHING SLEEVE	7
2			50-7588-1		SLEEVE	6
1			50-7587-1		CAP	5
4			50-7586-4		SPACER	4
4			50-7586-3		SPACER	3
4			50-7586-2		SPACER	12
4			50-7586-1		SPACER	11
1			50-7584-1		HOLDER, PHOTO XSTR	10
1			50-7583-1		HOLDER, L.E.D.	2
1			50-7582-1		MASS, ROTOR	8
1			50-7581-1		ENCLOSURE, ROTOR MASS	1
1			50-7580-1		SHUTTER, PHOTO SENSOR	6
1			50-7579-1		COVER, CAN	5
1			50-7578-1		HOUSING, MOTOR	4
1			50-7577-1		COVER, HOUSING	3
1			50-7576-1		HOUSING, SHIELD	2
1			50-7575-1		HOUSING, DIODE	1

PARTS LIST

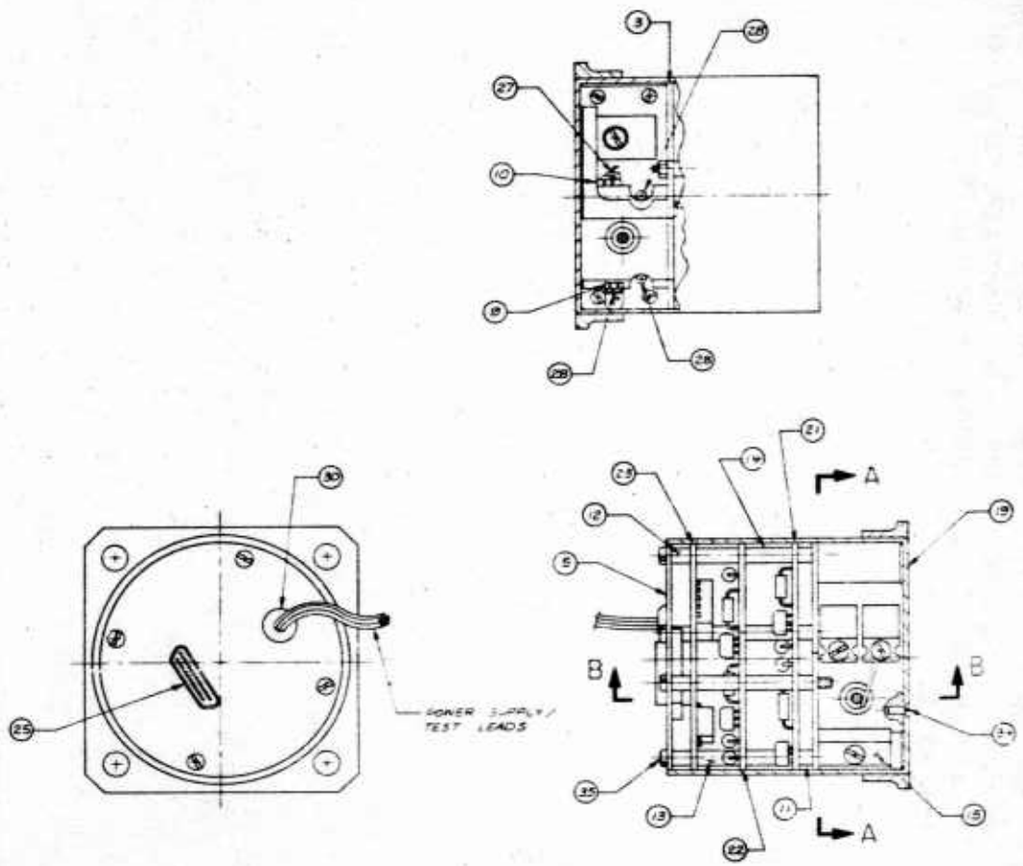

Figure 40. Final Prototype Safe Separation Sensor

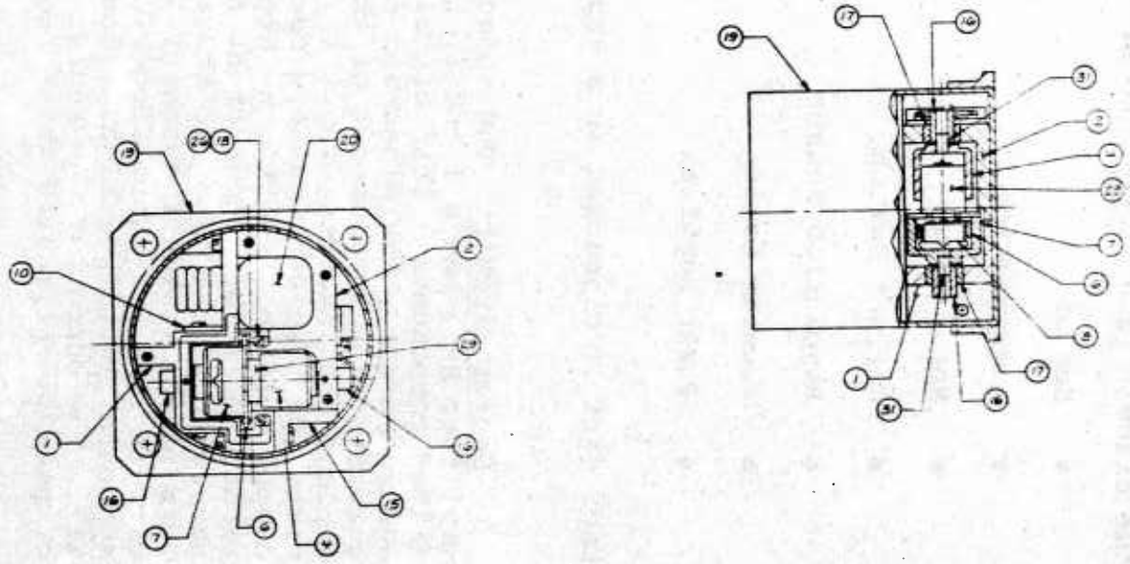

Figure 40. Final Prototype Safe Separation Sensor (Concluded)

SECTION XIII

FINAL PROTOTYPE CIRCUIT FUNCTIONAL DESCRIPTION

This section presents a functional description of the final prototype SSS. The circuit schematic is shown in Figure 41 and will be used in this discussion. For purposes of explanation, the circuit is divided into seven parts as follows:

- Sensor
- Compensation
- Motor Drive
- Current Switch
- Revolution Sensor
- Counter Logic
- Power Supplies

Each part is discussed in a separate subsection.

Sensor Circuit. The sensor circuit consists of operational amplifier AR1, LED's 1 and 2, photo diodes PD1 and 2, and associated components. This circuit functions as a current to voltage converter. The algebraic sum of the two photo diode reverse currents flow into or out of the input to the amplifier, which employs the inverting input terminal. Feedback resistor R1 converts the resultant photo diode current into a dual polarity output voltage. Due to the high input impedance of the operational amplifier, the current flow is very small, and the voltage swing at the input to the input terminal is also small. This is the reason the sensor amplifier presents a dynamic short circuit load for photo diode reverse current. This circuit approach provides a highly linear output as explained in Section XII. The output of the sensor is fed to the first stage of compensation circuits which begin at R4.

Compensation Circuits. The compensation circuits consist of two stages made up of operational amplifiers AR2 and AR3.

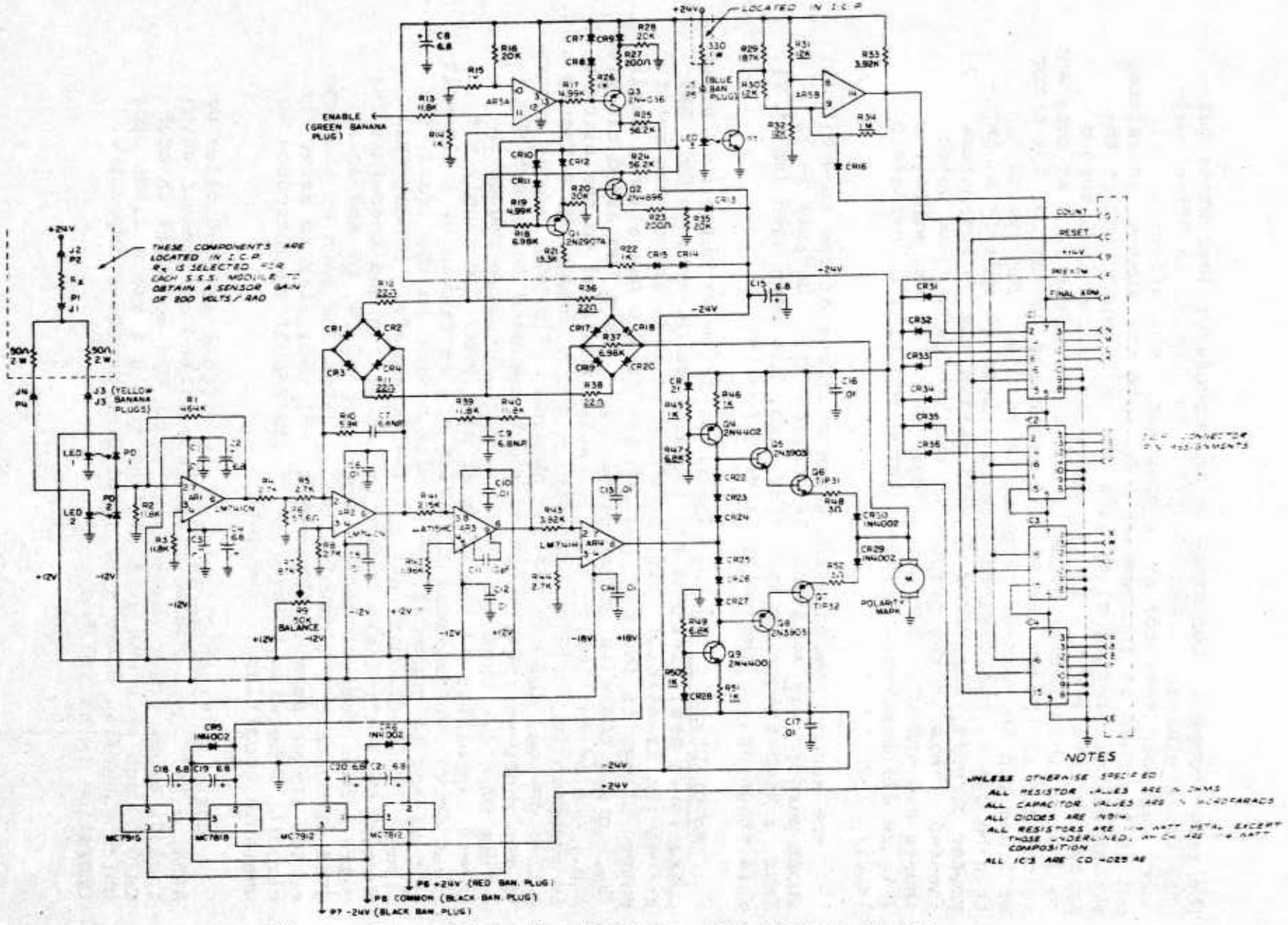

Figure 41. Schematic Circuit, SSS Torque Servo

The first compensation stage is an integrator lead whose purpose was explained in Section XII. To provide an offset balance, variable resistor R9 is provided. The effect of this pot is the same as introducing a T_a into the system; therefore, mechanical or electrical offsets can be balanced out of the system by this means. If the system is placed in a zero g condition, this pot is adjusted until the motor runs at constant velocity. If the system is then reset and restarted, the motor will not run in correct response to zero g. The system can then be run at the desired g level. Because this is an integrator circuit, capacitor C7 will retain its charge unless shunted. This is the purpose of the bridge circuit which shunts R10 and C7. The two bridges shown on the schematic (Figure 41) represent a reset system and will be explained later.

The second compensation stage consists of the lead circuit whose purpose was explained in Section XII. Because it is a lead, a high-frequency amplifier, AR3, has been used (uA715HC). This stage drives the motor drive circuits.

Motor Drive Circuits. The motor drive circuits consist of operational amplifier AR4 and transistors Q4 through Q9. AR4 drives the transistor circuit, which in turn drives the motor. Motor voltage is fed back through R37 to the operational amplifier to set the gain of the stage. This is a two sided circuit, i.e., one of the two polarities can be provided to the circuit in response to positive or negative g. Although the motor is a 6-volt device, the circuit can provide a ±18-volt supply across it for short periods. This approach was used to offset the effect of motor back emf, which would otherwise reduce the torque capability of the motor at high RPM. To supply sufficient drive, operational amplifier AR4 is driven by a ±18-volt supply; and to compensate for voltage drop in the transistor circuit, this circuit uses a ±24-volt supply. Diodes CR22 through CR27 eliminate crossover distortion and therefore require a bias current source consisting of Q4, Q9 and associated circuits. The combination of gains for each of the transistor stages permits the operational amplifier to drive the circuit; otherwise, distortion would result to introduce an unstable condition in the loop.

Current Switch Circuit. This circuit is controlled by AR5A, a voltage comparator, and associated components which include among other parts CR1 through CR4 and CR17 through CR20. Each of these sets of four diodes forms a diode ring which shunts an operational amplifier feedback impedance. Operation is as follows:

When the ENABLE is a logic level 1, the current source consisting of circuits made up of transistors Q1 through Q3 and associated components is off. In this event, resistors R24 and R25 reverse bias the ring or bridge diodes, and they are effectively removed from the circuit. In this instance the entire circuit is free to function as designed.

When the ENABLE is a logic zero, the current source is turned on, and all eight diodes are forward biased. The effective result is that the feedback for AR2 and the driver stage is a short circuit in series with a zero volt generator. Thus the output of each stage is zero. The basic purpose of these circuits is to ensure that the integrator charge is removed and that the motor is not running due to an offset condition. On this basis, the system loop can be controlled by a single enable input from the ICP.

Revolution Sensor. The rotor sensor signal is formed by LED 3 and photo transistor 1 and the rotor shutter as previously explained. Output of this circuit is characterized by slow rising and falling leading and trailing signals, respectively. Therefore, to shape these in a form acceptable to the counters, a voltage comparator, AR5B, is used. The relationships between the comparator output and the counters are the same as in the first two prototypes. When the final arm output at Pin 7 of IC1 goes low at the selected range, AR5B is disabled.

Counter Logic. The counter logic consisting of IC1 through IC4 is the same as that used in the first two prototypes.

Power Supplies. The ±18 and ±12-volt supplies are formulated by regulators MC7918 and MC7812, respectively. These regulators provide low output impedance sources for the operational amplifier to ensure electronic stability. Each of the circuits except the logic are driven by a ±24-VDC source from the ICP. A +15-volt source from the ICP powers the logic circuits. It should be noted that the source current for LED 1 and LED 2 is adjustable by means of resistor R_x. This feature is provided to set the gain of the sensor stage.

The circuit described above is significantly more complex than was originally anticipated. Due to the difficulties experienced in formulation of the design, no effort was made to simplify it within the scope of the present program. Several changes may, however, be made to simplify the circuit. First, if the power is removed from the system and applied at the start of a run, the integrator and drive circuit feedback bridges and associated components may be eliminated. These circuits were used to allow repeated runs for demonstration

purposes. Second, if the rotor moment of inertia is increased to reduce the velocity, less voltage will be necessary and a common source may be used. This will eliminate two regulators and will simplify the output drive circuit. It may also be possible to combine the compensation circuits into a single stage or combine the sensor, compensation and drive circuits into a single stage. During the investigation, a common compensation stage was designed, and it provided the desired response. This effort was conducted at a time when various oscillations were being removed from the system as explained. Separation of the stages was necessary to find the sources of oscillation and having solved these problems, the functional circuit was used.

SECTION XIV

FINAL PROTOTYPE TESTING

Final prototype testing was conducted at room ambient, low and high temperatures. In addition to these complete functional tests, numerous other tests were accomplished to characterize various design problems. These problems were in two areas: electronic oscillations and spring design. To provide the background for interpretation of the functional data, a discussion of the problem areas follows.

Following the analytical calculations which led to the compensation techniques described in Section XII, the circuits were designed and breadboarded for check out. Considerable difficulty was encountered with the lead compensation circuit. Despite numerous layout techniques, this circuit oscillated. Open loop testing of the μA715 operational amplifier was conducted to confirm the manufacturer's frequency response data. It was found that the open loop response was power supply voltage level dependent and that additional poles existed slightly beyond the manufacturer's reported data. Other operational amplifiers were tested and similar results were found. The μA715 was selected because its open loop response more closely matched the desired result when the supply voltage was increased and a lower stage gain was used. Following several layout designs and careful selection of passive parts, the oscillations were corrected and the desired closed loop frequency response achieved. It should be noted that the use of carbon resistors resulted in oscillations and metal film types were successfully substituted.

Following achievement of successful performance of the individual parts of the loop, the loop was closed to checkout the system. Again, oscillations persisted. The loop was opened at selected points and numerous frequency response data were taken. In general, the open loop empirical results matched the analytical predictions; however, several observations were made. First, it was found that when the loop was closed, the voltage at the motor was capacitively coupled to the nearby sensor circuits. Attempts to electrically isolate these two parts of the design proved to be difficult because of their close proximity and the need to transmit sensor light for proper null detection. The problem was finally solved by using a metal null shutter and eliminating direct path coupling. Physically, this amounted to shielding the sensor stage amplifier, its leads and the photo devices while permitting light transmission. It should be emphasized that breadboarding of the system is difficult because

of the shielding problem. It was necessary to fabricate several mounting designs to achieve the correct orientation of parts.

The second closed loop oscillation found was due to vertical spring motion. As the motor rotor velocity increased during a test, any inbalance in that member resulted in a slight displacement at the springs. This deflection was detected by the null sensor and processed in the same manner as T_a. Because of the sensor orientation, only the vertical component was detected, and this appeared within the loop as a sinusoid. The problem was solved by using two photo sensor pairs, one on each side of the motor. These sensors were then connected to the amplifier such that angular motion (in response to T_a) was sensed, and vertical displacement was subtracted. That is, vertical displacement was detected as a positive signal by one sensor pair and negative by the other sensor pair. If properly calibrated, the vertical displacement is thus eliminated from the electrical signals. Because of the unmatched photo parameters, it was necessary to provide a calibration circuit which permitted adjustment of the current through each sensor. In the third area, considerable electrical noise was generated by the photo diodes. This noise was large enough to cause saturation of the operational amplifiers and therefore destroyed loop performance. It was found during testing that the sensor gain could be increased by increasing the LED bias current without increasing the noise content. This permitted the amplified signal to be attenuated, thereby reducing the noise level and restoring the stage gain.

After all oscillations were eliminated and the noise reduced to an acceptable level, frequency response data were taken and found to be consistent with the analytical results presented in Section XII. It should be emphasized that closed loop performance was excellent, that is, null stability was achieved in accordance with the initial objectives.

Before conducting centrifuge and environmental testing, it was necessary to calibrate the system and confirm proper 1 g performance. The system is designed such that when placed in a 0 g condition, the sensor output voltage is 0, thus resulting in 0 motor voltage. Because the null sensors are mounted to the mechanical frame, the springs must be adjusted on a rotational basis until the sensor output voltage is 0. This is a difficult process because the sensor gain is very large and a very slight spring angular offset results in a substantial sensor voltage output. These springs are somewhat delicate and easily destroyed; therefore, they cannot be readily subjected to a press fit. The mounting holes are designed to permit adjustment by means of a set screw. Because there are 2 springs, calibration may result in 1 of 3 conditions. First, both springs are

at their 0 deflection point. Second, 1 spring may be offset, which is an incorrect calibration. Third, each spring is offset but in opposing directions such that sensor output voltage is 0. Any of these conditions may exist following set screw tightening; therefore, a potentiometer is placed at the integration-lead compensation stage input to zero the spring offset effect. The net result of this calibration process is that the motor voltage can be adjusted to 0 when the system is subjected to 0 g. If the motor is running during this calibration, the potentiometer is adjusted until motor velocity remains constant. Then if the system is shut off and restarted, the motor voltage should be 0. Adjustment of the potentiometer is effective, but system changes occur rapidly and recalibration is necessary.

The 1 g data shown in Table 12 is representative of system performance following calibration. Examination of the time column shows erratic performance and a general reduction in time as the run number increases. In addition, between runs, the system was placed in a 0 g condition and the motor accumulated velocity, thereby indicating that a change had taken place in the calibration.

To examine this problem, the integrator lead circuit input was grounded, thereby simulating a 0 sensor output. The potentiometer was also adjusted until the motor voltage was 0. Resulting drift was negligible, thereby indicating that the problem was either in the sensor stage or the springs. Next, the null was clamped to fix the sensor shutter. This removed the springs from the problem and the sensor output voltage remained constant, thus indicating that the problem was related to the spring. To confirm this, the system was placed in a static condition with power applied only to the sensor stage. Sensor output voltage was then monitored for several hours, and an approximate exponental drift occurred. This test was repeated several times with different springs, and the results were similar.

The drift observed above was believed to be related to spring migrations caused by temperature gradients. Such temperature conditions were thought to be the result of mounting power transistors near one of the springs. The transistors were removed and t' e static test repeated. This reduced the drift considerably but failed to eliminate it. It was therefore concluded that the basic drift was probably due to physical stress resulting from the mounting process and aggravated by temperature extremes.

Consultation with the spring manufacturer failed to produce additional spring or mounting information. The mounting technique being used was consistent with one of the manufacturer's

TABLE 12. 1g RUN DATA AT ROOM AMBIENT TEMPERATURE

Run Number	Range Setting (Feet)	Time (Sec.)	Actual Range (Feet)	Range Error (Feet)	Range Error (Percent)
1	1000	7.733	961.99	-38.009	-3.801
2		7.997	1028.8	28.796	+2.880
3		7.713	957.02	-42.979	-4.298
4		7.531	912.39	-87.610	-8.761
5		7.390	878.54	-121.46	-12.15
6		7.289	854.69	-145.31	-14.53
7		7.328	863.87	-136.13	-13.61
8		7.288	854.46	-145.54	-14.55
9		7.258	847.44	-152.56	-15.26
10		7.341	866.93	-133.07	-13.31
11		7.380	876.17	-123.83	-12.38
12		7.380	876.17	-123.83	-12.38
13		7.327	863.63	-136.37	-13.64
14		7.566	920.89	-79.110	-7.911
15		7.567	921.13	-78.867	-7.887
16		7.302	857.75	-142.25	-14.23
17		7.577	923.57	-76.430	-7.643
18		7.611	931.88	-68.123	-6.812
19		7.282	853.05	-146.95	-14.69
20		7.250	845.57	-154.43	-15.44
21		7.305	858.45	-141.55	-14.15
22		7.451	893.11	-106.89	-10.69
23	1000	7.675	947.61	-52.385	-5.239

recommended designs. Because the motor will transmit heat to the springs and environmental temperature changes will occur, relocating the transistors was not accomplished.

To find a solution to the drift problem, the various observations were re-examined and the following conclusions made. First, reduced drift was observed if the springs were lightly held. Second, performance was much less erratic on occasion, thereby indicating that a tightly held spring is less susceptible to location changes due to the application of motor torque or outside forces such as shock or vibration. Table 13 contains data taken from 27 consecutive runs. Assuming a calibration error of 48 percent, the variational error (repeatability) seen is quite small (1 percent). This indicates that with moderately tight spring mounting, the device will perform reasonably well.

To provide further temperature data, the device was subjected to -65°F and +160°F. While at the low temperature, the device was run 25 times, and the resulting data are shown in Table 14. Here again, assuming a 53 percent calibration error due to drift during the soaking period, the variational or repeatability error is reasonably small at 3.4 percent. This data is similar to that taken at ambient temperature. Attempts to conduct temperature testing at +160°F failed because binding occurred between the rotor and the bearings. This problem could not be corrected because the basic motor construction prohibited disassembly. No further attempt was made to conduct high temperature tests.

To summarize the drift problem, no solution was found and further investigations were beyond the scope of the program. It is believed however, that the problem can be corrected by 2 approaches. First, a spring and mounting study should yield the most favorable design and assembly procedure. Second, various changes in other system parameters can be accomplished to permit a larger offset level. For example, a large 1 g T_a accompanied by a larger rotor moment of inertia will improve offset situations.

It was mentioned earlier that the springs were delicate and easily damaged. This problem was primarily due to fatigue and repeated handling. However, during this portion of the program, approximately 25 springs were damaged or otherwise rejected because of incorrect operating parameters or visual defects. For example, a very non-linear effect was observed as a spring was moved from positive deflection through 0 to negative deflection. The spring manufacturers refer to this condition as hysteresis. In many springs hysteresis was negligible; however, it was quite prominent in others. On the basis of these types

TABLE 13. DATA FOR CONSECUTIVE 1g RUNS AT ROOM AMBIENT TEMPERATURE

Number	Range Setting (Feet)	Time (Sec.)	Actual Range) (Feet)	Range Error (Feet)	Range Error (Percent)	Variational Range Error (Percent)
1	1000	5.672	517.54	-482.46	-48.25	-0.1365
2		5.703	523.22	-476.78	-47.68	+0.4308
3		5.722	526.71	-473.29	-47.33	+0.7800
4		5.716	525.61	-474.40	-47.44	+0.6696
5		5.708	524.13	-475.87	-47.59	+0.5226
6		5.675	518.09	-481.91	-48.19	-0.08170
7		5.701	522.85	-477.15	-47.72	+0.3941
8		5.736	529.29	-470.71	-47.07	+1.038
9		5.674	517.91	-482.09	-48.21	-0.09995
10		5.692	521.20	-478.80	-47.88	+0.2292
11		5.693	521.38	-478.62	-47.86	+0.2475
12		5.664	516.09	-483.91	-48.39	-0.2823
13		5.699	522.48	-477.52	-47.75	+0.3574
14		5.696	521.93	-478.07	-47.81	+0.3025
15		5.660	515.36	-484.64	-48.46	-0.3552
16		5.679	518.82	-481.18	-48.12	-0.008638
17		5.695	521.75	-478.25	-47.83	+0.2841
18		5.677	518.46	-481.54	-48.15	-0.04517
19		5.663	515.90	-484.10	-48.41	-0.3006
20		5.636	511.00	-489.00	-48.90	-0.7913
21		5.646	512.81	-487.19	-48.72	-0.6093
22		5.646	512.81	-487.19	-48.72	-0.6098
23		5.662	515.72	-484.28	-48.43	-0.3188
24		5.691	521.02	-478.98	-47.90	+0.2109
25		5.642	512.08	-487.92	-48.70	-0.6825
26		5.621	508.28	-491.72	-49.17	-1.063
27	1000	5.675	518.09	-481.91	-48.19	-0.08170

TABLE 14. LOW TEMPERATURE 1g RUN DATA

Run Number	Range Setting (Feet)	Time (Sec.)	Actual Range (Feet)	Range Error (Feet)	Range Error (Percent)	Variational Range Error (Percent)
1	1000	5.599	504.31	-495.69	-49.57	+3.423
2		5.540	493.74	-506.26	-50.63	+2.366
3		5.368	463.55	-536.45	-53.64	-0.6522
4		5.424	473.28	-526.72	-52.67	+0.3200
5		5.428	473.97	-526.03	-52.60	+0.3899
6		5.378	465.28	-534.72	-53.47	-0.4793
7		5.378	460.11	-539.89	-53.99	-0.9969
8		5.439	475.90	-524.10	-52.41	+0.5822
9		5.442	476.42	-523.58	-52.36	+0.6347
10		5.299	451.71	-548.29	-54.83	-1.836
11		5.473	481.87	-518.13	-51.81	+1.179
12		5.449	477.65	-522.35	-52.24	+0.7573
13		5.496	485.92	-514.08	-51.41	+1.585
14		5.332	457.36	-542.64	-54.26	-1.272
15		5.492	485.22	-514.78	-51.48	+1.514
16		5.320	455.30	-544.70	-54.47	-1.477
17		5.342	459.07	-540.93	-54.09	-1.100
18		5.348	460.11	-539.89	-53.99	-0.9969
19		5.359	462.00	-538.00	-53.80	-0.8075
20		5.375	464.76	-535.24	-53.52	-0.5312
21		5.298	451.54	-548.46	-54.85	-1.853
22		5.403	469.62	-530.38	-53.04	-0.04571
23		5.472	581.69	-518.31	-51.83	+1.161
24		5.300	451.88	-548.12	-54.81	-1.819
25	1000	5.403	469.62	-530.38	-53.04	-0.04571

of observations, it was concluded that characterization of acceptable spring performance is necessary prior to use of the design. Attempts to conduct centrifuge testing on the final prototype were not successful. In each of two separate tests, at least 1 spring was damaged. This spring fatigue problem coupled with temperature drift resulted in unusable data.

SECTION XV

FAILURE MODES AND EFFECTS ANALYSIS

This section includes a qualitative analysis of various failure modes and their resulting effects. In general, all SSS design approaches accomplish the same basic functions; therefore the analysis presented here is concerned with those failure modes which will be common to all types. There probably are no specific failure modes unique to a particular design technique from the standpoint of functions that need to be implemented for correct operation. Unique failure aspects are normally characteristic of the specific part or configuration used to accomplish a particular function. Normally if two radically different designs are used to accomplish the same task, it is likely that a failure in either case will produce the same functional result. Aside from cost considerations, one design approach will be picked over another on the basis of reliability or probability of a particular type of failure. In the analysis that follows, failure modes are discussed first from the broad functional viewpoint. This is followed by a more detailed account of specific part or component performances. Lastly, techniques are presented for overcoming or minimizing various failure modes.

Functional Failure Modes. The SSS is a distance measuring device which controls or implements arming functions at specified ranges from the launch vehicle. Any failure which reduces the arming range to dangerous proportions is therefore obviously undesirable from the safety viewpoint. Failures which increase the range may result in a dud or fail-safe mode which denies mission accomplishment. These are the two primary modes of failure. It should be noted that in most low-cost designs there will be a specified range tolerance. For the present purposes, a failure exists if the range measured by the SSS is outside the specified tolerance.

Any system failure causing motor acceleration beyond that which the system is experiencing due to missile performance will result in a short arming range. Such a failure may be either electrical or mechanical as follows.

Electrical Failure Modes - In the SSS design, it is necessary to provide proportional electrical energy to the motor as required to accomplish the function of double integration. Any electrical failure which upsets the ability of the system to

provide proportional energy will result in a range error. Such an electrical failure may be total or intermittent, with a shorted motor across terminals being the most catastrophic. In all designs, whether the null tracks or oscillates, one or more transistors will be used to supply power to the motor. If this transistor circuit fails by shorting, dangerously short ranges will be experienced. The transistor circuit is driven either directly or indirectly by the null sensor. The sensor may be either electrical or mechanical, and failure of this mechanism can result in either removal of power or application of full power.

A mechanical null sensor is normally a switch. A shorted switch will result in a runaway motor which provides short ranges. An open switch failure will provide long ranges. The electrical null sensor can experience the same failure modes as any other electrical circuit.

Range information can be accumulated either electrically or mechanically. To date, digital counting techniques have been used to accumulate and determine coincidence with the selected range. Circuits which accomplish this function may fail independently of SSS operation. For example, undesirable electrical pulses may be accumulated by the counter, and since each pulse represents an increment of distance, the range will be shortened. Since coincidence is also accomplished electrically, an undesirable pulse or electrical signal can occur which forces the circuit to assume the coincidence condition. For example, if the counters are designed to operate in the count-down mode, coincidence will occur when the total count reaches zero. An inadvertent reset pulse on the counters can result in a zero count output, thereby signaling that final range is reached.

Mechanical devices which accumulate the range information are normally a part of the SSS itself or are controlled by the SSS. This simply means that to advance toward arm, the range accumulation mechanism must receive its power from the SSS. Therefore, it is reasonable to conclude that range failures will be SSS oriented and thus characterized by SSS failure modes.

Mechanical Failure Modes - The most important mechanism whose failure can produce undesirable range information is the null mount. To accomplish correct acceleration detection, the null must be free to move under the influence of motor torque and missile acceleration torque. Any other torques or disturbances which are not of this variety will result in range error. Such a failure in most cases involves a sticking null caused by

bearing contamination or other foreign materials to inhibit or restrict normal null operation. If a null sticks in the power portion of its normal travel range (toward the aft of the missile), the null sensor will command the motor to run. This will produce a short range. If the switch sticks in the upper portion of normal travel, a long range is experienced.

Aside from those mechanical failures mentioned in previous paragraphs, a sticking null is the only mechanical failure mode which has been envisioned. However, it is the most difficult to overcome with appropriate design procedure. Specific details on this failure mode are discussed later.

To summarize the general analysis, it can be concluded that all failure modes which can exist to supply excessive electrical power to the motor will result in dangerously short ranges unless appropriate design techniques are implemented to detect and overcome such an occurrence. Any failure mode which inhibits or rations the electrical power which the motor receives will result in a long range.

Detailed Component Analysis. These paragraphs include specific failure information on individual components which contribute to the addition or subtraction of electrical motor energy. As stated previously, entirely different hardware configurations may be used to accomplish the same function. The basic functions are:

- Null Sensing
- Electrical Control
- Range Accumulation
- Arming Functions

Each of these functions is discussed in detail below along with the various techniques used to accomplish them.

Null Sensing - For discussion purposes, null sensing includes the null sensor, associated electronics and null assembly consisting of the motor stator and the unbalanced mass. As previously stated, the sensor may be either a mechanical switch or an electronic design. The mechanical switch is the simplest design with the fewest parts; however, it is the least accurate of the two approaches, since it inherently increases null friction. The basic configuration is shown in Figure 42. Figure 42 shows a general null switch configuration and its relative orientation to the overall physical arrangement. When the null or unbalanced mass is torqued counterclockwise in response to missile acceleration in the direction

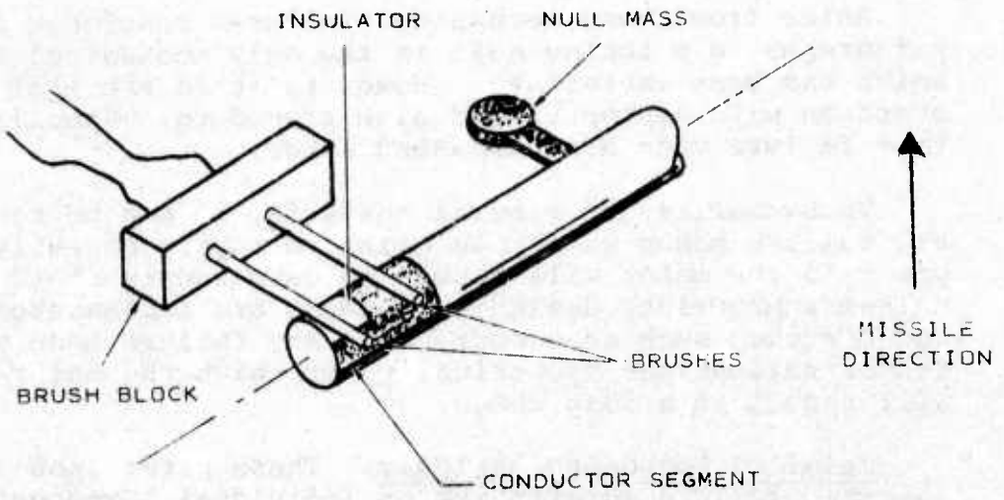

Figure 42. Null Sensing Design

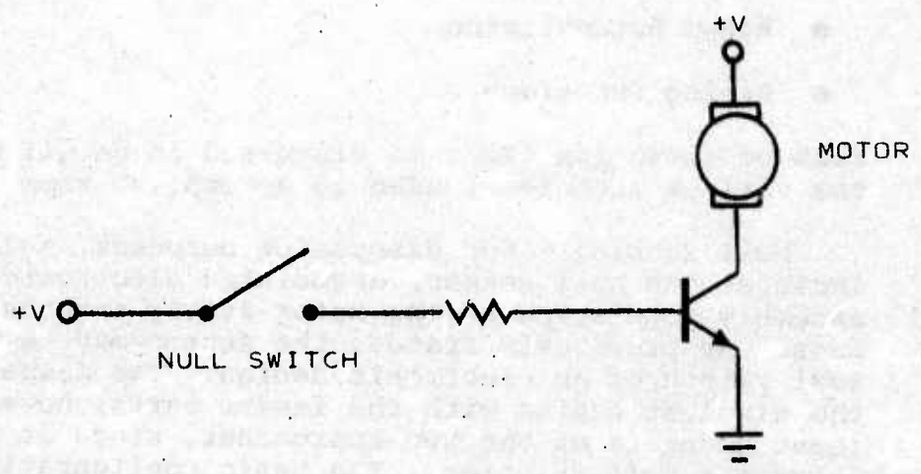

Figure 43. Motor Power Schematic

shown, the null switch is closed by the two brushes and the conductor segment. Closing the switch permits power to be supplied to the motor in the simplified manner shown in Figure 43. When the null switch closes, the transistor is turned on, thus supplying current to the motor. A motor torque is developed on the null mass in opposition to the torque caused by missile acceleration. In the oscillatory mode, this motor torque is greater than the acceleration torque. Therefore, the null mass moves clockwise to open the switch. The switch design can only be used for the oscillatory mode, since it is a bang-bang device. If the switch brushes short or a short occurs anywhere in the circuit such that the switch contacts are electrically bridged, the motor will accelerate at its full capacity, thereby introducing a dangerously short range.

Contamination on the insulator, if conductive, can also produce continuous current to the motor and cause a short range. Contamination which insulates would be the more usual failure condition and would result in a long range. Experience during the SRAM program has shown that insulating types of contamination are the most common and are of the fail safe variety.

Since the brushes must be in contact with the null for proper electrical operation, they contribute frictional torque to the null assembly and thereby influence its operation. If this friction becomes excessive, the null can be held in either the closed or the open position. The result of each of these failures has been characterized. The likelihood of excessive null brush friction is dependent on the particular SSS design. If the motor is quite large with ample torque, such excessive friction can be tolerated to a much larger extent than with a very small motor. In other words, if the brush pressure becomes excessive in a large motor, the motor torque applied will always be greater than any friction which can be developed. In this instance the switch will probably stick in the off position, resulting in a long range or a fail safe condition.

The second technique used to date for sensing null operation consists of a photo diode (LED)-photo transistor (PD) pair. The typical simplified schematic is shown in Figure 44. The LED is oriented relative to the PD such that its emitted light impinges on the PD unless interrupted by the null shutter. If the null shutter falls down under the influence of missile acceleration, the LED light will be sensed by the PD. This turns on the PD and therby turns on the motor transistor. Motor torque is then developed to move the shutter upward and interrupt the light. This shuts off the PD and removes motor power.

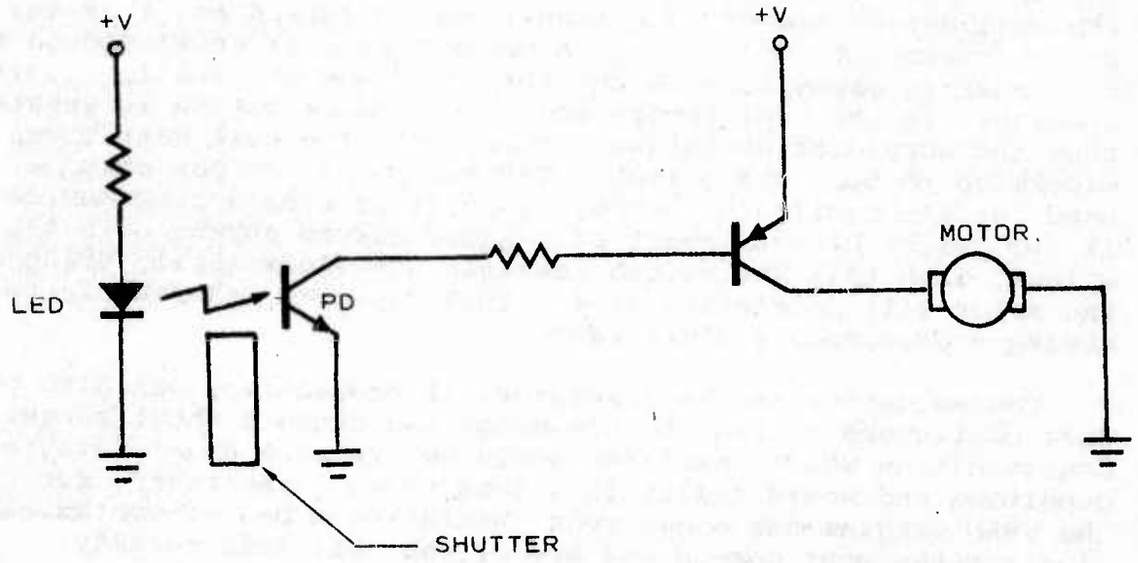

Figure 44. Optical Null Sensing Schematic

This arrangement may fail in a manner similar to that for the mechanical null switch. Since the LED emits light at all times, its failure can only produce a fail safe condition. For example, without light impingement on the PD, it cannot turn on. Therefore, no power can be supplied to the motor to produce range. The photo transistor performs the same task as the mechanical switch, so if it shorts by any mode the motor transistor will be turned on to produce a runaway condition. The advantage of using this approach is that there is no physical contact between the null assembly and the sensor. Frictional sticking is thus not present due to the sensor. In addition, contamination will not present a problem with this design approach. There are no contacts, since all components are hand wired.

For purposes of the present discussion, the technique used to mount the null assembly relative to the missile frame is considered part of the sensing elements. The two basic design approaches used for this program have failure modes which are quite different. In the first two design iterations, ball bearings mounted the null and provided the appropriate degree of freedom. The third (last) iteration uses torsional or pivotal springs. For the ball bearing approach, the mechanism which contributes to failure is quite well known. Ball bearing contamination or other bearing failure modes can contribute to

a sticking null, and the system may either run away or stop. Ball bearing malfunction is the most significant failure mode which has been considered, since in general all other problems can be detected and overcome by reasonably simple means. To date the best defense against such bearing failure mechanisms is through appropriate assembly and quality control procedures.

Though more costly, the flexural or pivotal spring approach used in the final prototype is probably the more reliable. This must be a qualified statement, since adequate life information has not been accumulated. For example, the springs may be correctly designed to withstand loading and other effects; however, under the influence of normal operation and vibration, metal fatigue may occur to the extent that a failure could result. The spring manufacturer indicates that for small deflections the total number of deflections which can be realised is unlimited, and this is the normal mode of operation. If, however, a spring fails such as to permit improper null operation, either a runaway or stopping failure mode is possible. The likelihood of such spring failure is very small compared with the possibility of null bearing failure or contamination. It is interesting to note that contamination of the ball bearings may result in freezing of the null when the system is at low temperatures. The springs are not particularly susceptible to contamination unless the accumulation of foreign materials is excessive.

Electrical Control Functions - Figures 42 through 44 illustrate motor power control. Such control consists primarily of one or more transistors, depending on the size of the motor and the null mode of operation. If an oscillating null is used, the circuit is basically very simple. If a tracking null is implemented, compensating circuits are needed which can be accomplished with transistors or operational amplifiers. In either situation, any circuit short or open that removes or alters sensor control of the motor will result in a failure. The failures can be of either the runaway or stop variety. For example, shorting of the motor transistor will supply enough motor power to produce a runaway condition. An open circuit will produce the opposite result. As will be seen later, almost any electrical failure mode may be overcome by a simple low cost mechanism to produce a fail safe condition.

Range Accumulation - Range information is accumulated by two basic techniques. First, a digital or electronic/electrical design is used where one or more pulses are generated per revolution. These pulses may be generated mechanically by brushes or electronically by LED-PD pairs. Pulses can be accumulated either on electronic counters or used to

drive a stepping motor. The stepping motor serves the function of reducing the motor turns count to less than one revolution. In other words, the SSS motor may turn 1,000 revolutions and provide 1,000 output pulses, while the stepping motor being driven will turn its output less than one turn. This means that range coincidence may be accomplished by activating frame mounted switches and/or moving a barrier plate a specified angular displacement less than 360 degrees.

If an electronic counter approach is used, the counters will be responsive to pulses introduced by external or internal sources. These pulses can advance the counters to produce a false range; however, it should be noted that such processing of unwanted signals will occur only with a malfunction of a correctly designed circuit. Such failures may include an intermittent ground, failure of the counter chip or various shorting mechanisms.

The stepping motor approach is much less susceptible to inadvertent advancement due to the introduction of unwanted pulses, since much greater power is required. The stepping motor may be advanced, however, if an intermittent short occurs at its input terminals. Failure to receive advance pulses will result in a longer range.

Motor Failure Modes - Since the motor is both electrical and mechanical, it is discussed as a separate item. In general, no motor failure mechanism could be formulated which can result in very short ranges. Typically any motor malfunction will result in a loss of performance, leading to a longer range. Depending on the g profile, certain motor failures may occur which simply reduce the efficiency or performance of the motor. Correct SSS operation may still occur. Motor failure modes are:

- Brush Failure
- Commutator Failure
- Loss of Magnetism
- Winding Shorts or Opens
- Motor Bearing Failure
- Motor Power Supply Failure

Each is discussed below.

Brush Failure - Brush Failure may consist of an open, an increase in apparent motor resistance or shorting to ground.

An open in a two-brush motor will result in a fail safe system if such failure occurs prior to beginning a run. Otherwise the arming range will be increased. A two-brush open prohibits power from being supplied to the motor, thus destroying the ability to integrate. If a motor has more than two brushes, the system can provide a limited capability, since motor torque, though reduced, may still be developed.

Any contamination between the brush and commutator strap can result in an increase in apparent motor resistance. Again, this reduces the capability of the system to integrate large levels of acceleration. This is because total current which the motor can draw is reduced. Since motor torque is proportional to current, the reduction in current reduces the ability of the motor to accelerate in response to missile acceleration. The exact amount of reduction in capability is dependent on the increase in apparent resistance. If an insulator which separates the brush from the grounded portions of the assembly fails, the motor will not run. It is probably true that a fail safe condition can occur in this case, because either the motor will not run at all or if velocity is present at the time the short occurs, the motor will stop quickly and stop further accumulation of range.

Commutator Failure - Again, a commutator failure cannot produce a shortened range. A shorted commutator is the same as shorting the motor coils; therefore, the ability of the motor to develop torque is reduced or eliminated. The result of a shorted commutator is either a fail safe or lengthened range. An open commutator will produce a similar result, except a lengthened range is more likely than a fail safe condition. This is highly dependent on the number of motor coils, the point in a run where the failure occurs, and the g level which must be sensed. For example, a DC motor having 36 commutators will undergo a small reduction in performance if one opens. If there are four commutator segments, the motor assumes a two-pole posture if one opens, thereby reducing the torque which can be developed to 50 percent or less. If there is no velocity at the time failure occurs, the motor will not commutate properly and may not accelerate at all.

Loss of Magnetism - Normally, two magnets are used in a permanent magnet motor. It is a very rare occurrence to see the total loss of magnetism; however, loss in any form will reduce the torque producing capability of the motor. Again, this will produce a long range. Some magnetic materials are susceptible to temperature extremes. For example, ceramic magnets experience a reduction in field strength at low temperatures; however, if used, the design can be set to overcome such a condition.

Winding Shorts or Opens - These problems are similar to commutator failures, except much less reduction in motor torque may result if the short occurs in a coil at a point where very few windings are involved.

Motor Bearing Failure - Bearing failure will result in a lengthened range, since such failure as may be defined consists of an increase in friction. An increase in bearing friction beyond an acceptable value means that a larger portion of the available motor torque will be consumed. This will reduce the amount of torque which can be used to accelerate the rotor. Therefore, the motor cannot follow the demanded acceleration rate, and a larger range will result.

Motor Power Supply Failure - Loss of power to the SSS will result in failure to arm or arming at a long range if failure occurs near the end of the integration process.

Failure Mode Safeguards. For the present purposes, it is assumed from a safety standpoint that a larger than desired range is more tolerable than a shortened range. On this basis, such designs or parts added to the system to detect and correct failures should be those which prevent the motor from accelerating beyond the desired rate. In the paragraphs that follow, recommendations are made for design approach selections and techniques for safeguarding.

Every SSS design will be formulated such that the motor can accelerate at a larger rate than required for the worst case g profile which is to be detected. Because of this, the motor can cause short ranges if a malfunction occurs, even if a very large g is seen by the device at the time of malfunction. Therefore, to provide appropriate safeguards, it is necessary to select a design approach where the number of failure possibilities which contribute to runaway is reduced. The design should be such that runaway conditions are easily detected and corrected. Without a parallel or redundant system, correction of a runaway device amounts to dudding or fail safe operation.

As stated in previous paragraphs, there are two general conditions which can produce a runaway system. These are sticking null bearings and electronic failur s which result in application of full motor power. Examination of these conditions reveals that the application of excessive motor torque due to an electronics problem will result in a very large null excursion. This means that the null will travel outside its normal operating range; therefore, a reasonably simple mechanical device may be used to capture the null and remove all system power. This will produce a fail safe condition.

Motor runaway caused by a sticking null is a difficult problem. To date no safeguard design technique has been formulated except to place emphasis on reliability of null bearing performance. To reduce the number of failure mechanisms which can result in shortened ranges, the range accumulator device should be connected to and be a part of the motor rotor. This may be accomplished by the addition of gear trains or alteration of the K factor. Since the sticking null is more difficult to overcome than an electrical short, null detection should be accomplished by a means which does not require mechanical attachment such as that seen by the null switch design. Such mechanical attachment will result in the increased possibility of a sticking null, while electronic means can produce the short failure which can be overcome.

To summarize the FMEA, it is clear that many failures may occur which can contribute to either short or long ranges. Of these, only one failure can occur for which a safeguard other than reliability consideration has not yet been found. This is the sticking null.

SECTION XVI
SUMMARY AND CONCLUSIONS

The basic function of an S&A is to provide a safe separation distance between the missile and launch vehicle before arming may occur. Any inaccuracy in the acceleration/distance measuring capability of the S&A will result in either decreased operational capability or increased risk to the launch vehicle. Of the various launch parameters which contribute to the determination of safe separation, distance is usually the best indicator of risk level. Because boost or acceleration profiles vary widely, measurement of the distance is difficult.

Most conventional missile S&A's employ timers or pseudo-integrators individually or in various combinations. They provide only a rough indication of distance travelled. Typical errors in safe separation distance measurement are from ±20 to ±40 percent. Whenever a new munition is being developed, severe tradeoffs between launch vehicle safety and operational capability must be made because of these accuracy limitations. Launch safety is not entirely determined by distance but by a complicated interaction of the aircraft flight parameters and fragment trajectories. However, separation distance can be the most valuable index of safety if sufficient accuracy can be achieved. Because missile motor performance varies as a function of temperature and design tolerances, it is necessary to detect acceleration and perform double integration to yield accurate distance information. A device which will accurately perform this double-integrating function is the Flight Environment Sensor (FES) aboard the Air Force SRAM missile.

The basic objective of the present program was to determine if the SRAM FES double-integrating feature could be successfully adapted to conventional S&A devices. Specifically, the acceleration detection range was to be extended and space consumption reduced while maintaining a high level of accuracy and reliability. This program produced hardware and performance data which supports the conclusion that a significant improvement in range information can be realized if an SSS is used in a conventional S&A.

When subjected to acceleration up to 6g, the SRAM FES produced an accuracy of about 0.5 percent in an optimum range of 13,000 feet. It was packaged in a container 11 by 4 by 3 inches. The SSS prototypes designed and fabricated during this program demonstrated a potential distance accuracy of 1 percent when subjected to acceleration profiles up to 27g's. The device is

packaged in a cylindrical container 2.59 inches in diameter by 2.62 inches deep. Power consumption was comparable to existing fuzes such as the Maverick Missile S&A. Additionally, the flexibility of the concept was demonstrated as reflected by Table 15.

In summarizing advantages offered by the SSS concept, it is necessary to emphasize that the SSS will process negative acceleration as well as positive. It can integrate varying and very small accelerations, including fractions of a g. At 0g, it will maintain the existing velocity. From a compatibility viewpoint, it is important that the SSS is not a delicate instrument. The care which must be exercised in assembly is similar to that required for fuzes now in use. From the viewpoint of producibility, the SSS may be characterized as merely a permanent magnet DC motor mounted on a set of ball bearings to provide a second degree of freedom. Based on information collected during the SRAM SAF development program and this exploratory development program, almost any DC motor can be used in an SSS design. Because motors of all types have a long history of success in military applications, ruggedness has been thoroughly demonstrated. The combined features described here and in the body of this report suggest a broad range of S&A applications for the SSS concept. Because the device can be packaged in a variety of sizes and can integrate a broad range of accelerations, the processing of accurate arming information for both powered and unpowered munitions appears to be within reach.

As stated, this program consisted of exploratory development. The effort provided the necessary information to proceed into advanced development. The next logical step is to adapt the SSS to a full-scale S&A. At this writing, such a program is being conducted under sponsorship of the Air Force Armament Laboratory. To implement the SSS into an S&A, the advantages and disadvantages of each configuration previously built were evaluated. This evaluation led to a unique technique for accumulating range information. Because internal motor friction does not affect accuracy, a reduction gear train can be mounted between the motor rotor and stator. This gear train can in turn drive an explosive barrier plate toward armed alignment as a function of missile displacement. The gear train and barrier plate are assemblies normally used in conventional S&A's. Because of this design similarity, use of the SSS can be described as a device which eliminates the frictional effects contributing to the basic inaccuracies of a typical S&A. From this viewpoint, the SSS does not represent a radical departure from the usual design approaches. As an example, consider one of any number of S&A's now in use which feature two arming functions consisting of explosive barrier

TABLE 15. COMPARISON OF BASIC SSS DESIGNS

Feature	SRAM FES	Breadboard SSS	Preliminary Prototype SSS	Final Prototype SSS
Motor Size (Diameter x length in inches)	1.5 x 1.0	1.0 x 0.35	1.0 x 0.35	0.5 x 0.5
Commutator Type	Carbon Brushes	Photo	Photo	Wire Brushes
Null Detection	Mechanical Switches	Photo	Photo	Photo
Mounting	Ball Bearings	Ball Bearings	Ball Bearings	Springs
Motor Bearings	Ball	Ball	Journal	Ball
g Detection Range	+6, -5	+27, -5	+27, -5	±50
Range Accumulation	Stepping Motor	Digital	Digital	Digital
Programmable Range	No	Yes	Yes	Yes
Motor Power Consumption (watts)	90	45	45	25
Null Performance	Oscillatory	Semi-Tracking	Semi-Tracking	Tracking

plate alignment and closing of firing circuits. The firing circuits are normally mechanically connected to the barrier, which is driven by an escapement coupled to a g weight.

With the SSS/gear train design described briefly above, implementation is essentially identical to in-use S&A's. It may therefore be concluded that on a comparative basis, the difference in cost between an SSS-based S&A and an in-use S&A is approximately the cost of one permanent magnet DC motor. Such a difference will be typically a small percentage of the total fuze cost; however, this comparison is much less significant than the possible cost savings which can be realized if an SSS-based S&A can significantly improve the effectivity of the missile. Based on the information gathered during these exploratory programs, the promise of an accuracy improvement to the extent necessary to provide operational flexibility with safety appears quite feasible.

(The reverse of this page is blank)

APPENDIX

INSTRUMENT CONTROL PACKAGE (ICP)
FUNCTIONAL AND OPERATING DESCRIPTIONS

FUNCTIONAL DESCRIPTION

The ICP has been modified so that both position system and torque system SSS modules may be functioned. The operational procedures listed apply to both systems except where noted. Two circuit schematics are provided (Figure 45), one of the ICP, the other for the modification performed to accommodate the final prototype. For explanation purposes, the circuit is divided into the following sections:

- Time and Range Displays
- Clock Circuits
- Timer Circuits
- Range Selection
- Power Supplies
- Control Logic

Each of these circuits is discussed below.

Time and Range Displays. The two display circuits, time and range, are identical except that provisions for a decimal are made on the time circuits. Input count is accumulated by four TTL decade counters, P/N N8280A. The four binary outputs of the four counters are routed to decoder-drivers, S/N 7446N. Decoder-drivers accept the binary information for decoding into seven segment display signals. The equivalent circuit for each segment is shown in Figure 46. As shown, the S/N 7446N provides a ground for a segment to be lighted; otherwise the output is high at 2.9 volts. The 68-ohm resistors limit the current to each display segment.

Segments are checked by placing a high at the L/T input or pin 3 of each display. A switch on the control panel is used to place this high for illuminating all segments of both displays. Thus, when this switch is depressed, each digit shows an 8. Depressing the L/T switch also illuminates the arm and prearm indicators.

Switch S7B is used to place the decimal point for the elapsed time display. For 10-millisecond accuracy, it is moved one digit to the right. The time measurement capability is then up to 99.99 seconds for the 10-millisecond selection and 9.999 for the 1-millisecond selection. Range limits are 9999 feet.

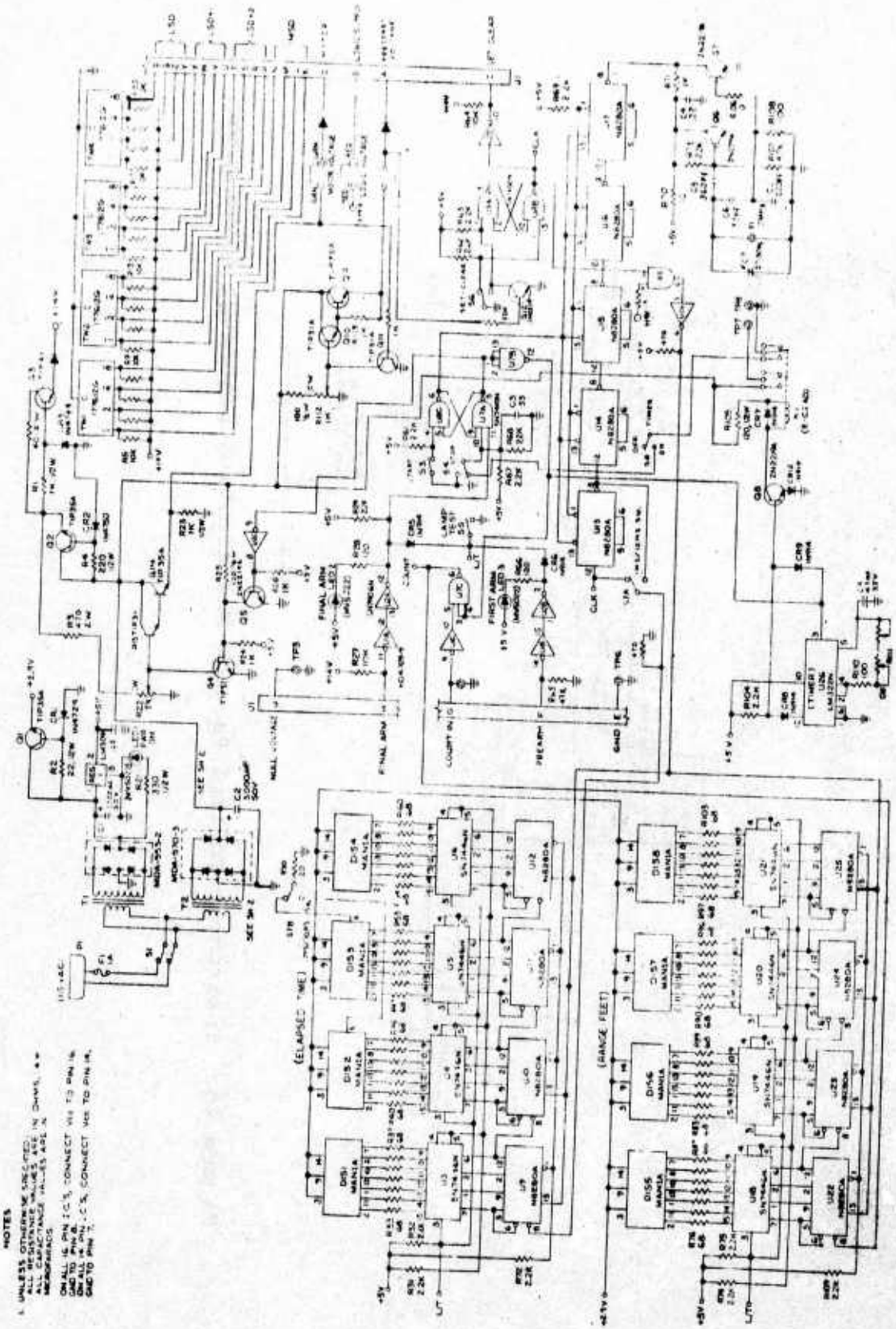

Figure 45. Instrument Control Package Schematic

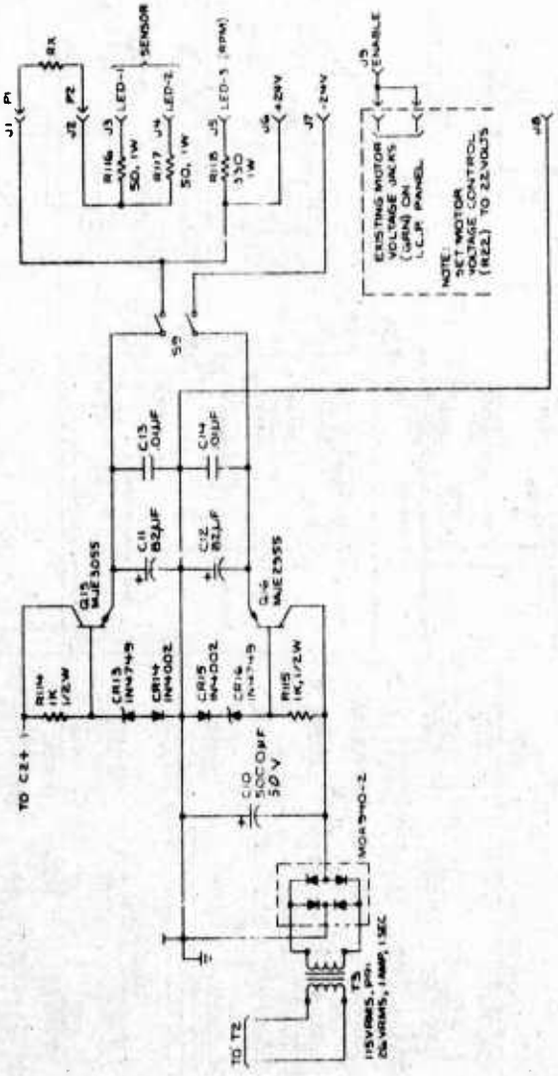

Figure 45. Instrument Control Package Modification Schematic (Concluded)

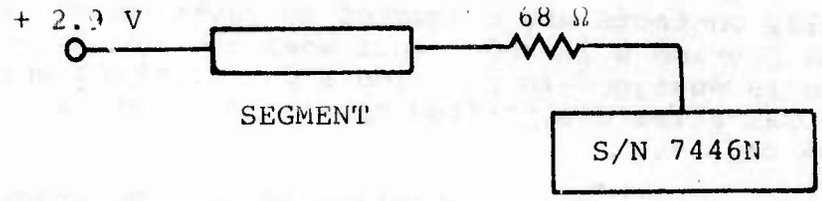

Figure 46. Display Circuit

The clock input for the range is routed from the SSS via connector pin G through an inverter (U1C) and NAND gate (U7C). This logic will be explained later. Pin 13 of each counter is the clear point. A logic zero at these pins results in a zero display for all digits.

Clock Circuits. The clock input for the elapsed time circuit is provided by a 10-megahertz crystal and oscillator circuit plus 5 divide-by-10 counters U13 through U17. The output of the 10-MHz clock is present at the collector of transistor Q7, which is fed to the first divide-by-10 counter U17. Pin 12 of U17 is then a 1-MHz clock and each subsequent pin 12 of U16, U15, etc., divides the previous frequency by 10. The output of pin 12 of U14 is 1 KHz and pin 12 of U13 is 100 KHz. With the use of switch S7A, either of these clock rates may be selected. If the 1-KHz rate is selected, the system can count to the nearest millisecond. Similarly, the 100-Hz clock provides accuracy to the nearest 10 milliseconds.

Timer Circuit. The timer circuit consists of U26, a National Semiconductor LM322N chip designed for timing. The timing period is selected by two variable resistors, one for coarse and the other for fine settings. When a high is placed at pin 3, the timing cycle begins. This can be seen by a low at pin 12. Therefore, before the timing cycle starts, a low exists at pin 3 and diode CR9 is conducting to establish a 0.7 volt bias at the base of Q8, keeping it off. When the high is placed at pin 3 and pin 12 goes low, again the base of Q8 is at 0.7 volt to keep it off.

When the timer completes its cycle, pin 12 goes back to high and pin 3 is still high. Then current can flow through R104 to the base of Q8, turning it on. With Q8 on, current flows through the relay coil to pull in the contacts. If switch S8 is off, the circuit functions as explained during each operation of the ICP. If S8 is turned on, a ground is placed on the stop circuits via the relay contacts. Therefore, the system is stopped on the basis of time delay the same as stopping occurs on range. The final arm signal (based on range) is removed and the time signal is placed to the stop circuits by means of switch S8.

The relay contacts are connected to jacks on the front of the panel to provide a 28-VDC output when the timing has run out. This feature is designed to function a device which shifts the axis of the SSS after a specified time to simulate a change in acceleration levels.

Range Selection. Range selection is made by means of four thumbwheel switches, TW1 through TW4. These are 10-position switches having four binary-coded outputs which are the jam inputs or range selections for the four SSS counters. The binary outputs are routed directly to 16 connector pins as shown in Figure 45. These outputs are present at all times, and simultaneous entry is made by depressing the set-clear switch S6.

Power Supply Circuits. There are seven supply voltages generated in the ICP. A 2.9-volt supply is set by Q1 and regulated by Zener diode CR1. This supply is used to operate the display segments. A 14-volt supply is provided by Q3 and is used for all logic circuits in the position system SSS and for the counting circuits only in the torque system. This voltage is supplied to the SSS through connector pin B and is also available at the logic voltage jacks on the ICP front panel. A 5-volt supply is provided by REG-1 and is used to operate all TTL devices in the ICP. The motor voltage supply is formed by a Darlington pair whose base is controlled by R22. By adjusting R22, the motor supply voltage is variable from 0 to approximately 24 volts. This supply is accessible at the motor voltage jacks on the ICP front panel. The motor voltage via these jacks is used for the enable input in the torque system and should be adjusted to maximum for proper operation. A prestart voltage is provided by Q9 and Q10 and can be varied by R112.

Two other voltages are provided for use with the torque system. These are +24 volts and -24 volts and are shown on the ICP power supply modification schematic (Figure 45). These voltages are supplied to the SSS through jacks mounted on the ICP side panel. A switch, S9, is mounted with these jacks and turns the 24-volt supplies on or off. Also located on the side panel are 5 other jacks which provide various current levels required in the torque system. These currents are obtained through resistors in series with the +24-volt supply.

Three transformers are used along with three bridge rectifiers and three filter capacitors to provide the basic DC levels. LED 1 indicates the power-on status of the ICP, and S1 is the power switch. When the power switch is turned on, all voltages are available and providing current except the motor and prestart outputs. These are controlled by switches and other circuitry explained below.

Control Logic. To explain the control logic, the best starting point is the set-clear function. This circuit consists of NAND gates U8A and U8B which are wired as a flip-flop. When the set-clear switch S6 is depressed, a ground is placed on pin 1 of U8A to force a logic 0 at pin 11. This signal is routed to pin 10 of U8D, which results in a logic 1 at pin 8. Pin 8 is connected to pin 5 of inverter U2E whose output (pin 6) is then a low. This point is bus connected to all reset pins of the range and elapsed time circuits. The logic low resets all display circuits. NAND gate U8B output, pin 11, also drives U2D whose output is routed to connector pin C and thence to the SSS counters to set them to the range selected by the thumbwheel switches. The set-clear switch is a spring-loaded pushbutton type; therefore, when released, a ground is placed at pin 13 of U8B to return the system to the ready state. Since TTL circuits require a 5-volt supply and CMOS a 14-volt supply, interface circuits are needed. This is the purpose of U2D, which accepts TTL and provides a CMOS level output for use in the SSS.

Following set-clear operation, the system may be started by depressing S3. This action sets a flip-flop consisting of NAND gates U8C and U7A. Depressing the start button places a 0 at pin 4, and U8C output is then at 1. This 1 is fed back to pin 9 of U7A, and since pins 10 and 11 are high via U2A and R67, its output at pin 8 is low. This flip-flop will remain in this state regardless of the position of S3, and that switch may be released. Other input signals are necessary to change the start state as will be explained later.

The 0 output of pin 8 of U7A is routed to inverter U2C whose output is a high to turn on Q5. With Q5 on, Q4 is turned off and motor power is applied to the SSS via the Darlington and connector pin D. Stated differently, motor power is not supplied to the SSS until the start button is depressed.

At the same time, the output of pin 8 of U7A is routed to NAND gate U7B, whose output becomes high with operation of start switch S3. This high is routed to the timer to start its cycle and to pins 3 and 4 of NAND gate U7C. With a high at these pins, the count at connector pin G is processed via interface inverter U1C and pin 5 of U7C. With a 0 at pins 3 and 4 of U7C, no range count can be processed. The signal at pin 6 of U73 is the motor velocity whose count is now accumulated by the range counters displayed. Therefore, the purpose of U7C is to gate on or off to accept or reject the range clock on the basis of the state of the flip-flop of U8C and U7A. This flip-flop is controlled by the start switch.

Meanwhile, the output of U8C is a logic high following operation of the start switch. This high is routed to the timer clock circuit U13 through U17 on the reset bus. This allows the clock to function and the elapsed time circuits to count up.

If a low signal is applied to pin 10 or pin 11 of U7A, the flip-flop will take up the opposite state which then removes motor voltage, inhibits the time clock, and gates off the range input count. When this condition occurs, the total elapsed time and range is displayed and held until the set-clear is depressed. Such stop signals are available from 3 possible sources. First, if the stop switch S4 is depressed, this places a low at pin 10 of U7A to change the state of the flip-flop. Second, the arrival of a final arm signal at connector pin H from the SSS is placed at pin 11 of interface inverter U1A. This signal is again inverted by U2A whose output is routed to pin 11 of the flip-flop to stop and display data. The final arm signal is a low which occurs when all SSS counters have reached a logic 0 output, which is the condition reached when the preselected range has been accumulated. A low at pin 12 of U2A provides a ground for LED 2, the final arm display provided on the front of the ICP control panel.

The third stopping technique is provided by the timer. When S8 is turned on, the realy contacts force a low at pin 10 of U7A following timer run out. Therefore, the system will stop on the basis of time, range or manual action. It should be stated that when used in the time mode, the input range should be set to a level which cannot be reached for the time selected. Otherwise, the system will stop if the range is reached prior to timer run out.

The restart voltage is applied to the SSS (position system only) by means of S2. However, when the start button is depressed, the motor voltage thus applied is routed to turn on a TIP31A transistor whose collector is pulled down to shut off Q10 and Q9, the prestart source. Therefore, when the system is started, prestart voltage is removed if it has been turned on. Following runout, the motor voltage is removed and the pre-start voltage reapplied automatically.

The prearm indication is provided by U1B and U2B. A prearm signal is a low which is inverted twice by U1B and U2B to provide a ground for LED 3. This LED is controlled by the SSS counters; therefore, if the SSS is disconnected and the ICP turned on, the prearm will be on.

Both the null voltage and the motor velocity can be monitored at the ICP. Connector jacks are provided on the control panel via connector pins J and G.

Since the total supply sources to the SSS are the motor and logic voltages, the power consumption can be measured by means of shorting bars shown in series with connector pins D and B. By removing the shorting bars and replacing them with precision 0.1-ohm resistors, the power from each source can be determined. This is done by measuring the voltage across the resistor and dividing by the resistance to obtain the current. Multiplying this current by the applied voltage yields the power.

OPERATION PROCEDURES

These paragraphs provide a description of operating procedures and techniques for interfacing the ICP to the SSS. Illustrations of the control and side panels are shown in Figures 47 and 48, and Figure 49 shows the electrical interface between the SSS and ICP. Operating procedures are outlined in a step-by-step sequence for various functional options.

Connection Procedure.

a. Position System SSS:

(1) Power switch off.

(2) Connect cable.

(3) Proceed to range limit procedure.

b. Torque System SSS:

(1) Power switch off.

(2) 24-volt supply switch off.

(3) Connect cable.

(4) Connect leads as follows:

(a) Yellow plugs to sensor current jacks (order not important).

(b) Red plug to +24V jack.

(c) Black plug on white wire to -24V jack.

(d) Blue plug to RPM current jack.

(e) Green plug to motor voltage jack on ICP front panel. Use a GR plug shunt to connect the 2 motor voltage (green) jacks.

(f) Black plug or brown wire to ground.

(5) Insert proper resistor into R_X jacks.

(6) Turn motor voltage control full CW.

(7) Proceed to range limit procedure.

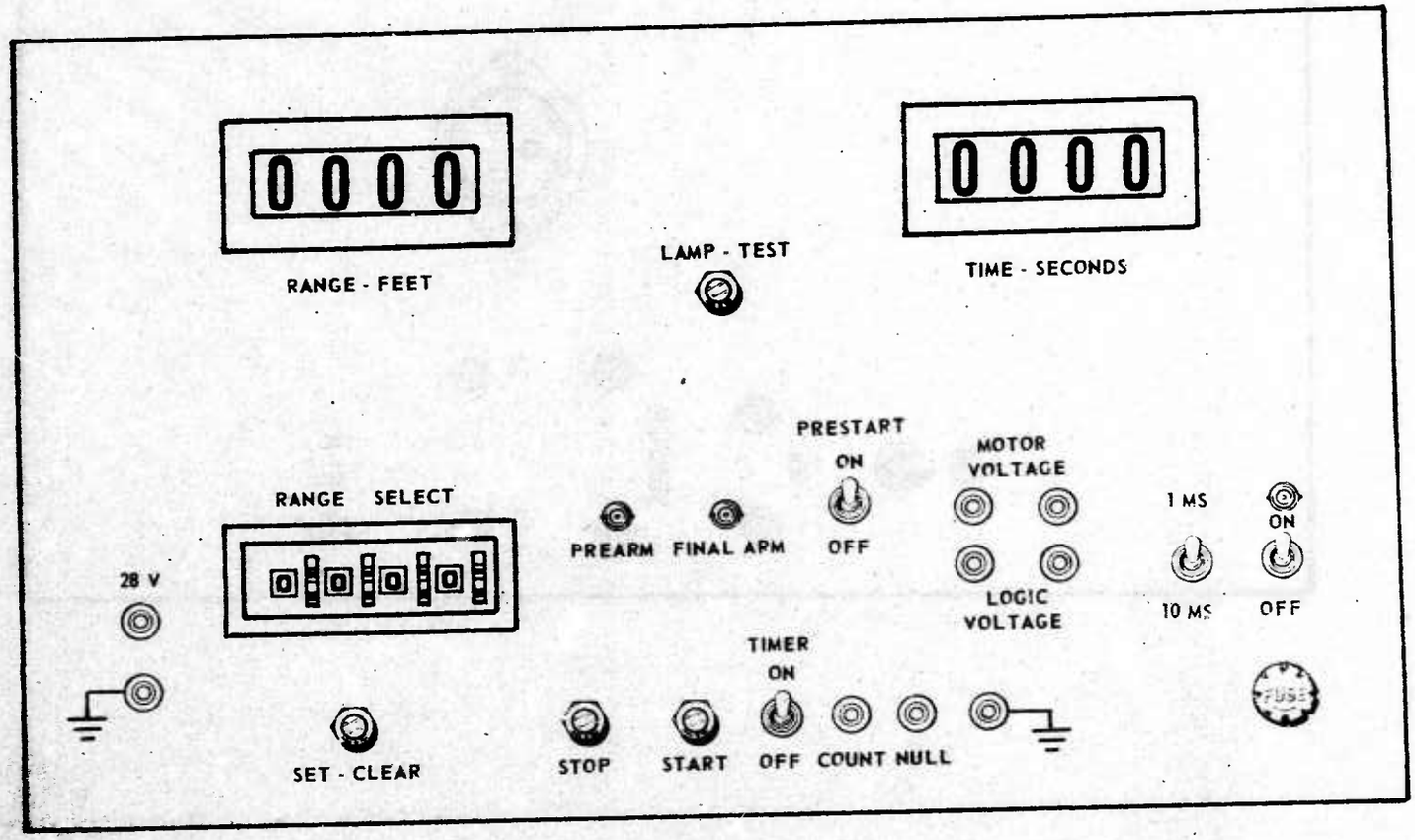

Figure 47. ICP Control Panel

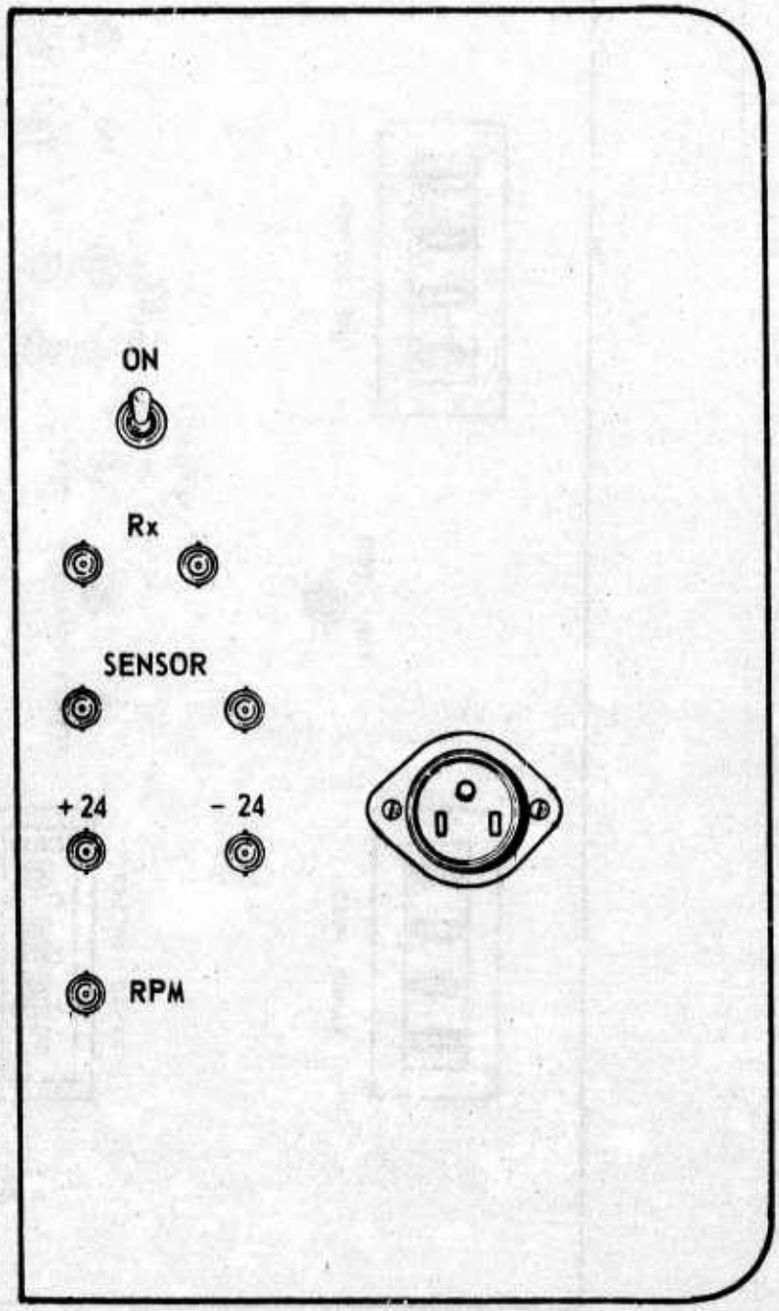

Figure 48. ICP Side Panel

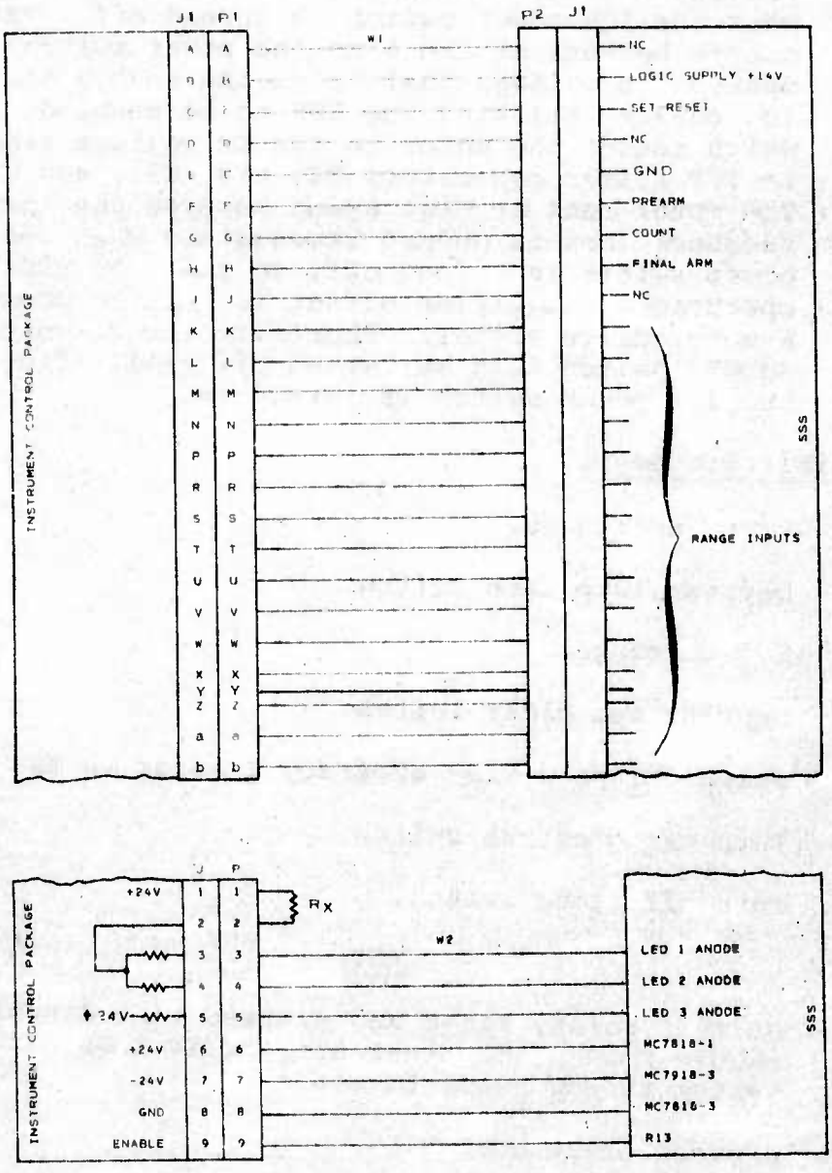

NOTES:

1. J1 THROUGH J8 ARE BANANA JACKS.
2. J9 IS THE OUTPUT FROM THE EXISTING MOTOR VOLTAGE JACKS (GREEN) ON ICP FRONT PANEL.
3. RX IS MOUNTED ON GR PLUG P1/P2.
4. P3 THROUGH P9 ARE BANANA PLUGS.

Figure 49. Final Prototype SSS Electrical Interface with ICP

NOTE

The 24-volt supply switch, S9, is provided to prevent voltage from being applied to the motor when the ICP power switch is turned off. This occurs because at the time the power switch is opened the voltage that holds the enable signal low ceases, allowing the SSS to be enabled, which causes the motor to run on voltage stored in ICP filter capacitors C2, C10, C11, and C12. The motor runs at high speed because the torque feedback loop is opened immediately when the power switch is turned off, so that the SSS operational amplifier offset is able to provide a motor drive signal. Therefore the 24-volt supply switch must be turned off until after the ICP power switch is turned on.

Range Limit Procedure.

(1) Power switch on.

(2) Depress lamp test switch.

(3) Select range.

(4) Depress set-clear switch.

(5) Select elapsed time accuracy 1 ms or 10 ms.

(6) Turn off prestart switch.

(7) Turn off timer switch.

NOTE

At this point, range and elapsed time displays should read 0 and final arm/prearm LEDS off. System is now ready to start.

(8) Depress start button.

NOTE

The system will now function until the selected range is reached. At the final range, the system will stop automatically, displaying range and elapsed time. The final arm and prearm LED's will be on.

To repeat a run under the same conditions or a different range, the operation is as follows:

(1) Set range.

(2) Depress set-clear.

(3) Depress start.

Timer Operation.

(1) Remove the SSS.

(2) Turn on timer switch.

(3) Select accuracy, 1 ms or 10 ms.

(4) Depress start button.

(5) Record the run time.

(6) Adjust the potentiometer - CW to increase time, CCW to decrease.

(7) Depress set-clear.

(8) Depress start.

(9) Repeat steps (5) through (8) until desired time is recorded.

(10) Reconnect SSS.

(11) Set range above expected level.

(12) Depress set-clear.

(13) Depress start.

NOTE

If the selected time is short, the start button must be released quickly.

(14) Record range and time.

To repeat this run, repeat steps (12) and (13).

NOTE

For repeating runs, it is necessary to allow sufficient time for the motor to run down prior to starting a new run. Otherwise when the set-clear is depressed, the SSS counters will begin accumulating run down distance. The ICP is not affected; however, the final range seen on the display will be less than the selected range and the elapsed time will be shorted than expected.

Prestart Operation. Position system only.

CAUTION

When the ICP is to be functioned with the SSS connected, the prestart voltage potentiometer should be turned full counterclockwise to remove all prestart voltage. If the pot is full clockwise, excessive power will be supplied to the SSS motor.

To use the prestart function, proceed as before, following the steps below:

(1) Turn the prestart voltage pot full CCW.

(2) Turn on prestart voltage switch.

(3) Connect oscilloscope or counter to count jack.

(4) Adjust pot until the desired velocity is recorded.

CAUTION

If velocity is greater than 200 Hz, the prestart voltage should be turned off when the system is not being functioned.

(5) To operate, depress set-clear and start buttons simultaneously. A quick release is necessary. This is because the count is accumulated in the SSS counters while the motor is running; therefore, to start from 0 count, the set-clear must be depressed along with the start.

INITIAL DISTRIBUTION

HQS USAF/RDQRM	2	TAWC/TRADOCLO	1
HQ USAF/SAMI	1	ADTC/SES	1
HQ USAF/XOXFM	1	ADTC/SD23	1
AFIS/INTA	1	AFATL/DL	1
AFSC/DLCA	1	AFATL/DLOSL	9
AFSC/IGFG	1	AFATL/DLY	1
AFSC/SDZA	1	AFATL/DLJ	1
AFAL/DHO	1	AFATL/DLJC	1
AFWAL/Tech Lib	1	AFATL/DLJF	10
ASD/ENFEA	1	AFATL/DLJK	1
FTD/PDXA-2	1	AFATL/DLJM	1
AFWL/NSC	1	SARPA-ND-C	1
AFWL/NSE	1	USNWC (Code 335)	1
AFWL/SUL	1	USAF/AFRD	1
AFEWC/SUR	4	HARRY DIAMOND LAB/DRXDO-DA	1
AUL (AU/LSE-70-239)	2	NAVAL WPNS EVAL FAC	1
DDC	2	AFML/MXE	1
NRSLC/MMIRBD	1	MERADCOM/DRXFB-XS	1
OGDEN ALC/MMWM	2	AFATL/DLM	1
SAC/LGW	1	SAFRD	1
SAC/NRI	1	USAFE/LGWM	1
TAC/DRA	1		
57 FWW/DOS	1		
USAFTFWC/TA	1		
6510 ABG/SSD	1		
HQUSAFE/DOA	1		
HQUSAFE/DOQ	1		
HQPACAF/LGWSE	1		
HQPACAF/DOO	1		
SARRI-LW	1		
SARPA-TS-S#59	1		
DRXSY-J	1		
DRXSY-A	1		
REDSTONE SCI INFO CEN/Doc Sec	2		
NAV RES LAB/Code 2627	1		
NAVAIR SYS COMD/Code 530C	1		
NAVAIR SYS COMD/AIR-954	1		
NAV SUR WPN CEN/Tech Lib	2		
NAV ORD STN/Tech Lib	1		
NAV AIR TEST CEN/CT-176 TID	2		
USNWC (Code 533)	1		
SANDIA LAB/Tech Lib Div 3141	1		
THE RAND CORP/Lib-D	1		
TACTEC/BATTELLE COLUMBUS LAB	1		
USAFTAWC/TEFA	1		

(The reverse of this page is blank)